PhD degree in Molecular Medicine (curriculum in Molecular Oncology)

European School of Molecular Medicine (SEMM),

University of Milan and University of Naples “Federico II”

ATR mediated regulation of cellular and nuclear plasticity

Gururaj Rao Kidiyoor

IFOM, Milan

Matricola n. R10786

Supervisor: Prof. Marco Foiani

IFOM, Milan

Anno accademico 2016-2017

TABLE OF CONTENTS

Page number

List of Abbreviations

ATR	Ataxia Telangiectasia and Rad3-related
CIN	Chromosomal instability
MIN	mini-satellite instability
GCR	Gross chromosomal rearrangements
MMR	mis-match repair
HR	Homologous recombination
UV	Ultra-violet radiation
ROS	Reactive oxygen species
DDR	DNA damage response
ATM	Ataxia Telangiectasia Mutated
RPA	Replication protein A complex
PCNA	Proliferating cell nuclear antigen
BER	Base excision repair
NER	Nucleotide excision repair
NHEJ	Non-homologous end joining
TC-NER	Transcription coupled Nucleotide excision repair
GG-NER	Global genomic Nucleotide excision repair
BRCA1	Breast cancer susceptibility 1
53BP1	Tumor suppressor p53 binding protein
NBS	Nijmegen breakage syndrome
MDC1	Mediator of DNA damage checkpoint protein 1
ATRIP	ATR interacting protein
TopBP1	Topoisomerase binding protein 1
PTEN	Phosphatase and tensin homolog
CDKN2A	Cyclin dependent kinase inhibitor 2A

EGFR	Epidermal growth factor receptor
PNKP	Polynucleotide Kinase/Phosphatase
TTD	Trichothiodystrophy
COFS	Clinical diagnosis of cerebro-oculo-facio-skeletal syndrome
NE	Nuclear envelope
PCNT	Pericentrin
LINC	Linker of the nucleus and cytoskeleton complex
ESCRT	Endosomal sorting complex required for transport
PIKK	Phosphatidylinositol 3-kinase-related kinases
DNA-PK	DNA dependent protein kinase
mTOR	Mechanistic target of Rapamycin
SMG1	Suppressor of morphogenesis in genitalia 1
TRRAP	Transcription/transformation domain associated protein
MEC1	mitotic entry checkpoint 1
9-1-1	Rad9-Rad1-Hus1 (9-1-1) complex
HEAT repeat	Huntingtin, Elongation factor 3, Alpha-regulatory subunit of protein phosphatase 2A and TOR1
FAT domain	FRAP-ATM-TRRAP domain
PTM	post-translational modification
ETAA1	Ewing tumour-associated antigen 1
PC	Phosphatidyl Choline
EM	Electron microscope
CHK1	Checkpoint kinase 1
VPR	Viral protein R
MAPK	Mitogen-activated protein kinase
ERK1 and 2	Extracellular signal-regulated kinase 1and 2
VAMP2	Vesicle-associated membrane protein

STAT3	Signal transducer and activator of transcription 3
UPF1	RNA helicase and ATPase
RRM2	Ribonucleoside-diphosphate reductase subunit M2
dNTP	Deoxynucleotide
NEBD	Nuclear envelope breakdown
ER	Endoplasmic Reticulum
IP	Immuno-precpitation
SILAC	stable isotopes labeling with amino acids in cell culture
HU	Hydroxyurea
DAVID	The database for visualization and integrated discovery
STRING	Search Tool for the Retrieval of Interacting Genes/Proteins
GO	Gene ontology
ARP	Actin-related protein
FMN2	Formin 2
AFM	Atomic Force Microscopy
FRET	Fluorescence Resonance Energy Transfer
PDMS	Polydimethylsiloxane

Figures Index

Page number

Abstract

Protein kinase ATR (Ataxia Telangiectasia and Rad3-related) is a key regulator of genomic integrity. In addition to its vital, well-understood role in maintaining replication fork stability, ATR is also involved in mediating mechanical stress response at the nuclear envelope preventing potential threats to the genome. Our data from sub-cellular distribution and interactome analysis of ATR suggests that ATR contributes to several cellular processes in multiple organelles such as mitochondria, actin cytoskeleton, Golgi and nuclear envelope. At the nuclear envelope ATR is present on both inner and outer nuclear membranes, on the nuclear pores and bound to perinuclear chromatin and to perinuclear actin fibers. In this study we show that ATR regulates nuclear membrane integrity by maintaining nuclear morphology and optimal membrane tension, by counteracting mechanical force imbalances at the NE and by coordinating nuclear events with nuclear and cell migration. We report a novel role of ATR in preventing and protecting nuclear envelope damage and DNA damage caused by mechanical constrains acting on the nucleus. Further we show that by maintaining nuclear envelope integrity ATR facilitates cell migration on 2D surfaces and by regulating nuclear membrane components and by limiting nuclear envelope damage it aids cell survival during confined 3D migrations. Loss of ATR dampens neuronal migration during development and cancer cells lacking ATR are inefficient in extravasation, do not survive circulation and fail to successfully metastasize into the host environment. Therefore, by promoting cell survival in altering mechanical microenvironment and during metastasis and invasion, ATR assists tumor development, suggesting a dual role for this kinase in tumorigenisis

Introduction

1. Genomic instability during development, aging and cancer

Genome contains all the necessary information for cellular and organismal existence, thus making its maintenance and faithful transfer a vital task. These genetic materials are biological molecules that are susceptible to damage. Considering that it is the only source of information for cell survival, cells employ numerous processes to ensure the preservation of their integrity and to promote faithful propagation. While in proliferating cells, efficient and error-free DNA replication and chromosome segregation renders threat to genome integrity; in senescent cells, inefficient repair of damaged DNA renders the major for genome integrity.

Genome instability broadly refers to all genetic alterations ranging from point mutations to chromosome rearrangements, leading to incorrect or loss of genetic information (Aguilera and Gomez-Gonzalez, 2008, Hoeijmakers, 2009, Hanahan and Weinberg, 2011). Major categories of genome instability are-

1. Chromosomal instability (CIN) - changes in chromosome number leading to chromosome gain or loss, caused by aberrant chromosome segregation during mitosis.
2. Micro- and mini satellite instability (MIN) - Alterations in repetitive-DNA sequences occurring due to replication slippage and defective mismatch repair (MMR) or homologous recombination (HR).
3. Instability resulting from base substitutions, micro-insertions and micro-deletions.
4. Gross chromosomal rearrangements (GCRs) – genome instability caused by translocations, duplications, inversions and deletions.

Since genetic material is never renewed completely after mitosis, time dependent deterioration of DNA would lead to genome instability. In addition, intrinsic stresses such as reactive oxygen species and aberrant replication also contribute to genome instability. Genome is also constantly exposed to assaults of varying degrees from several external

sources including ultra-violet (UV) light, ionizing radiation (IR) and chemical toxins (Figure 1). In some cases, organisms utilize genetic instability positively for generating variability to drive evolution and variations in immunoglobulin. However, majority of genome instability is associated with pathological disorders including premature ageing, cancer predisposition, neuronal disorders and inherited developmental disorders (Hoeijmakers, 2009).

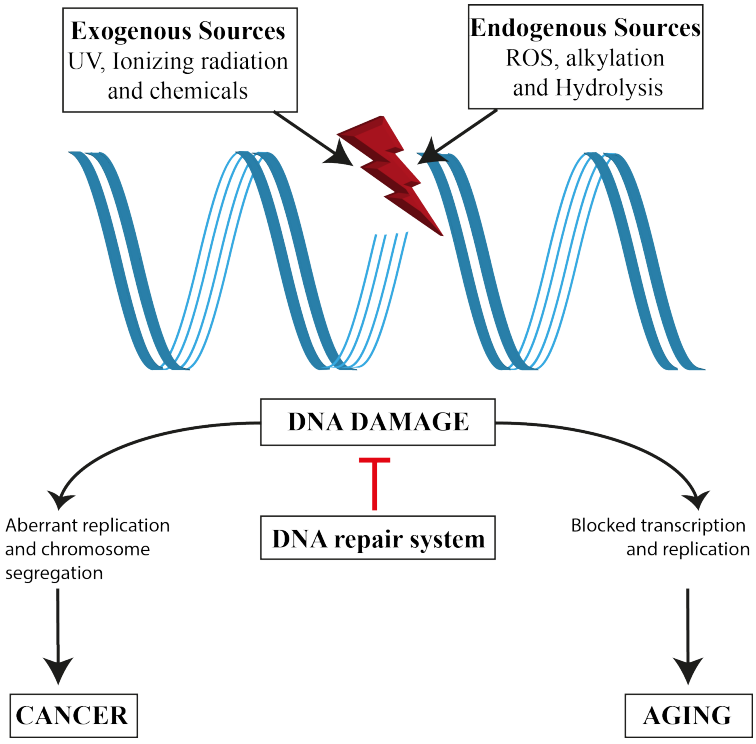

Figure 1 – Causes and consequences of DNA damage (image modified from Hoeijmakers et al., 2009, NEJM)
Both internal and external stress on the DNA leads to its damage. Failure to repair and defective repairing leads to genome instability. Genome instability could consequently hinder transcription and replication; blocking protein synthesis and cell proliferation thereby accelerating aging process or it could result in oncogenic mutations and aberrant chromosomal segregation causing cancer.

1.1. DNA repair and maintenance of genome integrity

Cells maintain genome integrity by employing elaborate apparatus consisting of repair pathways and genome surveillance systems ensuring damage free genome and error free replication. Cellular responses to DNA damage are collectively called DNA damage checkpoint, including initiation of DNA repair, arrest of cell cycle progression, and apoptosis if the damage is beyond repair. The process of DNA damage checkpoint consists of four components: sensors, mediators, signal transducers, and effectors. Sensors are proteins involved in recognition of DNA damage to initiate subsequent

events. Replication protein A complex (RPA), Proliferating cell nuclear antigen (PCNA), 9-1-1 complexes, ATM and ATR are categorized as sensors of DNA damage. The class of mediator includes Breast cancer susceptibility 1 (BRCA1), Claspin, tumor suppressor p53 binding protein 1 (53BP1), and mediator of DNA damage checkpoint protein 1 (MDC1); they even can participate in more than one step of the checkpoint response. In humans, two checkpoint kinases, Chk1 and Chk2 function as signal transducers. Double-strand breaks are sensed by ATM and are transduced by Chk2, UV-damage signal are sensed by ATR and are transduced by Chk1. Signal transducers phosphorylate a series of effector proteins to carry out processes including repair and cell cycle arrest. Effector proteins including Cell division cycle protein 25 (Cdc25) and p53 are involved in implementing checkpoint-mediated responses such as cell cycle arrest and apoptosis.

Cells employ multiple repair pathways, based on the category of DNA lesion (Figure 2). DNA repair pathways are divided into four major categories: base excision repair, nucleotide excision repair, double-strand break repair, and repair of interstrand cross-links.

Base-excision repair (BER) is employed to eliminate subtle modifications including oxidative lesions, small alkylation products, and several other kinds of single-strand breaks. First the damaged base is removed, and then the gap is refilled by DNA synthesis.

Nucleotide-excision repair (NER) is employed to eliminate the helix-distorting single strand DNA damage. NER are broadly divided into two sub-categories: TC-NER and GG-NER. Global genome NER (GG-NER) represents NER mediated repair across the whole genome, while Transcription-coupled NER (TC-NER), is strictly linked with nucleotide-excision repair of lesions that obstruct transcription.

Non-homologous end joining (NHEJ) and homologous recombination (HR) repair are the two major repair pathways employed for repairing various types of double strand breaks. In NHEJ, two ends of broken DNA are brought together and sealed. NHEJ are

highly error prone and mostly occur in non-cycling cells including neurons where the identical copy of DNA is absent. Homologous recombination is the most sophisticated and preferred mode of double strand break repair in proliferating cells. It acts through a series of complex DNA transactions involving a large set of proteins. HR uses the identical sister chromatid to properly align the broken ends and accurately insert missing information at the site of damage.

Interstrand cross-link repair resolves cytotoxic cross-links that covalently attach two strands, thereby preventing strand separation and effectively arresting transcription and replication at the site of damage (Sancar et al., 2004, Hoeijmakers, 2009).

Cells also have DNA damage tolerance pathways that facilitate the duplication of the genome, even in the presence of unrepaired lesions. These lesion bypass pathways function through two mechanisms, translesion synthesis and template switching. In translesion synthesis, special DNA polymerases that can synthesize DNA with low fidelity replaces the replicative polymerase blocked at the damage site, catalyzes the addition of a few nucleotides across the lesion, and then dissociates allowing the main replicative helicase to return. In template switching model the 3'end of the blocked strand dissociates from the damaged template and re-anneals to the complementary nascent DNA strand (Nikolaishvili-Feinberg and Cordeiro-Stone, 2000, Hoeijmakers, 2009).

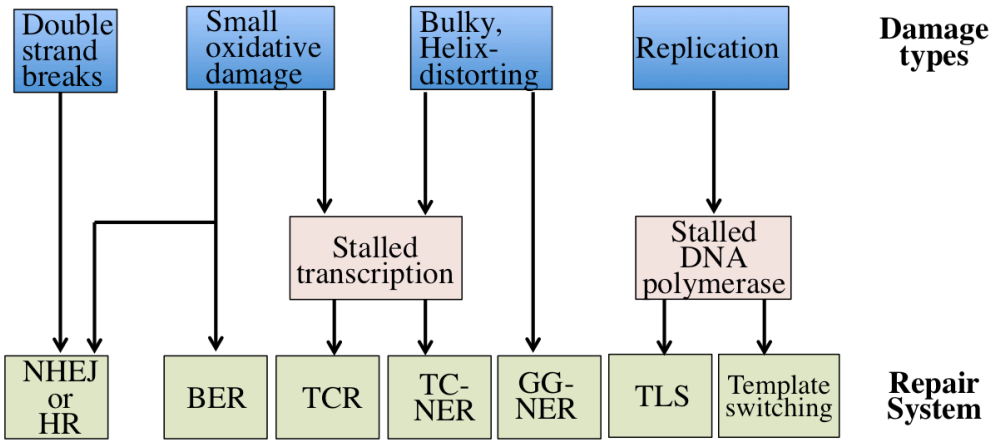

Figure 2 – Types of DNA lesions and their respective DNA repair pathway (image modified from Hoeijmakers et al., 2009, NEJM) This figure summarizes the major DNA damage classes and the repair pathways employed by the cells to efficiently repair the damage. TCR- transcription-coupled repair, TLS - translesional synthesis.

1.2. Genome instability in aging

Aging is defined as the time-dependent deterioration of physiological integrity and function of cells and organs of an organism. Accumulation of cellular and genomic damage over time is considered to be one of the main causes for aging. The hallmarks of aging are genomic instability, telomere attrition, epigenetic alterations, loss of proteostasis, deregulated nutrient sensing, mitochondrial dysfunction, cellular senescence, stem cell exhaustion, and altered intercellular communication (Lopez-Otin et al., 2013). Genome instability is not only the hallmark of aging but it is also the driving force since it can directly influence other hallmarks, thereby accelerating aging process. Aging also increases the risk for several cardiovascular diseases, cancer and neurodegenerative disorders (Figure 3). Cancer could also be considered an age related disease since they both share a common origin at the mechanistic level i.e., accumulation of genomic and cellular damage. Broadly, cancer and aging are two different manifestations of genome instability (Figure 1). While, aging stems from a gradual decline of fitness due to the accumulation of genomic damage, cancers are formed by a sub-population of rare mutations that can increase cellular fitness and provide aberrant advantages towards cell survival and proliferation (Niccoli and Partridge, 2012). Genome instability also contributes directly towards age related cardiovascular and neurodegenerative diseases.

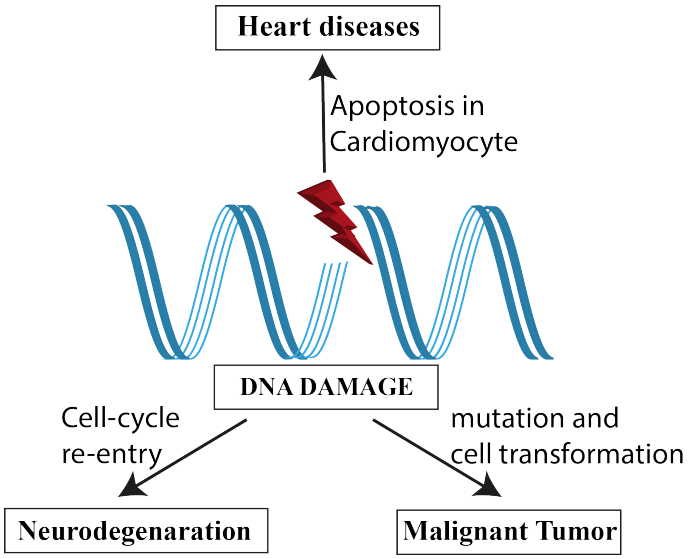

Figure 3 –Effects of DNA damage on aging
Genome instability due to defective repair and telomere shortening leads to (A) cardiovascular diseases (B) neurodegeneration (C) cancer.

a. Cardiovascular diseases

High levels of DNA damage and shortened telomeres in the vascular endothelium promote cellular senescence and inflammatory responses. This consequently leads to plaque deposition, atherosclerosis, coronary artery disease and heart failure. In ageing cardiomyocytes telomere shortening and reduced DNA damage response (DDR) by mutations in repair pathway may limit the proliferative potential of cardiac progenitor cells, deplete progenitor pool by increasing cellular senescence and apoptosis consequently increasing the risk of heart failure. In mice models with short telomeres, cardiomyocyte numbers are reduced to half the number present in control heart (Kovacic et al., 2011, Niccoli and Partridge, 2012). Patients with mutations in ATM and ATR exhibit high risk of developing ischaemic heart disease (Ruzankina et al., 2007).

b. Neurodegenerative diseases

Genome stability is essential for proper development and function of the nervous system. In developing brains, DNA damage could occur during DNA replication and in mature neurons spontaneous double-strand breaks could arise due to neuronal activity (Figure 4). Accumulation of DNA damage in the brain can affect gene expression, which consequently impact processes involving memory and neuronal survival. Neurons utilize multiple repair pathways to ensure genome integrity and neuronal homeostasis (Figure 4). Maintaining genome integrity against replication stress is essential for the survival of early-born neural progenitors. Replication-associated DNA damage in neural progenitors utilizes HR or NHEJ for repairing Double-strand breaks and MMR for correcting replication errors. Compromised genome during development as in case of Topoisomerase II binding protein 1(TopBP1) inactivated mice, leads to substantial neurodevelopmental abnormalities throughout the cortex (Lee et al., 2012). In post-mitotic neurons, HR is unavailable for repair (Shull et al., 2009), therefore NHEJ remains the sole pathway available to prevent accumulation of DNA double-stranded breaks.

Oxidative stress is one of the primary sources of breaks in mature neurons generating single strand DNA breaks. This breaks are repaired using BER or by TC-NER (McKinnon, 2013). An overview of representative neurologic diseases associated with defective DNA damage response is listed in table 1.

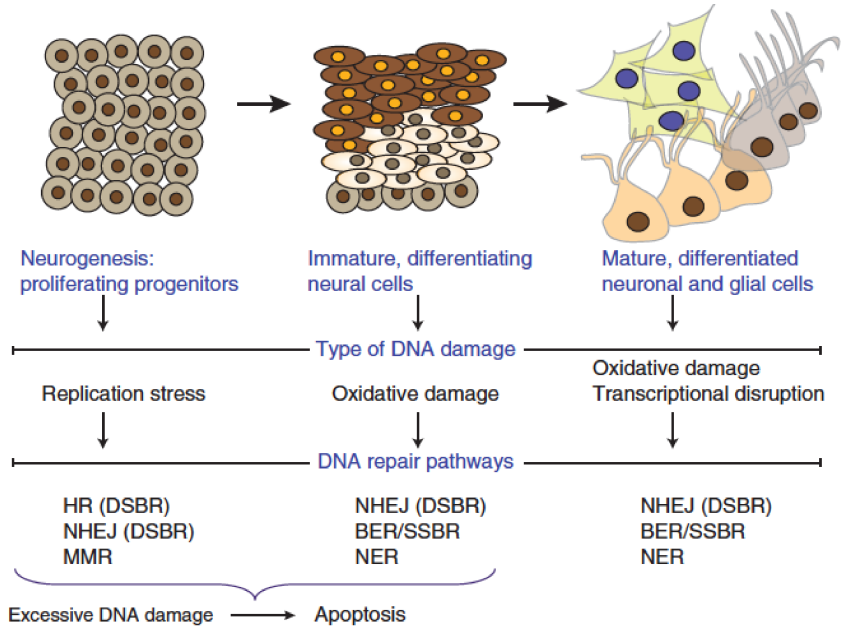

Figure 4 – DNA damage signaling in the nervous system and neurogenesis (image adapted from McKinnon, 2013, Nature neuroscience)
This figure summarises various DNA repair pathways utilized by neuronal progenitors and mature neurons.

Table 1 – neural disorders associated with DNA damage signaling.

DNA damage	Repair pathway	Disease	Neuropathology
Double strand break	NHEJ & HR	Lig4 syndrome Severe combined immunodeficiency (SCID) Fanconi anemiaa	Neurodevelopmental defects/microcephaly Brain tumors
Single strand break	BER	AOA1 SCAN1 MCSZ	Microcephaly Neurodegeneration
DNA interstrand crosslink	Fanconi Anemia pathway	Fanconi anemia	Neurodegeneration Brain tumors Neurodevelopmental defect
Helix-distorting lesion/bulky adduct	Transcription coupled NER	Xeroderma pigmentosum Trichothiodystrophy Cockayne syndrome	Neurodegeneration
Mis-incorporated nucleotide (during replication	Mismatch Repair	Lynch syndrome Nijmegen breakage syndrome ATLD	Brain tumors Microcephaly Neurodegeneration
Replication stress	ATR mediated repair	ATR-Seckel syndrome	Neurodevelopmental microcephaly

1.3. Genome instability in cancer

Genomic instability is the hallmark of almost all human cancers. Most cancers have chromosomal instability (CIN), with high rate of chromosome structure and number variation. Compared to normal cells, cancer cells are genetically unstable and continue to acquire chromosomal abnormalities over time. Cancers can be broadly categorized into two groups: Hereditary cancers and sporadic cancers.

a. Hereditary cancers

In hereditary cancers genomic instability is attributed to mutations in DNA repair genes. Since germline mutation targeting DNA repair proteins are present in every cell of the patient, loosing the remaining wild-type allele could lead to genomic instability and drive tumor development (Loeb, 1991). BRCA1, BRCA2, RAD50, Nijmegen breakage syndrome protein 1 (NBS1), p53, and ATM are few examples of DNA repair genes that are mutated in various hereditary cancers (Negrini et al., 2010).

b. Sporadic cancers

In sporadic cancers two different models explain accumulation of genomic instability: first one is similar to hereditary cancers, caused by mutations in DNA repair genes and the second is caused by the oncogene-induced DNA replication stress at the common fragile sites. However, genome-wide studies suggest that around 69–97% of sporadic cancers do not have mutations in DNA repair (caretaker) genes, indicating genomic instability in many sporadic cancers is not due to inactivation of caretaker genes. The major mutations in sporadic cancers include the tumor suppressor protein p53 and genes that regulate cell growth either positively such as the oncogenes Epidermal growth factor receptor (EGFR) and RAS or negatively such as the tumor suppressor genes Cyclin dependent kinase inhibitor 2A (CDKN2A) and Phosphatase and tensin homolog (PTEN) (Halazonetis et al., 2008). In addition, mutations in genes that regulate growth lead to self-sufficiency of growth signals. Mutations in cytoskeletal and secretome components

assist cancers to alter cellular properties, acquire stem-like status and facilitate cancer metastasis and invasion (Negrini et al., 2010). Though, it is evident that genomic instability is the driving force in cancer development, molecular basis of genomic instability in most of sporadic cancers is less defined, demanding further studies.

1.4. Genomic instability during development

Interestingly germline mutations of several genome stability proteins are also associated with developmental defects. Severities of the defects range from mild to severe depending on the protein that is mutated and the penetration of the mutation. Several diseases associated with DNA repair molecules exhibit neurodevelopmental defects, microcephaly, craniofacial defects and dwarfism. Cockayne's Syndrome caused by impaired TC-NER exhibit severe progeroid syndrome, premature termination of growth and development, severe neuronal dysfunction and hearing loss. Another disease called trichothiodystrophy (TTD), associated with defective TC-NER, also shows similar phenotypes (Hoeijmakers, 2009). Multiple mutations in single strand break repair protein, PNKP (Polynucleotide Kinase/Phosphatase) leads to severe microcephaly, developmental delay, hyperactivity, and intractable seizures. LIG4 syndrome (caused by mutations in DNA ligase IV) and Cernunnos syndrome (XLF-severe combined immunodeficiency) patients also show microcephaly. Clinical diagnosis of cerebro-oculo-facio-skeletal (COFS) syndrome is caused by mutations in ERCC1, CSB/ERCC6, XPG/ERCC5 or XPD/ERCC2, is characterized by growth retardation, microcephaly, congenital cataracts, facial dysmorphism, kyphoscoliosis, osteoporosis and psychomotor disability. Xpf-mutant mouse and Ercc1 deficiency mouse also showed similar overt postnatal growth delay and premature death typical of progeria. Heterozygous mutations in ATR are associated with Seckel syndrome characterized by microcephaly and reduced body size (O'Driscoll et al., 2003). Similar phenotypes were observed in a patients with

Seckel syndrome caused by ATRIP (ATR interacting protein) mutation. Humanized ATR Seckel and conditional ATR knockout mice exhibit strong premature aging and progeroid phenotypes, along with other phenotypes reported of seckel patients (Ruzankina et al., 2007, Murga et al., 2009). Nijmegen breakage syndrome (NBS) associated with NBS1 mutations is characterized by growth retardation, microcephaly, combined immunodeficiency (O'Driscoll, 2012). We should also note that other developmental and age related diseases including the centrosomal protein pericentrin (PCNT) associated Seckel syndrome and nuclear envelope protein lamin (LMNA) associated progeria also exhibit genome instability, defective DDR and accumulation of DNA damage (Isermann and Lammerding, 2013).

In summary, developmental diseases, almost all cancers and several age related disorders form an intricate feedback network with genome instability as the common factor. Inefficient repairing of replication-mediated damages leads to accumulation of damage and developmental defects. This accumulated damage could consequently accelerate aging. On the other hand, cancer is considered an age related disease; during aging due to accumulating DNA damage the risk of cancer disposition increases. Therefore studying genome stability could help us understand better the causes of these disorders and develop better therapeutic strategies.

2. Nuclear integrity influences genome integrity

The Nuclear Envelope (NE) is a phospholipid bilayer separating the nucleoplasm from the cytoplasm. It is composed of a bilayer embedded with nuclear pores, lamins and LINC (linker of the nucleus and cytoskeleton) complex proteins (Figure 5) (Prunuske and Ullman, 2006, Zwerger et al., 2011). Apart from being a physical barrier, NE regulates protein and RNA transport, transcription, replication, DNA repair, RNA synthesis, cell fate/differentiation and migration among other processes. NE also mediates nuclear homeostasis by functioning as a signal inducer, integrator and transducer for a variety of

cellar signals (Dauer and Worman, 2009). Loss of NE integrity is strongly associated with the genomic integrity. Abnormal nuclear shape is the biomarker of several cancers. Altered nuclear shape is one of the key diagnostic tools used for identifying cancer cells. Changes in nuclear morphology causes changes in chromosome organization consequently affecting gene expression and alter nuclear mechanics which could also facilitate metastasis (Webster et al., 2009, Dahl et al., 2008). Lamins provide a scaffold for tethering chromatin to the NE and protein complexes that regulate genome stability; therefore defects in the nuclear lamina can cause genome instability. The current opinion in the field suggests that transient loss of NE integrity (common in cancer cells) could contribute to the genomic instability, and lead to higher genetic variability in cancer cells (Bell and Lammerding, 2016).

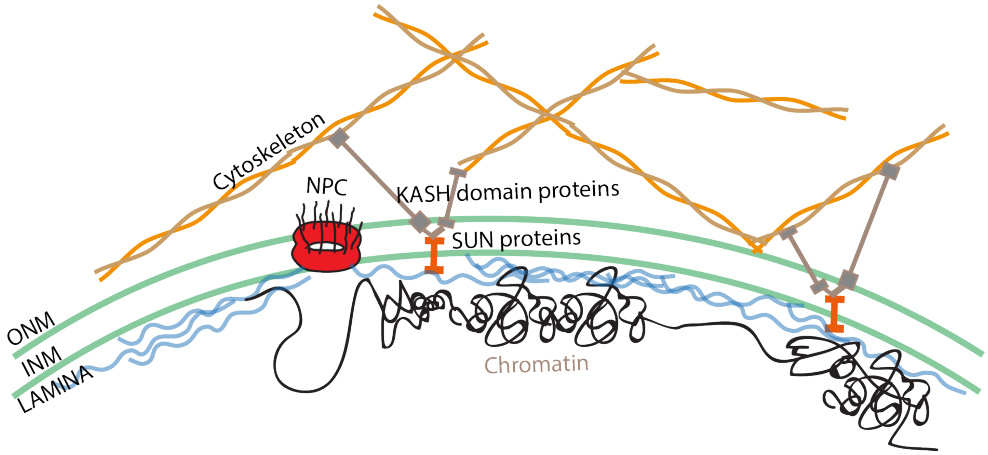

Figure 5 – Nuclear envelope components and organization
This figure depicts NE organization including connections to the Actin, microtubules and intermediate filaments via the LINC complex and lamin associated chromatin.

2.1. Nuclear envelope rupture and repair in dormant cells

During mitosis, nuclear lamina disassembles by phosphorylation of nuclear pore proteins, lamins, and other NE proteins. At the end of mitosis, NE reassembles forming new nuclei by a process assisted by components of the Endosomal sorting complex required for transport-III (ESCRT-III) membrane repair machinery (Vietri et al., 2015, Olmos et al., 2015, Raab et al., 2016). This is an example of naturally occurring controlled NE rupture and repair. Compromises at the NE level would lead to defective

mitosis resulting in abnormal segregation, loss of nuclear shape and micronuclei formation. Micronuclei, are chromosome fragments that get mis-segregated during mitosis and have acquired their own NE, independently from the primary nucleus. Micronuclei are a common feature of cancer cells and a major contributor to genomic instability. Losses of NE integrity in micronuclei are frequent causing massive double strand breaks and chromothripsis contributing to further genomic instability (Zhang et al., 2015). Interestingly transient NE rupture also occurs in dormant cells with defective lamina and in cancer cells. These are repaired rapidly within 90 minutes and they do not cause cell mortality (Vargas et al., 2012, De Vos et al., 2011). However, mechanical forces acting on the nucleus from external load or from cytoskeleton also generate NE ruptures, which may lead to cell-death in cells with compromised nuclear integrity (Bell and Lammerding, 2016, Lammerding and Wolf, 2016).

2.2. Nuclear envelope rupture and repair during migration

Metastasis and Invasion is a hallmark for several cancer types (Hanahan and Weinberg, 2011). Spreading of tumor to additional tissues increases the mortality rate in most cancer types. During *in-vivo* migration, cells pass-through spaces in extracellular matrix (ECM) that are substantially smaller than the size of the nucleus. While the dynamic cytoplasm deforms easily and passes through narrow pores, the nucleus being the largest and stiffest cellular organelle, renders a rate-limiting step. In addition, nuclear deformation imposes a challenge to nuclear integrity in 3D environments (Bell and Lammerding, 2016). NE rupture, occurring during migration through confined spaces, starts by the local detachment of nuclear membranes from the underlying nuclear lamina at the leading edge of the deformed nucleus, resulting in bleb formation. These blebs are devoid of nuclear pores and many other NE proteins including LINC complex. Under continued nuclear pressure, the nuclear membrane bleb expands with chromatin

accumulating into the blebs forming 'chromatin herniations'. Finally, the nuclear membrane in the bleb ruptures, allowing uncontrolled exchange of soluble contents between the nucleus and cytoplasm resulting in DNA damage (Figure 6). In severe cases, the nucleus can fragment, with pieces of chromatin separating from the primary nucleus, resembling the formation of micronuclei (Figure 7). ESCRT-III proteins immediately repair NE ruptures while the DNA damages persist and are repaired slowly over time (Raab et al., 2016, Denais et al., 2016).

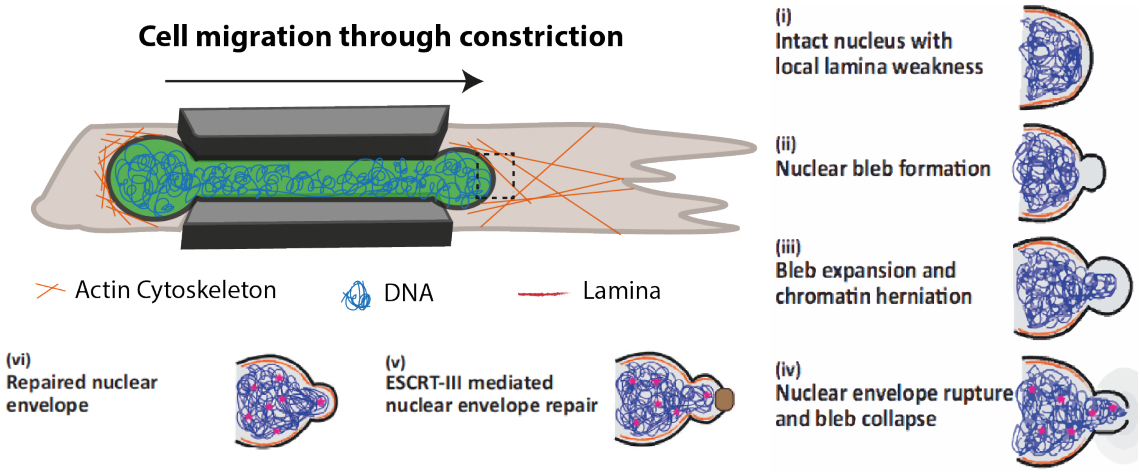

Figure 6 – Mechanism of NE rupture during migration (modified from Shah et al.,2017, TCB)
Stepwise analysis of NE rupture and repair at the leading edge of a cell migrating through narrow pore.

Compression of the nucleus during interstitial migration though narrow pores result in severe nuclear deformation and NE rupture, allowing uncontrolled entry of cytoplasmic nucleases into the nucleus, which would damage the DNA. In addition to this, mechanical shearing of DNA could also lead to DNA damage, leakage of mobile DNA repair proteins from the nucleus to cytoplasm could delay DNA repair, chromatin protrusion could expose DNA to the cytoplasm resulting in DNA damage and facilitate micronuclei formation. Finally, cytoplasmic organelles such as mitochondria can also enter the nucleus and cause DNA damage by producing reactive oxygen species (ROS) (Figure 7) (Raab et al., 2016, Denais et al., 2016, Zwerger et al., 2011, Irianto et al., 2017, Shah et al., 2017).

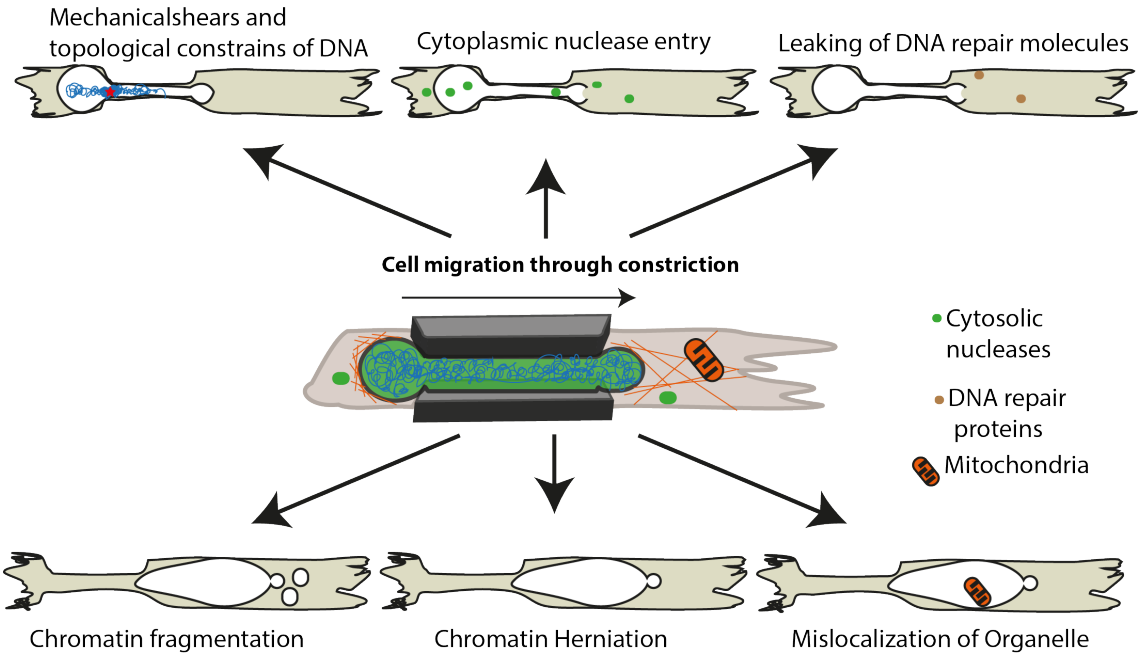

Figure 7 – Consequences of Nuclear deformation and rupture during migration
Schematic representation of defects that could occur during and due to migration through narrow pores.

From these studies it is clear that nuclear envelope integrity and genome integrity are interlinked to one another. Recent reports elegantly show that mechanical forces acting on the nucleus pose a threat to the NE as well as the DNA. Severe nuclear stress as in case of migration through narrow pores could promote genomic instability and in case of cancer cells genomic instability can lead to higher clonal variability.

3. ATR maintains Genome integrity

3.1. PIKK family kinases

Phosphatidylinositol 3-kinase-related kinases (PIKKs) family is constituted of six proteins - mechanistic target of rapamycin (mTOR), ataxia-telangiectasia mutated (ATM), Ataxia Telangiectasia mutated and Rad 3 Related (ATR), DNA-dependent protein kinase (DNA-PK), suppressor of morphogenesis in genitalia-1 (SMG-1), and transformation/transcription domain-associated protein (TRRAP). PIKK are structurally similar to PI3 kinases, but instead of lipid kinase activity they function as protein kinases PIKKs mediate variety of stress responses, including DNA damage, mitochondrial stress, membrane stress, hypoxia, nutrient starvation and errors in mRNA splicing. PIKKs regulate diverse biological functions at different cellular compartments (Lempiainen and Halazonetis, 2009). As mentioned previously, ATM, ATR and DNA-PKcs are involved in the DNA damage response in the nucleus. mTOR kinase is mainly cytoplasmic and controls a wide variety of metabolism pathways and cell growth. SMG-1 regulates nonsense-mediated mRNA decay and TRRAP functions as a regulator of transcriptional activity. Though TRRAP is considered as a true PIKK member it lacks kinase activity. From the prospective of this study, we will be discussing only about ATR since it is the focus of this study. ATR is an essential PIKK kinase conserved in all eukaryotes (Baretic and Williams, 2014). Mecl in S. *cerevisiae*, Rad3 in S. *pombe* and ATL in C. *elegans* and mei-41 in D. melanogaster are homologs of ATR in other model organisms (Saldivar et al., 2017, Cimprich and Cortez, 2008).

3.2 Structure of ATR

ATR is a member of PIKK family sharing strong structural similarities with other members. ATR protein constitutes of 2644-amino acids comprising of N-terminus α-solenoid HEAT repeat (Huntingtin, Elongation factor 3, Alpha-regulatory subunit of protein phosphatase 2A and TOR1), FAT domain (FRAP-ATM-TRRAP), KD (kinase

domain), PRD (PIKK regulatory domain) and a FAT-C-terminal (FATC) domain (Figure 8). ATR contains 45 HEAT repeats at the N-terminus (Perry and Kleckner, 2003). HEAT repeats mediate protein-protein interactions. ATR HEAT repeats include the binding site for ATRIP, BH-3 like domain and nuclear localization sequence (NLS). ATRIP binding is dispensable for stability of ATRIP-ATR complex as well as ATR activity. ATRs potential UV damaged DNA binding region are also contained within the HEAT repeats (Kidiyoor et al., 2016). FAT domain is composed of Helix-turn Helix repeats. They wrap around the kinase domain providing structural integrity and regulating binding partners. The PIKK Regulatory domain (PRD domain) of ATR is a 30 amino acids long unique sequence at the end of FAT domain regulating ATR activity by regulating its interaction with TopBP1. The kinase domain of ATR is embedded in the shell of FAT domain. ATM and ATR have phosphorylation site specificity towards Serine or Threonine residues, which are followed by glutamine (SQ/TQ) (Kim et al., 1999). The most c-terminal FAT (FATC) domain of ATR constitutes 33 mostly hydrophobic aromatic amino acids. FATC domain is dispensable for PIKK kinase activity. FATC domain is functionally identical amongst PIKK members, however replacing the FATC domain of ATR with that of ATM deactivates ATR suggesting that FATC domain of ATR is unique (Mordes et al., 2008). FATC domain of mec1 mediates its kinase activity, nuclear localization and stability of the protein (DaSilva et al., 2013). Additionally, ATR FATC domain can bind to membrane mimetics (Sommer et al., 2013).

Figure 8 – Structural domains of ATR (taken from Kidiyoor et al.,2016)
Distribution of various domains across the amino acid sequence of ATR.

3.3. Activation at the site of DNA damage:

In eukaryotes, ATR is an essential kinase. Its most characterized role is in maintaining genome integrity during DNA replication. ATR maintains genome integrity by ensuring replication fork stability, recruiting appropriate repair machinery at the site of replication stress and finally by coordinating cell cycle progression with DDR via checkpoint activities (Cimprich and Cortez, 2008). ATR is involved in repairing of ssDNA lesions, commonly generated during DNA replication stress such as oncogene induced replication artifacts and stalled replication forks. Many genotoxins includng Hydroxy Urea (HU), UV rays, DNApolymerase inhibitors and topoisomerase poisons also lead to formation of long stretches of ssDNA. ATR heterodimer formation with its obligatory partner ATRIP is essential for ATR activity. Genomic assaults generate long stretches of single stranded DNA (ssDNA) that immediately gets coated with ssDNA binding protein complex RPA. This RPA coated ssDNA serves as a substrate for activation of ATR. ATR-ATRIP complex is recruited at the damage site in a Rad9-Rad1-Hus1 (9-1-1) complex dependent manner. TopBP1 interacts with ATR at the PRD domain and activates ATR. ATR also undergoes auto phosphorylation at Thr1989, serving as a feedback loop for signal amplification. ATR can also be activated at the damage site independently of TopBP1 by Ewing tumor-associated antigen 1 (ETAA1), which is also recruited to damage site through direct interactions with RPA (Haahr et al., 2016). ATR also undergoes auto phosphorylation at Thr1989, serving as a feedback loop for signal amplification (Liu et al., 2011, Nam et al., 2011). Once activated ATR phosphorylates a battery of repair and response proteins including the checkpoint kinase 1(CHK1) (Figure 9). Recent reports suggest that posttranslational modifications (PTM) of RPA (ubiquitination of RPA) (Marechal et al., 2014)and ATRIP (SUMOylation of ATRIP) (Wu and Zou, 2016)can also influence ATR activity.

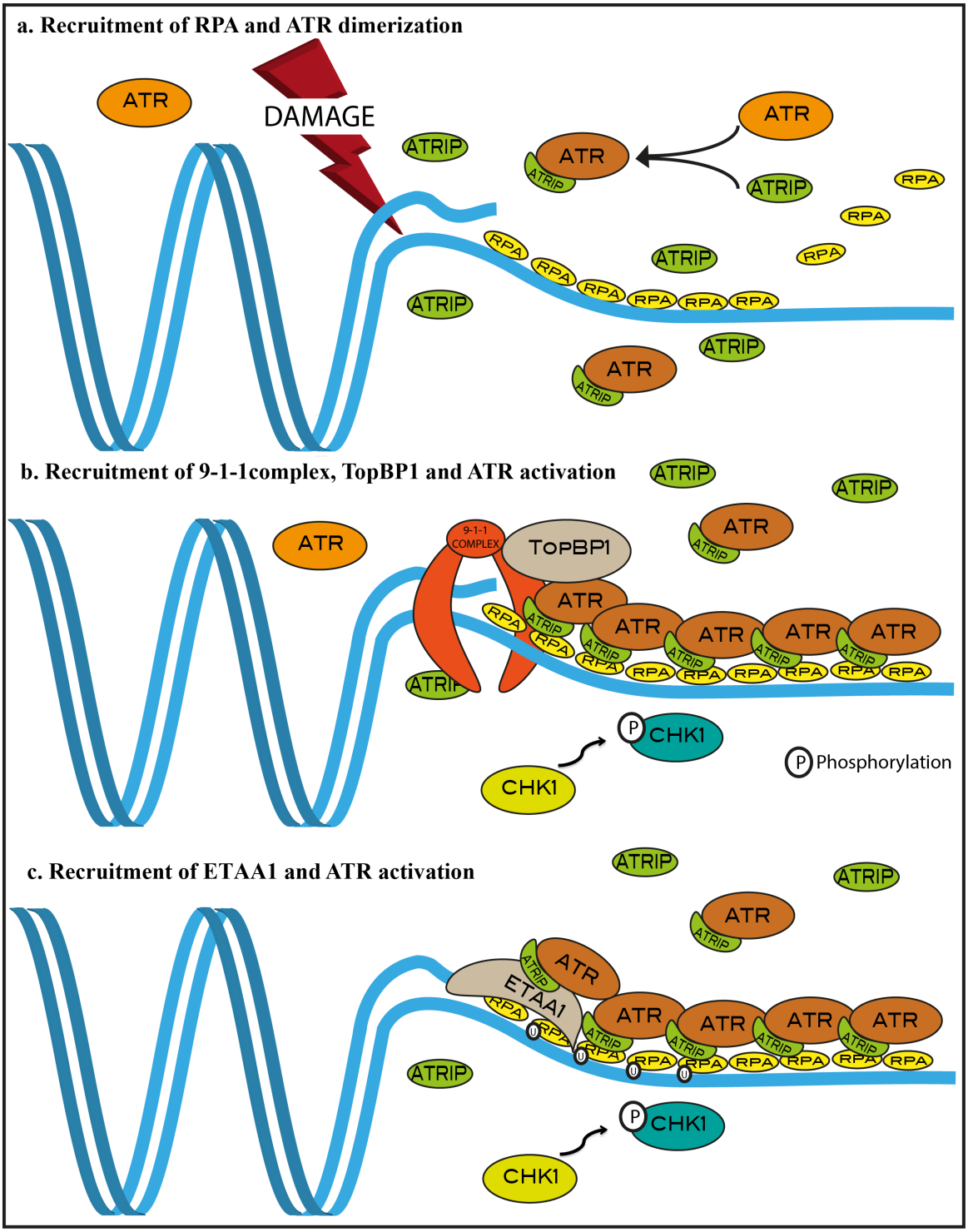

Figure 9 – Activation of ATR at the site of DNA damage
(Modified from Kidiyoor et al.,2016)
(a) ATR is recruited with its binding partner ATRIP on the RPA –ssDNA complex at the site of damage. Once recruited it can be activated by TopBP1 (b) or by ETAA1 (c)

3.4. DNA damage independent activation of ATR

a. Nuclear envelope

At the NE, ATR functions as a stress sensor, responding to changes in phospholipid composition, lamin architecture, NE rupture, membrane stress and NE deformations (Kidiyoor et al., 2016). Our lab and others had shown that ATR could sense mechanical stress imposed by external forces or by the condensing chromatin at the NE (Kumar et al., 2014) (Bozler et al., 2015). In response to such stress, ATR relocalizes to the NE and locally phosphorylates CHK1 kinase and potentially other proteins required to resolve stress (Kumar et al., 2014) (Figure 10). Similarly, *S. cerevisiae,* we demonstrated that Mec1 resolves fork collision with transcription machinery by untethering the RNA from the nuclear pore and relaxing the DNA (Bermejo et al., 2011).

Nuclear membrane contains a high proportion of saturated Phosphatidylcholine (PC) compared to polyunsaturated PCs. ATR monitors this composition and inhibitors that alter this ratio by reducing levels of saturated PCs and increasing polyunsaturated PCs, results in altered membrane fluidity and ATR activation. ATR consequently phosphorylates p-53 and arrests cell cycle in G1 phase (Zhang et al., 2007b). Transfecting cells with HIV-1 Viral protein R (VPR) localizes to the NE and induces NE disruption leading to ATR activation and subsequent CHK1 phosphorylation and cell cycle arrest (Figure 10)(Roshal et al., 2003, de Noronha et al., 2001, Jacquot et al., 2007). Phosphorylated ATR (S428) localizes at the NE in a lamin dependent manner (Chandris et al., 2010).

b. Nucleoli

ATR is detected in the nucleoli (Andersen et al., 2005), and this localization is amplified in presence of nucleolar stress (Kidiyoor et al., 2016). ATR maintains nucleolar homeostasis responding to stress stimuli that damage morphology or normal functioning of nucleoli, while ATM plays a central role in repairing nucleolar DNA

lesions (Larsen and Stucki, 2015). In senescent cells, ATR localizes at the nucleolus, and this subpopulation of nucleolar ATR is devoid of phosphorylation at Ser-428 (Chandris et al., 2010). When cells are challenged with hypo-osmotic stress, mechanical stress or thermal shock (hypothermia), ATR rapidly relocates into the nucleolus (Figure 10) phosphorylates downstream targets such as Chk1, p53 (S15) and consequently inducing cell cycle arrest (Kumar et al., 2014, Roobol et al., 2011).

Tumor suppressor protein ARF ($p14^{ARF}$) induction also results in nucleolar relocalization of ATR along with BRCA1, followed by phosphorylation of p53(S15) and cell cycle arrest. ARF also activates the ATR/CHK1 pathway, which then deactivates RelA, a component of NF-kB, by phosphorylation (Rocha et al., 2005). In cells lacking the MAPK members ERK1 or ERK2, upon HU treatment induced ATR re-localizion to the nucleolus instead of getting recruited at the ssDNA-RPA foci (Wei et al., 2011). Moreover, ATR can also assist other proteins such as Rad9B (a Rad9A paralog) to relocate on to the nucleoli upon UV-induced nucleolar disruption (Perez-Castro and Freire, 2012). Ectopic expression of TopBP1 induces nucleolar stress and causes nucleoli segregation through a process dependent on nucleolar ATR. The authors also demonstrate that the nuclolar hyperactive ATR/TopBP1 combination also inhibits rRNA synthesis, indicating the involvement of ATR in rRNA metabolism (Kumagai et al., 2006).

c. Centrosomes

The relation between ATR and centrosomes appear to bidirectional, ATR and centrosomes can influence each other's function significantly, impacting at the organismal level. ATR localizes to centrosomes during mitosis and cellular stress (unpublished data). During mitosis, ATR is recruited at the centrosomes in its phosphorylated form (Ser-428) along with other members of DDR pathway ATRIP, CHK1, p53 and BRCA1 (Zhang et al., 2007a, Chandris et al., 2010). Furthermore, NBS1/ATR/BRCA1 pathway is necessary for mono-ubiquitination of γ-Tubulin,

regulating tubulin-nucleation process and for regulating centrosome amplification (Shimada et al., 2009, Zhang et al., 2007a).

ATR Seckel patient cells have supernumerary centrosomes and defective mitosis (Griffith et al., 2008). Overexpression of ATR in myoblasts inhibits differentiation of myoblasts into muscles by inhibiting MyoD, this also induces abnormal centrosomal amplifications, aneuploidy and defective cell cycle arrest (Smith et al., 1998). This altered number of centrosomes (also the case for many cancers) in absence of ATR results in higher number of multipolar cell divisions, aneuploidy and mitotic catastrophe.

Seckel syndrome is also caused by mutations affecting the gene encoding the centrosomal protein Pericentrin (PCNT), which is involved in the ATR-dependent signaling pathway (Tibelius et al., 2009). Surprisingly, PCNT-Seckel patients also show defective ATR signaling pathway (Griffith et al., 2008, Rauch et al., 2008). Other centrosomal gene mutations including CEP152, CPAP, MCPH1 also cause microcephaly and dwarfism. Most of them, if not all, are involved in ATR signaling and patient cells have defective ATR signaling (Klingseisen and Jackson, 2011).

ATR also regulates centriole and cilia formation and functioning. Centrioles are basal bodies for cilia and flagella (Nigg and Raff, 2009, Conduit et al., 2015). A report showed that ATR localizes to the cilia of Photo Receptor (PR) cells of mice retina and it is essential for cilia maintenance. Heterozygous ATR seckel mice had no ATR in cilia of their PR cells, exhibited significant shortening of cilia and severe degeneration (Valdes-Sanchez et al., 2013). Similar study on Seckel patient-derived cells also reported slightly shorter cilia with drastic impairment in cilia-dependent signaling, and functions in absence of ATR (Stiff et al., 2016).

d. Actin cytoskeleton

During mechanical stress induced NE deformations and during mitosis ATR localizes to perinuclear actin fibers (Kumar et al., 2014). ATR Seckel fibroblasts exhibit elevated

levels of stress fibers and increased levels of phospho-Cofilin, a regulator of actin dynamics (Tivey et al., 2013). They also have active p38 stress response and as a result undergo premature senescence. A screen performed on *D.melanogaster,* identified Mei-41 as one of the cytoskeletal organization factors (Kiger et al., 2003). It is also important to note that, a large number of cytoskeletal proteins are phosphorylated by ATM/ATR upon genomic stress (Matsuoka et al., 2007). Recently a study revealed a crosstalk between ATR and Rho signaling. Alterations in the Rho pathway reduced ATR signaling and ATR defects reduced active RhoA and phosho-myosin light chain 2, leading to defective Rho signaling (Beveridge et al., 2014).

e. Mitochondria and other cytoplasmic functions

ATR associates with mitochondria through BH3 domain. In mitochondria ATR interacts with mitochondrial proteins, promotes anti-apoptotic pathways. This novel non-DDR function of ATR is independent of classical ATR activation components including RPA and ATRIP (Hilton et al., 2015). In *C.elegans* defects ATL-1 (ATR ortholog) results in reduction of mitochondrial DNA copy number, but activation of mild oxidative stress altered lifespan of the organism (Mori et al., 2008, Suetomi et al., 2013).

In brain tissues, ATR was shown to be more cytoplasmic, interacting with ATM and phosphorylating the synaptic vesicle protein VAMP2, suggesting a role in neuronal synapses(Li et al., 2009). ATR Seckel fibroblasts exhibit hyper phosphorylation of endocytosis protein Caveolin-1 (Tivey et al., 2013). Another study reported a novel role of ATR in regulating leptin-dependent STAT3 signaling, suggesting a potential involvement in maintenance of cellular energy balance (Ericson et al., 2015). ATR was also reported to be regulating the translation initiation factor eIF-3 complex in presence of replication stress by phosphorylating UPF1 (Choe et al., 2014).

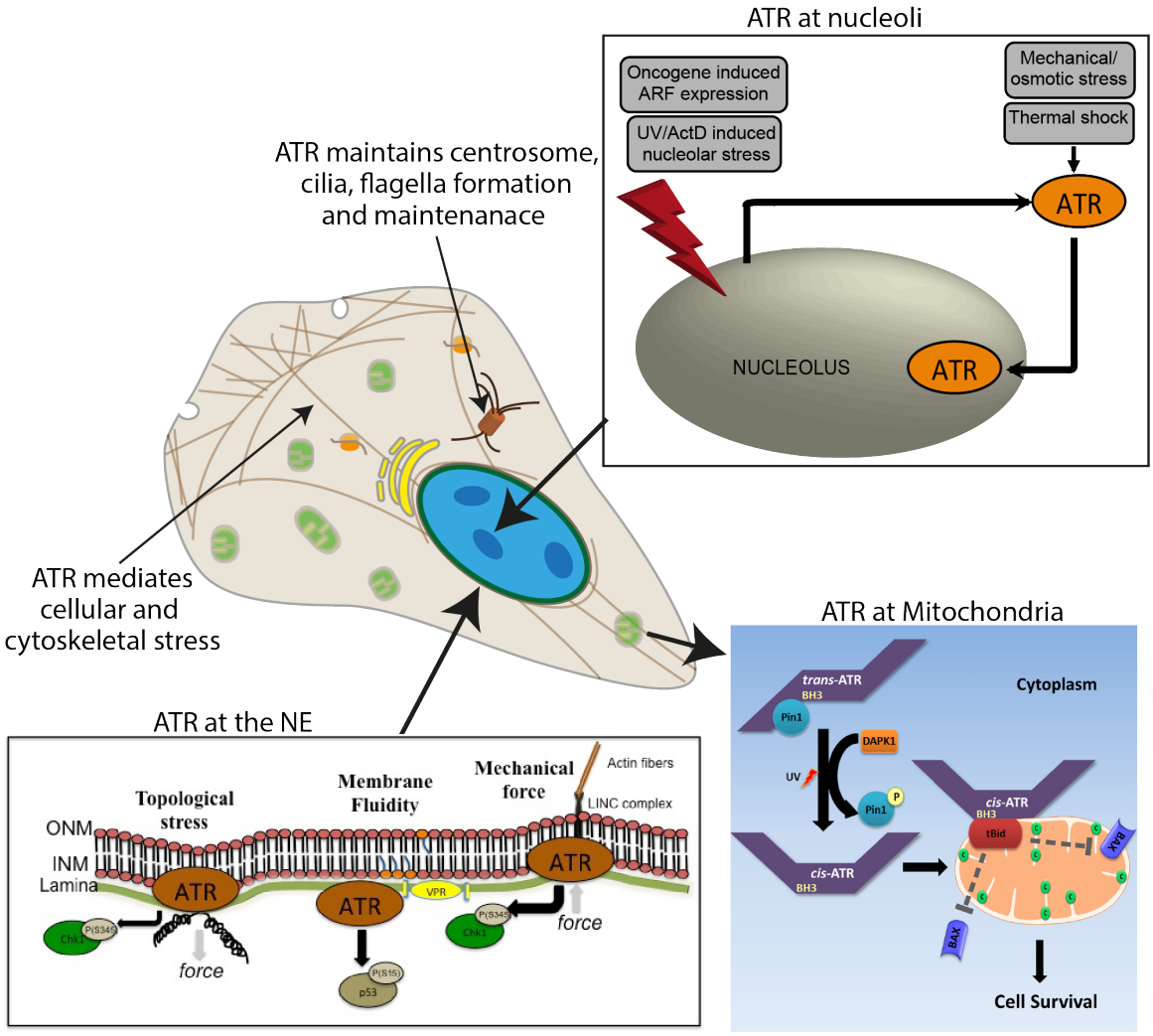

Figure 10 – Non-canonical activation of ATR, independent of DNA damage
(Modified from Kidiyoor et al.,2016 and Hilton et al.,2015)
Summary of cellular activators of ATR. Activation of ATR at the NE, nucleoli and mitochondria, and its functions at centrosomes and actin fibers.

3.5. Pathologies associated with ATR

ATR is essential for cell survival; ATR-deficiency is embryonic lethal and embryos exhibit shattered chromosomes (Brown and Baltimore, 2000, de Klein et al., 2000). A rare autosomal recessive disorder caused by hypomorphic mutation of ATR called the Seckel syndrome (OMIM 210600) (O'Driscoll et al., 2003) is the only known genetic disorder associated with ATR. Seckel syndrome is a developmental disorder characterized by mild to severe mental retardation, growth retardation, dwarfism, microcephaly and other craniofacial abnormalities (Shanske et al., 1997, O'Driscoll et al.,

2003). Seckel patient cells exhibit compromised nuclear architecture, defective DDR pathways, replication arrests and senescence (Gordon et al., 2014).

Two mice models were developed to study the role of ATR during development and homeostasis; humanized seckel mice and inducible ATR mosaic knockout mice. Seckel mice have ATR levels equivalent of what is observed in human Seckel patients. Seckel mice exhibit chromosomal instability, severe developmental abnormalities, dwarfism, progeria like accelerated aging, craniofacial disorders and pancytopenia. Premature deaths in Seckel mice were associated with a generalized organ failure caused by age-related dysfunction. Though ATR is a tumor suppressor, Seckel mice did not develop any tumors, even in the absence of tumor suppressor protein p53 (Murga et al., 2009). In presence of damage, ATR maintains dNTP levels by regulating Ribonucleoside-diphosphate reductase subunit M2 (RRM2) protein expression. RRM2 regulates synthesis of DNA precursors. Crossing Seckel mouse with the mice expressing supra-physiological levels of RRM2 ameliorated several phenotypes of Seckel mice including the overall size and lifespan of the mice suggesting the importance of ATR in regulation of dNTP biosynthesis and DDR (Lopez-Contreras et al., 2015).

Deleting ATR in 8 to 12 week old inducible ATR mosaic knockout mice lead to hair-loss and graying, kyphosis, age related defects including osteoporosis, fibrosis of the heart and kidney, reduced thymopoiesis, and spermatogenesis. In ATR knockout mice stem and progenitor cell draining lead to reduced regenerative capacity consequently ameliorating tissue renewal and homeostatic capacity, which in turn lead to the premature onset of age-related phenotypes. This study also demonstrated the role of ATR in maintenance of tissue structures and showed that the age-related phenotypes of ATR knockout mice are not influenced by or the direct consequences of developmental abnormalities (Ruzankina et al., 2007).

4. ATR regulates nuclear envelope integrity.

Previous work from our laboratory shows that ATR responds rapidly to NE deformation caused by mechanical forces (Kumar et al., 2014, Bermejo et al., 2011). Chromatin condensation before NE breakdown and DNA replication during S phase, are the two physiological situations where DNA topological constraints exert mechanical stress at the NE generating invaginations (Bozler et al., 2015) (Figure 11). Local nuclear membrane stress recruits ATR-ATRIP to the NE. The ATR response then coordinates chromosome replication and condensation with the nuclear envelope by modulating the chromatin and NE association.

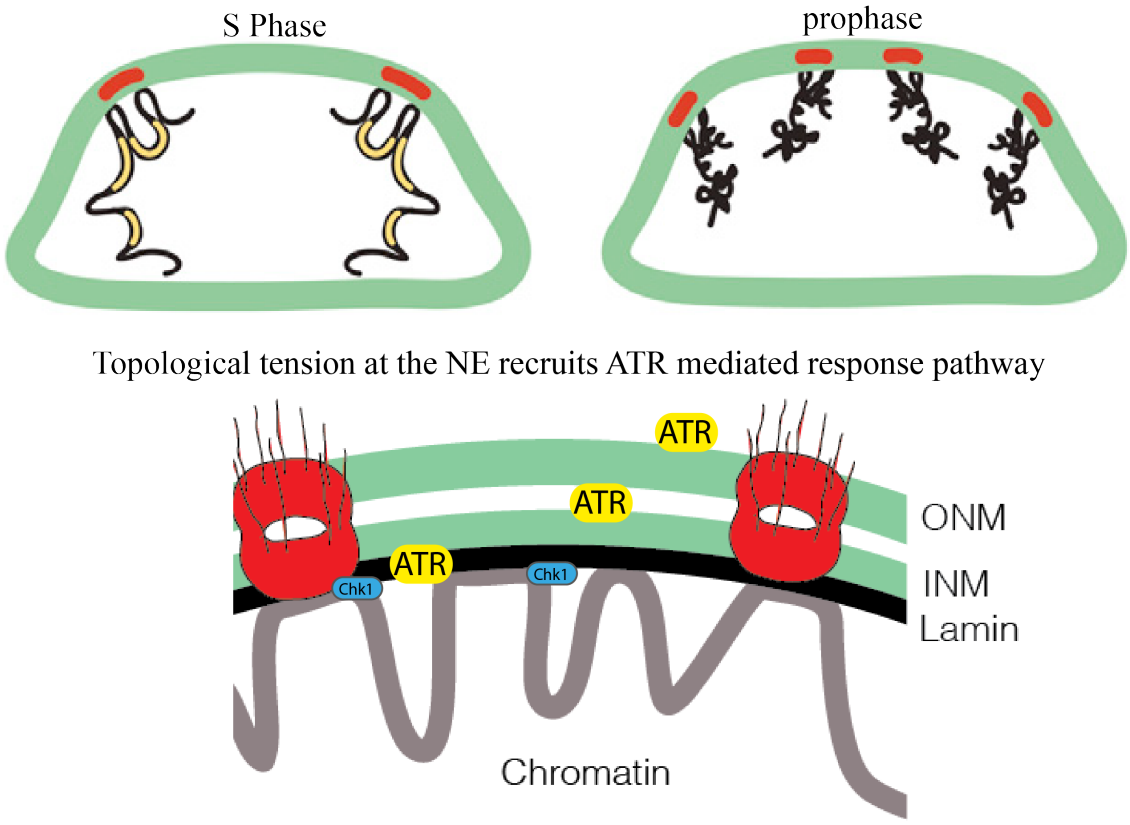

Figure 11 – Activation of ATR at the Nuclear envelope
(Modified from Kumar et al.,2014, Cell)
Topological constrains during replication and condensation excert mechanical forces to the NE, ATR senses this, relocates to nuclear rnveope and phosphorylates Chk1 at the NE

Consistent with this, ATR was enriched at NE invaginations, structures that are generated by the internal mechanical forces. This recruitment of ATR to the NE in response to membrane stress is independent of RPA-ssDNA complex and does not require its kinase activity. ATR inhibited cells as well as Seckel patient fibroblasts exhibited a delay in the processes leading to chromatin condensation and nuclear envelope break-down (NEBD) and resulted in several mitotic defects including nuclear fragmentation, prolonged association of chromatin to the NE and increased micronuclei formation. Further, Kumar et al., also showed that hyperosmotic conditions that shrink the nucleus and induce raffles in the NE and compression load induced mechanical stress conditions also relocate ATR into the NE consequently phosphorylating CHK1 locally (Kumar et al., 2014) in a reversible way. This osmotic challenge is also known to induce chromatin compaction (Irianto et al., 2013), similar to prophase.

These studies indicate that ATR is needed to protect the perinuclear chromatin from mechanical assaults on the nucleus. Given that NE integrity is prerequisite for genome integrity and mechanical insults on the NE could drive genomic instability, we predicted that the regulators of genomic integrity would also respond to such mechanical stimulus to prevent the potential threat to the genome. Since, ATR can sense the mechanical force induced nuclear alterations and coordinate nuclear dynamics accordingly, we hypothesized ATR to be involved in protecting nucleus against mechanical insults. Considering NE is the prime target of such mechanical insults; cells can exploit it as a platform for sensing such mechanical stress and initiate an appropriate response. Therefore, in the current study we assessed the contribution of ATR in maintaining nuclear integrity and homeostasis under several mechanical alterations Our goal is to understand the role of ATR in maintenance of chromosome architecture, nuclear shape and its impact on cell motility, cell migration, and cancer metastasis.

Materials and methods

Plasmids and siRNAs

ATR shRNA and control (pLKO1) plasmids were from Dr. Oscar Capetillo (CNIO, Spain) (Toledo et al., 2011); the GFP-ATR plasmid was from Dr. Randal Tibbetts (Tibbetts et al., 2000). Control and Chk1 siRNA (s503) were ordered from Life technologies Silencer Select Pre-Designed siRNA. Nesprin tension sensor (pcDNA nesprin TS; plasmid #68127) and nesprin headless control (pcDNA nesprin HL; plasmid #68128) (Arsenovic et al., 2016) were purchased from Addgene.

Reagents

Antibody	**Source**	**Cat. number**
1. ATR	Cell signal	2790
2. TopBP1	Abcam	ab2402
3. Nup133	SantaCruz	sc-27392
4. Tubulin	Sigma	T5168
5. Lamin B1	Abcam	ab16048
6. Lamin A/C	Santa cruz	sc-7292
7. Total chk1	Santa cruz	sc-7898
8. Nesprin 2	Thermoscientific	MA5-18075
9. Histone H3 (tri-methyl K9)	Abcam	ab8898
10. Total Histone H3	Abcam	ab1791

Secondary antibodies Alexa488, AlexaCy3, AlexaCy5 (Life Technologies) were obtained from IFOM imaging facility.

Other reagents	**Source**	**Cat.Number**
1.DNAse I	NEB	M0303S

2. ATR inhibitors

ETP46464	Calbiochem	500508
AZ-20	Tocris	5198
3. Benzonase	Sigma	E1014
4.Anti-GFP mAb-Magnetic beads	MBL,japan	D153-11
5. Mem-PER plus Kit	Thermofisher	89842
6. Duolink® PLA kit	Sigma	DUO92102
7. BCA Protein Assay	Thermofisher	23227
8. RTV-615 (PDMS)	Momentive Performance materials	RTV615

Cell lines

HeLa and U2OS cells were obtained from IFOM cell culture facility. U2OS cells stably expressing 53BP1-GFP and GFP-ATR were kind gift from Jiri Bartek. HeLa stable cell lines with GFP-H2B and m-cherry-H2B were from IFOM imaging facility. The stable U2OS line expressing the FUCCI reporter was from Libor Macůrek (Macurek et al., 2013). hTert -RPE-1 expressing 53BP1 were from M.Piel (Institute curie, Paris). Immortalized mouse fibroblasts of wild-type and Seckel were kind gift of Oscar Capetillo. Human primary fibroblasts derived from Seckel patient (GM18366) were purchased from Coriell biorepository and control fibroblast IMR90 from IFOM cell culture facility. HCT116 and $ATR^{flox/-}$ cells were from The American Type Culture Collection (ATCC). Primary fibroblasts from progeria (HGADFN167) and control (HGFDFN168) were obtained from the Progeria Research Foundation Cell and Tissue Bank.

Cell culture

HeLa, HEK 293T and U2OS cells were maintained in DMEM (Dulbecco's

Modified Eagle's medium) with GlutaMAX and 25mM HEPES (Life Technologies) supplemented with 10% (vol/vol) fetal bovine serum (FBS) South America (Biowest), and penicillin-streptomycin (Microtech). Human primary fibroblasts derived Seckel patient were maintained in DMEM supplemented with 15% FBS North America (Sigma-Aldrich). And primary fibroblasts from Progeria and controls, and IMR90 were grown in 10% FBS North America. Primary mouse embryonic fibroblasts were cultured in Dulbecco's Modified Eagle's Medium (DMEM, Lonza BE12-614F) supplemented with 15% FCS and 1% L-Glutamine (Microtech X0550). All cells were grown in a humidified incubator atmosphere at 37 degree and 5% CO_2. During trypsinization, cells were washed once with sterile PBS, incubated with trypsin-EDTA (1ml for 10cm plates) at 37˚C until detachment was visible (maximum 5 minutes). Cells were well re-suspended in complete medium, centrifuged at 1200rpm, for 3 minutes, re-suspended in complete and split to new dishes.

Lipofectamine transfection

(protocol from IFOM cell biology unit)

1. The day before transfection, cells are plated to achieve about 70% confluence on the day of transfection.

2. For one well of 6-well, dilute 1-2 µg DNA in 250 µl of serum-free medium; leave 5' at room temperature.

3. Dilute 4 µl of L2000 in 250 µl of serum-free medium; leave 5' at room temperature

4. Combine the diluted DNA with diluted L2000, mix gently and incubate for 20' at room temperature. Transfection volume: 1,5 ml complete growth medium.

5. Add DNA/L2000 complex mixture to the cells and mix gently by rocking the plate back and forth; incubate for 24 hours in a CO2 incubator at 37°C.

6. At the end of incubation time change medium and return the cells

Lipo2000: lipofectamine 2000 Life Technologies 11668-019

Opti-MEM: OPTIMEM-I w/Glutamax Life Technologies 51985-042

Lentiviral transduction

(protocol from IFOM cell biology unit)

Day 1:

1. Plate HEK293T cells in a 10cm plate at 5x 106 cells/plate

HEK239T calcium phosphate transfection:

ENV (VSV-G)	2.8mg
pMDL (gag&pol)	5mg
REV	2.5mg
Lentiviral vector	10mg
CaCl2 2M	62.4mg

add 0.1x TE (pH 8) sterile to make volume up to 500ml

2. Mix and add bubbling into 500µL of 2xHBS. Incubate for 5 minutes at RT.

3. Add drop wise to the medium (1mL/plate) and leave overnight at 37°C.

Day 2:

4. Replace 293T transfection medium with 5.5mL of fresh medium.

5. Plate target cells so that they will be 50% confluent the day of infection.

Day 3:

6. Filter the viral supernatant with 0.45µm filters and add polybrene (8µg/mL).

7. Infect target cells with 5mL (10cm plate) of viral supernatant or 2 ml in one 6-well.

8. Incubate for 24 hours and then replace the viral supernatant with normal medium with selection.

Day 5:

9. From successfully infected cells after selection for 2 days, the efficiency of knockdown

was assayed by western blot. For the whole duration of the experiments the cells were cultured under puromycin selection and were used fro experiments for a maximum duration of 10 days.

siRNA transfection protocol

1. At day of transfection change medium and leave only 3,5ml/6cm dish DMEM without antibiotics

2. Prepare 20µM (=20 000 nM) siRNA stock: add 250 µl of sterile Ambion water to 5nmol powder stock

3. Mix 250 µl of Optimem medium with 5 µl siRNA from 20µM stock

4. Mix 250 µl of Optimem medium with plus 5 µl RNAiMax

5. Mix well and combine both mixes and incubate for 15 min at RT

6. Add mix into 6 cm dish containing 3.5 ml of DMEM medium

7. Split cells 36 h after transfection and proceed with experiment 72h after transfection

FACS analysis

1. Harvest cells using trypsinization and wash cells once in 1ml PBS

2. Resuspend pellet in 250µl PBS and fix cells by adding 750µl pure ethanol drop wise while vortexing. Leave cells in fixative at least 30 min on ice.

3. Wash once in 1ml PBS 1% BSA

4. Resuspend pellet in 1ml PI (50µg/ml) + RNase and incubate for 3hr at room temperature or overnight at 4 degree, and store stained cells at 4 degree until analysis

Immunofluorescence of fixed samples

For the IF, cells were plated on coverslips, day before. On the day of the experiment cells were washed with 1x PBS and then fixed with 4% formaldehyde (15 minutes at RT). After fixation cells were washed three times with 1X PBS and permeabilized with 0.2% TritonX-100 PBS for 15 minutes at RT (0.5% for 5 mins for

ATR ab). Blocking was done after permeabilization incubating the cells with 1% BSA 0.1% TX-100 PBS (referred as blocking solution from here on) for one hour. Primary antibodies were diluted in blocking solution, staining was done by inverting the coverslip on Ab solution on a parafilm and incubating for 1 hour at RT. Following this coverslips were given three washes with 0.1% TX-100 PBS (10 minutes each). Species-specific secondary antibodies diluted in blocking solution were added to samples similarly as primary Ab and incubated in dark for 1 hour, at RT, followed by three washes with 0.1% TX-100 PBS. Samples were mounted on coverslips with mounting medium containing DAPI (VectaShield). Cells were then visualized and images captured using Leica TCS SP2 confocal scanning microscope, equipped with a 633/1.4 NA objective. Images were then processed using ImageJ and smoothed to reduce the background noise.

Live cell imaging

The live cell imaging acquisitions were performed in microscopes equipped with incubators with maintained 37°C and 5% CO_2 throughout the duration of experiment. Time–lapse live imaging were performed using these microscopes depending on the requirements and availability: UltraVIEW VoX spinning-disk confocal system (PerkinElmer) equipped with an EclipseTi inverted microscope (Nikon) provided with a Nikon Perfect Focus System and a Hamamatsu CCD camera (C9100-50) and driven by Volocity software (Improvision; Perkin Elmer) and using a DeltaVision Elite imaging system (Applied Precision) driven by softWoRx software and equipped with a CoolSNAP HQ2 CCD camera (Photometrics). Single cell migration and wound healing live imaging were captured with a bright-field NIKON Eclipse TE2000-E microscope equipped with a Prior Stage and CascadeII-512 camera (Photometrics) using 10X or 20X dry objective.

Buffers

1. Lysis buffer

Tris-HCl	pH 8.0 50mM
$MgCl_2$	1mM
NaCl	200mM
$CaCl_2$	1mM
Glycerol	10%
NP-40	1%

Stock solutions were stored at 4^0C upto a month. Protease inhibitors 1:100 (complete inhibitors, Roche) and phosphatase inhibitors 1:200 (phosphatase inhibitor cocktail 2, Sigma) are added at the time of experiment. Benzonase (50U) added only if the protein of interest was DNA bound.

2. Laemmli buffer (1X)

Tris-HCl pH 6.8	50mM
SDS	2%
Glycerol	10%
β−mercaptoethanol	0.1%
Bromophenol blue	0.0005%

Western blotting

Proteins were separated by SDS-page electrophoresis using polyacrylamide-precast gels (Bio-Rad) in a SDS-PAGE running buffer. Gradient precast gels and percentage of acrylamide were chosen according to the experiment and protein size. The separated proteins were transferred on a nitrocellulose membrane of 0.2 μm (small molecular weight proteins or 0.45 μm pore sizes (higher molecular weight). The transfer was carried for 1.5 hour at 90V or 30V overnight in cold room using wet/tank blotting systems (Bio-Rad) and transfer buffer (Glycin 1%, Tris-HCl 0.02 M) with 20% methanol. After the transfer nitrocellulose membrane was coloured with Ponceau staining solution

to check the quality of the transfer. The Ponceau staining was removed washing the membrane with washing buffer PBST (0.2% Tween 20 PBS). Blocking was performed for 1 hour with 5% milk in PBST. After the blocking, the primary antibody diluted in 5% milk PBST was added for 2 hours at RT or overnight at 4 degree, then washed with PBST for three times (10 minutes each) to remove the excess of antibody. The horseradish peroxidase-conjugated secondary antibody diluted in 5% milk PBST was added for 1 hour followed by 3X PBST washings of 10 minutes. Blots were developed using SuperSignal West Dura Extended Duration Substrate (Thermo Scientific) or SuperSignal West Femto Chemiluminescent Substrate (Thermo Scientific) and signal acquisition performed using ChemiDoc (Bio-Rad, Molecular Imager ChemiDoc XRS+).

Electron microscopy (EM) sample preparation (protocols from A. Mironov and G. Beznusenko)

The EM analysis were performed by the IFOM EM facility (G. Beznusenko and A. Mironov) (Kweon et al., 2004, Beznoussenko et al., 2007). Grids, osmium tetraoxide, paraformaldehyde and glutaraldehyde were purchased from Electron Microscopy Sciences (EMS, USA). Sodium cacodylate, saponin, NH_4Cl, lead citrate and Epoxy resin kit were purchased from Fluka (SIGMA). Potassium ferrocyanide, ethanol and acetone were purchased from Carlo Erba (Italy), and Mat Tek dishes (P35G-1.5-14-C-GRID) from MatTek Corp (USA). Fab'fragments conjugated with nanogold (1.4 nm gold particles) and Goldenhance^{TM} –EM were from Nanoprobes (USA).

1. For Gold-labeling:

Pre-embedding techniques: The name of these techniques derives from the fact that labeling is performed before sample embedding. Briefly, the sample is chemically fixed and the antigen is labelled by means of a specific primary antibody that is recognized by a

secondary antibody conjugated with ultra-small gold particles (1.4 nm gold conjugates that penetrate cells and tissues much more readily and have been used successfully to immuno-label intracellular structures).

Gold enhancement: The cells grown on Matteks were fixed with a mixture of 4% paraformaldehyde and 0.05% glutaraldehyde in 0.15 M Hepes for 5 min at RT and then placed into 4% paraformaldehyde in 0.15 M Hepes for 30 min RT. Afterwards, the cells were washed 6 times in PBS at RT and incubated with blocking solution for 30 min at RT. Finally, the cells were incubated with primary antibody diluted in blocking solution. On the following day, the cells were washed 6 times with PBS at RT and incubated with goat anti-rabbit or anti-mouse Fab' fragments coupled to 1.4 nm gold particles (diluted in blocking solution 1:100) for 2 h and finally washed 6 times with PBS at RT. Meanwhile, the activated Goldenhance^{TM}-EM was prepared according to the manufacturer's instructions and 100 µl were added into each Mattek. The reaction was monitored by a conventional light microscope and was stopped after 5-10 min when the cells had turned "dark enough" by washing several times with PBS. Osmification followed: the cells were incubated for 1 h at RT with a 1:1 mixture of 2% osmium tetraoxide in distilled water and 3% potassium ferrocyanide in 0.2 M sodium cacodylate pH 6.9 and then rinsed 6 times with PBS and then with distilled water. The samples were then dehydrated: 3x 10 min in 50% ethanol; 3x 10 min in 70% ethanol; 3x 10 min in 90% ethanol; 3x 10 min in 100% ethanol. The samples were subsequently incubated for 2 h in 1:1 mixture of 100% ethanol and Epoxy resin (Epon) at RT, the mixture was then removed with a pipette and finally samples were embedded for 2 h in Epoxy resin at RT. The resin was polymerized for at least 10 h at 60 °C in an oven.

Tomography: Thick (200 nm) Epon sections were cut with a Leica EM UC7 ultramicrotome (Leica, Germany) and ribbons of 6-12 serial sections were transferred onto formvar-coated copper slot grids. Colloidal gold particles (10 nm) were deposited on both surfaces of the sections and used as fiducial markers during the subsequent

alignment of the series of tilted images. Specimens were analysed with a Tecnai 20 High Voltage EM (FEI, Thermo Fisher Scientific, The Netherlands) operating at 200 kV. Once a cell was selected, the sample was tilted from +65° to –65° at 1° intervals, with magnification from 7,800X to 25,000X. The specimen was irradiated for 15 min with the electron beam before initiating the acquisition of the tilt series in order to limit anisotropic specimen thinning during data collection. Focus was regulated for each acquired image. The computer program IMOD 4.9 was then used to align the tilt series and to calculate the tomographic reconstruction from the aligned tilt series. At least 45 tomograms were analysed for each experimental condition. Values in the text are means ± S.D. Surfaces of Golgi membranes were rendered using the IMOD software.

2. Tomography:

Two-step CLEM based on the analysis of tomographic reconstructions acquired under low magnification with consecutive reacquisition of EM tomo box under high (60000x) magnification and its re-examination was used exactly as described (Beznoussenko et al., 2016). Briefly, an ultratome (LeicaEM UC7; Leica Microsystems, Vienna) was used to cut 60 nm serial thin sections and 200 nm serial semi-thick sections. Sections were collected onto 1 % Formvar films adhered to slot grids. Both sides of the grids were labeled with fiduciary 10 nm colloidal gold (British Biocell International). Tilt series were collected from the samples from ±65° with 1° increments at 200 kV in Tecnai 20 electron microscopes (FEI, Eindhoven. the Netherlands). Tilt series were recorded at a magnification of 20,000X or 60,000X using software supplied with the instrument. The nominal resolution in our tomograms was 4 nm, based upon section thickness, the number of tilts, tilt increments, and tilt angle range. The IMOD package and its newest viewer, 3DMOD 4.0.11, were used to construct individual tomograms and for the assignment of the outer leaflet of organelle membrane contours, and best-fit sphere models of the outer leaflet were used for vesicle measurements. Videos were made in 3DMOD and assembled

in QuickTime Pro 7.5 (Apple), and the saving of videos as an HD 720p reduced file size in QuickTime. CLEM was performed exactly as described (Beznoussenko et al., 2014).

3. FIBSEM:

FIBSEM analysis was performed on the same samples using a FEI Helios NanoLab 660 FEGSEM or G3 equipped with SEM Multi-Detector and ICD detector at accelerating voltage 2.0 kV. Access to both of which was kindly provided by FEI Co. For all high-resolution EFSEM images, a primary beam energy of 2.0 kV was used with a working distance of 1 mm, 3 ms dwell time and tube bias of 140 V. An Auriga 60 FIB-SEM (Zeiss) microscope with Atlas3D software (FIBICS) was additionally used to collect the 3D data of two cells. Acquisitions were performed according to instructions of manufacturers.

4. Image processing and analysis:

Image post-analysis were performed in ImageJ and Amira. All acquired images were aligned using the TrakEM2 plugin of FIJI. Images were segmented by thresholding with Amira (FEI). The number of ATR-tagged gold particles in different compartments of the cell was counted and percentages were calculated. The labeling density of ATR on different cellular structures was assessed and calculated as described in (Lucocq et al., 2004). For this we used the following criteria: Gold particles were considered to label the NE, ER or mitochondria when these particles were observed over lumens or membranes of these compartments; Gold particles were considered as a label of the PM when these particles were observed over the PM. Normality of variant distribution was assessed with Shapiro-Wilk tests. Cumulative probability distributions were compared using the Kolmogorov-Smirnov test. Estimation of the minimal set of samples was performed according to (Mironov and Mironov, 1998). Correlation between two variables was calculated using Pearson Product Moment Correlation.

5. Nuclear morphology analysis of cells in constriction

For analysis of cells undergoing migration in PDMS molds of micro-fabricated channels with constrictions, we mounted PDMS molds onto the MatTek dishes, fibronectin coated them and then loaded cells at the loading chambers and incubated for 24 hours. We scored cells migrating within the channels under the UltraVIEW VoX spinning-disc confocal unit (PerkinElmer), and indicated cells in which the nucleus is either just entering the constriction or the nucleus is completely in the constriction with the leading edge of the nucleus starting to exit the constriction. Next, we eliminated all the remaining cells from the loading wells and acquired images of cells suitable for the future CLEM analysis. 0.05% glutaraldehyde +4% formaldehyde in 0.1 M cacodylate buffer (pH 7.2) was added to the dish for 5 min. During this time, cells were examined again under a light microscope to confirm the nuclear position with respect to the constriction. Cells with unchanged morphology were then fixed with 2.5% glutaraldehyde + 4% formaldehyde in 0.2M cacodylate buffer (pH 7.2) for 10 days in order to make cell bodies resistant to the process of the mechanical detachment of mold from the MatTek. Then PDMS mold was detached from the MatTek dish and the cells attached to the dishes were processed for EM analysis as described above. After mold detachment, cells were additionally stained with 1% methylene blue in PBS for 3 min at RT and again examined under a light microscope in order to confirm the presence of selected cells on the MatTek glass.

Immuno-precipitation and Mass-spectrometry

Cells were grown in SILAC medium with dialyzed FBS and Heavy or Light isotope labeled amino acid (L-lysine and L-arginine) for 5 cell cycles. We tested the quality of incorporation to ensure high uptake. Then labeled U2OS GFP-ATR cells were cultured to 80-90% confluence (3 x 15 cm dish per condition).

Lysis buffer:

	Reagent	Final Concentration	Stock available in IFOM	Volume to make 50ml buffer
1	TRIS-HCl pH8.0	50mM	1M	2.5ml
2	$MgCl_2$	1mM	1M	50uL
3	NaCl	200mM	5M	2mL
4	$CaCl_2$	1mM	1M	50uL
5	Glycerol	10%	50%	10mL
6	NP-40	1%	10%	5mL

Add freshly according to the experiment being performed

1. Protease Inhibitor Roche Tablets (1 / 10 mL).

2. Phosphatase inhibitors – (1:200) Sigma cocktail 2

3. Benzonase – Only required for the fraction of the lysis buffer, which is used for cell lysis! (50 U / mL).

1. Wash plate 1x with PBS

2. Add 1 mL lysis buffer + benzonase (on ice)

3. Scrape off cells & store 1 h - 1.5 h on ice or on rotor in cold room

4. Bead preparation for pre-cleaning

Prepare 100 µL beads for removal of unspecific protein A binders from the lysate

wash beads 2 x with PBS (1 min, 4°C, 1000 rpm)

resuspend beads in 100µL lysis buffer & mix on rotor in cold room or on ice

5. Spin lysates (30 min, 4°C, max speed)

6. Transfer the supernatant and keep a small aliquot for protein concentration measurement (BCA)

7. Add 100 µL protein A/G agarose beads and rotate 1 h – 1.5 h in the cold room to remove unspecific protein A binders. Incubate for 1 hour on ice.

8. Spin (10 min, 4°C, max speed) and take the supernatant. Keep 50ul aliquot (as input sample).

9. Prepare anti-GFP magnetic beads, by washing them 3 times in PBST and once in lysis buffer.

10. Add 100ul of anti-GFP magnetic beads per condition.

11. Rotate O/N in the cold room

12. Wash beads 4 x with lysis buffer (5 min rotation in the cold room)

13. Remove supernatant completely and add 2 x Laemmli buffer (agarose beads: 1:1, dynabeads: 50 µL)

14. Boil 15 min (95° C) together with input and flow-through → IP

15. Analyse through western blotting the efficiency of the IP.

16. Run the samples on Precast Gel, stain it with Coomassie Blue and store in 1% glacial acidic acid solution until processed for mass-spec.

Proteomic analysis (protocol obtained from U. Restuccia)

IP elutes resolved on a 4-12% NuPAGE® pre-cast gel (Invitrogen) and stained by Coomassie colloidal blue were then cut into 8 or 10 slices each of which was reduced, alkylated and digested with trypsin as reported elsewhere (Restuccia et al., 2009). Peptides mixtures were desalted and concentrated on a home-made C18 desalting tip, and then peptides were injected in a nanoHPLC (EasyLC Proxeon, Denmark). Peptides separation occurred onto a 25 cm long column, reverse phase spraying fused silica capillary column (75 µm i.d.) home-made packed with 3µm ReproSil AQ C18 (Dr. Maisch GmbH, Germany). A gradient of eluents A (HPLC-grade water with 0.1% v/v formic acid) and B (ACN with 20% v/v water with 0.1% v/v formic acid) was used to achieve separation, from 7% to 60% of B in 30 minutes, at a constant flow rate of 250 nl/min. The LC system was connected to a QExactiveHF mass spectrometer (ThermoScientific, Bremen, Germany) equipped with a nano-electrospray ion source (Proxeon Biosystems, Odense, Denmark). Full scan mass spectra were acquired in the LTQ Orbitrap mass spectrometer with the resolution set to 60,000 (@200 m/z)

accumulating ions to a target value of 6,000,000. The acquisition mass range for each sample was from m/z 300 to 1650 Da and the analyses were made in duplicates. The fifteen most intense doubly and triply charged ions were automatically selected and fragmented in the ion trap after accumulation to a 'target value' of 15,000. Target ions already selected for the MS/MS were dynamically excluded for 20 s. Identification and quantification of peptides and proteins were performed with MaxQuant 1.5.2.8 against the human Uniprot complete proteome set, having identified a protein with at least 2 peptides (1 unique), 6 aminoacids of minimal length, FDR<1% and quantified with at least 2 ratio counts. Significant outliers scores were calculated using Perseus 1.5.2.6 (Cox and Mann, 2008) and those with a p-value <0.05 have been selected for further analysis. For label-free analysis, the procedure was the same, but immune-precipitated samples were kept separate and loaded separately, then digested and analysed by mass spectrometry. Proteins were identified using Mascot (v. 2.3.02) and quantification was done using Scaffold (v. 4.3.4). Exclusive unique peptide count was selected to evaluate changes in proteins abundance.

For analysis, we pooled one label-free and two SILAC experiments, selected candidates that were found as ATR-GFP interactors in at least two experiments and which were significantly enriched (8-fold) over GFP control in at least one SILAC experiment. We performed Gene ontology (GO) analysis using DAVID, to generate enriched terms for cellular compartments (GOTERM_CC) and biological processes (GOTERM_BP) (p value with Benjamini correction < 0.05). Revigo tool was utilized to simplify GO terms (resulting list size: 0.7, database: Homo sapiens, semantic similarity measure: SimRel) and R Studio for plotting of Revigo output (size = log size, color = log10 p value). Candidates where then manually curated to generate non-overlapping sub-categories of interest (for this study). A network was generated for each sub-category using STRING interaction analysis and the output was plotted using cytoscape.

Membrane Fractionation (Mem-Per Plus Kit)

1. Resuspend 5 × 106 cells in the growth media by scraping the cells off the surface of the plate with a cell scraper. Centrifuge harvested cell suspension at 300 × g for 5 minutes.

2. Wash cell pellet with 3ml of Cell Wash Solution and centrifuge at 300 × g, 5 minutes.

3. Carefully discard the supernatant and resuspend the pellet in 1.5mL of Cell Wash Solution and transfer to a 2mL centrifuge tube. Centrifuge at 300 × g for 5 minutes and discard supernatant.

4. Add 0.75mL of Permeabilization Buffer to the cell pellet (with or without Benzonase, 0.5ul). Vortex briefly to homogenize cell suspension and incubate 10 minutes at 4°C .

5. Centrifuge permeabilized cells for 15 minutes at 16,000 × g. Carefully remove the supernatant containing cytosolic proteins and transfer to a new tube.

6. Add 0.5mL of Solubilization Buffer to the pellet and resuspend by pipetting up and down. Incubate tubes at 4°C for 30 minutes with constant mixing.

7. Centrifuge tubes at 16,000 × g for 15 minutes at 4°C. Transfer supernatant containing solubilized membrane and membrane-associated proteins to a new tube, boil both cytoplasmic fraction and membrane fraction with Laemmli buffer.

RT-PCR

Faculty of Cogentech sequencing facility performed RT-PCR experiments in IFOM campus.

Proximity Ligation Assay

Experiment was performed according to the protocol suggested by the manufacturer. Cells were washed with 1x PBS and then fixed with 4% formaldehyde (15 minutes at RT). After fixation cells were washed three times with 1X PBS and permeabilized with 0.2% TritonX-100 PBS for 15 minutes at RT. Add 100µL of Duolink® Blocking Solution to sample and incubate the slides in a heated humidity

chamber for 60 minutes at 37°C. Dilute the ATR (1:100) and nesprin Ab (1:200) and add to coverslips, incubate for 1 hour. Wash the samples with PBS. Dilute the two PLA probes 1:5 in appropriate buffer and apply to samples. Incubate for 60 min at 37°C. Wash with Wash Buffer A for 2X 5min. Dilute the Ligation stock 1:5 in H_2O. Dilute the Ligase at 1:40 in the solution and apply the mix to samples. Incubate for 30 min at +37°C. Dilute the Amplification stocks 1:5 in H_2O. Dilute the Polymerase at 1:80 in the solution and apply the mix to samples. Incubate for 100 min at +37°C. Wash in 1x Wash Buffer B for 2 × 10 min. Wash in 0.01x Wash Buffer B for 1 min. Mount the samples with vectorshield Mounting Medium with DAPI, and analyze in a confocal microscope.

DNAse Assay

The cells were arrested in G1 by double thymidine block (2 time - 14 hours, 2mM thymidine) then washed once with PBS and permeabilised in CSK buffer supplemented with 0.2% Triton X-100 and protease inhibitor cocktail (Sigma-Aldrich, St. Louis, MO, USA) at room temperature for 5 minutes. Next, the samples were incubated in CSK buffer supplemented with 0.1% Triton X-100, protease inhibitor cocktail and DNase I (Sigma-Aldrich, St. Louis, MO, USA) at the indicated concentrations at room temperature for 20 minutes. Cells fixed with 4% PFA fro 15 minutes at room temperature. The remaining DNA is stained using DAPI at a concentration of 1 μg/mL in PBS for 10 minutes. Then, the nuclei are photographed using a fluorescence microscope and the area of the nucleus was measured using Image J software.

Atomic Force Microscope measurements

The AFM experiments were performed with Qingsen Li (Marco Foiani's lab) (Li et al., 2008) using Nanowizard 3 (JPK instruments, Germany), mounted on a light microscope. For AFM indentation we used a modified silicon nitride AFM cantilever (spring constant of 0.03N/m) with a 5mm diameter polystyrene bead adhered to the tip

(NovaScan, USA). The cells were grown on 24mm round glass coverslips, mounted on the AFM stage and were maintained at physiological temperature of 37 °C throughout the experiment using a heater (JPK instruments, Germany). Indentation was carried out at the center of cell using a loading rate of 1.5 mm/s. The ramp size used in this study was 3 mm and an indentation force of 2 nN was applied during the tests in order to ensure that a small deformation was exerted on the cell and minimize any substrate contributions. The Young's modulus was subsequently determined using Hertz's contact model

$$F = \frac{4}{3}\frac{E}{(1-\nu^2)}\sqrt{R\delta^3}$$

where, F is the indentation force, E is the Young's modulus to be determined, n is the Poisson's ratio, *R* is the radius of the spherical bead, and d is indentation depth. The cell was assumed incompressible and a Poisson's ratio of 0.5 was used.

Nuclear isolation for AFM analysis

HeLa cells were rinsed once with PBS and treated with 1 ml of a 0.01% Igepal CA-630 (a non-ionic detergent, Sigma), 1% citric acid solution in water for 5 min. Nuclei were expelled, while the cytoplasm remained adherent. The supernatant was collected, mixed with 5 ml PBS, and centrifuged at 300g for 5 minutes. The nuclei pellet was then re-suspended in PBS, spread onto coverslip for AFM experiments.

Preparation of micro-patterned channels

We received silicon wafers from Matthieu Piel's lab and the procedures to prepare the wafers are described in details in (Raab et al., 2016). Briefly, the silicon rubber (RTV-615, Momentive) was mixed with curing agent at a ratio of 10:1, and poured in the silicon wafer and allowed to polymerize in a vacuum chamber overnight. The next day, microfabricated PDMS structures were extracted from the mold. Punchers were used to drill the PDMS in the regions designed for seeding chambers, and then they were washed with ethanol to sterilize. Plasma treatment was performed to activate the surfaces of the

PDMS and glass to bind the PDMS covalently on the slide-glasses or petri dishes. Then they were boiled at 65 degree for 1 hour sterilized again with 30 sec plasma treatment, and then coated with fibronectin overnight. Cell were loaded the day before or 6 hours before the experiment to the wells.

Analysis of cell migration

For single cell migration, images captured using a bright-field microscope every 5 minutes and cell tracking was performed manually using the MtrackJ tool of ImageJ. For Cell migration and tracking in 2D lines were performed as described previously (Maiuri et al., 2015) in collaboration with P .Maiuri. U2OS cells with or without ATR inhibitor treatment were plated on glass slides micro-patterned with 10um thickness lines coated with fibronectin. After 3 hours later time-lapse experiment was run for 24 hours with 10-minute time intervals. Image analysis was done with a semi-automated in-house code.

For wound-healing assay images were captured with a bright-field NIKON Eclipse TE2000-E microscope every 10 minutes for 18 hours. Wound closure speed was analyzed with the assistance from IFOM imaging facility, using a semi-automated code in MATLAB. All the analysis of migration through constrictions were performed manually and 53BP1 foci were counted using imageJ.

Results

Chapter 1

Cellular distribution and interactome of ATR

ATR is expressed in all phases of cell cycle in several tissues including the ones that are terminally differentiated such as heart and brain. This suggests that ATR apart from its essential role during replication could also contribute to other cellular processes involving tissue maintenance. ATR and other members of the PIKK family were long proposed to be involved in regulating several cellular aspects, however, studies on the yeast ATR pathway (MEC1 and RAD3) (Bentley et al., 1996) highlighted the essential role of ATR in replication and ssDNA mediated DNA repair, overshadowing the DNA repair independent functions of ATR. Recent literature highlights several DDR independent roles of ATR in organelles including nuclear envelope, nucleoli, cilia and mitochondria (Kidiyoor et al., 2016). Though the essential well-characterized role of ATR is in the nucleus, several reports have demonstrated the presence of ATR in centrosomes, mitochondria (Hilton et al., 2016) and nuclear periphery(Kumar et al., 2014). Visualizing the GFP-ATR in cultured cells, revealed that ATR is distributed across nucleus as well as cytoplasm (Tibbetts et al., 2000), and in neurons ATR was reported to be more cytoplasmic, interacting with ATM and regulating synaptic functions (Li et al., 2009). Since there are no reports (other than proteomic database sites) summarizing the distribution of ATR across the cell, we decided to analyze distribution and interactome of ATR across HeLa cell.

1.1 Cellular distribution of ATR by electron- microscopic analysis.

We performed immune-gold labeled EM analysis of HeLa cells and quantified number of nanogold labelled ATR in different organelles (Kumar et al., 2014) (Figure 12). Overnight-cultured 70% confluent dishes of HeLa cells were prefixed with paraformaldehyde (PFA), stained, imaged with light microscope, then fixed with Glutaraldehyde and processed for gold labeling and EM analysis (Kumar et al., 2014) (see material and methods for detail). Total amount of gold particles were counted in different cellular compartments and percentages calculated with respect to the total gold

particles present in the cells. Amount Gold particles localized within 20 nm of the nuclear envelope or of the plasma membrane were considered as being on the membrane.

In our analysis of interphase cells (n>10) we observed ATR to be distributed throughout the cell with highest percentage in the nucleus accounting for 34 percent (Figure 12A) of total protein. Significant amount of cytosolic ATR was found to be membrane bound (in Golgi, ER and plasma membrane) or bound to actin structures (Figure 12A,B, C), however, majority of ATR was in free-floating form either in nucleus (34%) or in cytoplasm (24%) unbound or non-associated to any organelle. Approximately 19% of ATR was bound to actin fibers (Figure 12A, C), mainly to the NE associated perinuclear actin filaments (Figure 12D, G), to actin stress fibers (Figure 12C) and to actin networks of filopodia (Figure 12B). We also observed ATR enriched at both plasma membrane and actin fibers of filopodia (Figure 12B), suggesting a possible involvement of ATR in cell migration process.

Since we have evidence that mechanical stress at the NE induces relocalization of ATR (Kumar et al., 2014), we performed similar distribution analysis of ATR upon sorbitol treatment (osmotic stress) and in cells undergoing mitosis, particularly during prophase. Both conditions significantly reduced the free-floating ATR, increasing membrane bound and actin bound ATR (Kumar et al., 2014) (Figure 12A), correlating with the immunofluorescence data of ATR at the NE in both prophase cells and sorbitol treated cells (Kumar et al., 2014). Closer analysis of ATR near NE revealed that ATR was found on both sides of nuclear membrane, at the nuclear pores and associated to perinuclear actin fibers (Figure 12D, E, G). In prophase cells we observed an increase of NE bound ATR without any reduction in the nucleoplasm indicating that the increased ATR at the NE was mainly cytoplasmic ATR, moved towards NE. However, different from prophase cells, sorbitol treated cells had reduced levels of nuclear ATR (from 33% to 10%) and increased level of ATR bound to actin filament (from 19% to 39%)

suggesting a stress induced movement of nuclear ATR towards cytoplasm (Figure 12A). In case of prophase cells the condensing chromatins and the perinuclear actin cytoskeleton purely generates the membrane stress at the NE. But osmotic stress acts on whole adherent cell with intact cytoskeleton affecting plasma membrane, nuclear envelope and cytoskeleton. This could be the reason why we observed different distribution of ATR at cytoplasmic actin stress fibers, NE and nucleoplasm in sorbitol treated and prophase cells.

This analysis of ATR distribution also revealed the preference of ATR towards membranes. Approximately 13 percent of total ATR was distributed across NE, plasma membrane, endoplasmic reticulum, Golgi (Figure 12A, B, E), organelles mainly constituted of membranes. In addition, mitochondrial ATR was also attached to the mitochondrial inner membrane. Further, we observed a modest increase of membrane bound ATR, when membranes experienced mechanical stress such as osmotic challenge (Figure 12A), supporting the functional role of ATR in membrane stress response (Kumar et al., 2014). Though it was suggested that ATR and other PIKKs have phospholipid binding domains (Sommer et al., 2013, Kidiyoor et al., 2016), our analysis provides evidence supporting this. We show that in normal cells a fraction of ATR is always bound to membranes and treatments that induce membrane stress increases this association.

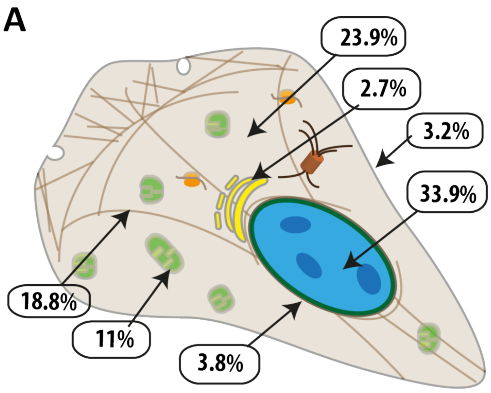

	interphase	Sorbitol treatment	prophase
Nuclear envelope	3.8%	14.3%	14.5%
Nucleoplasma	33.9%	10%	36.5%
Mitochondria	11%	11%	4.3%
Cytosol	23.9%	5.3%	14%
Plasma membrane	3.2%	4.4%	5.1%
Endo. Reticulum	2.7%	13.8%	5.2%
Actin	18.8%	38.8%	19.3%
Golgi	2.7%	2.6%	1.1%

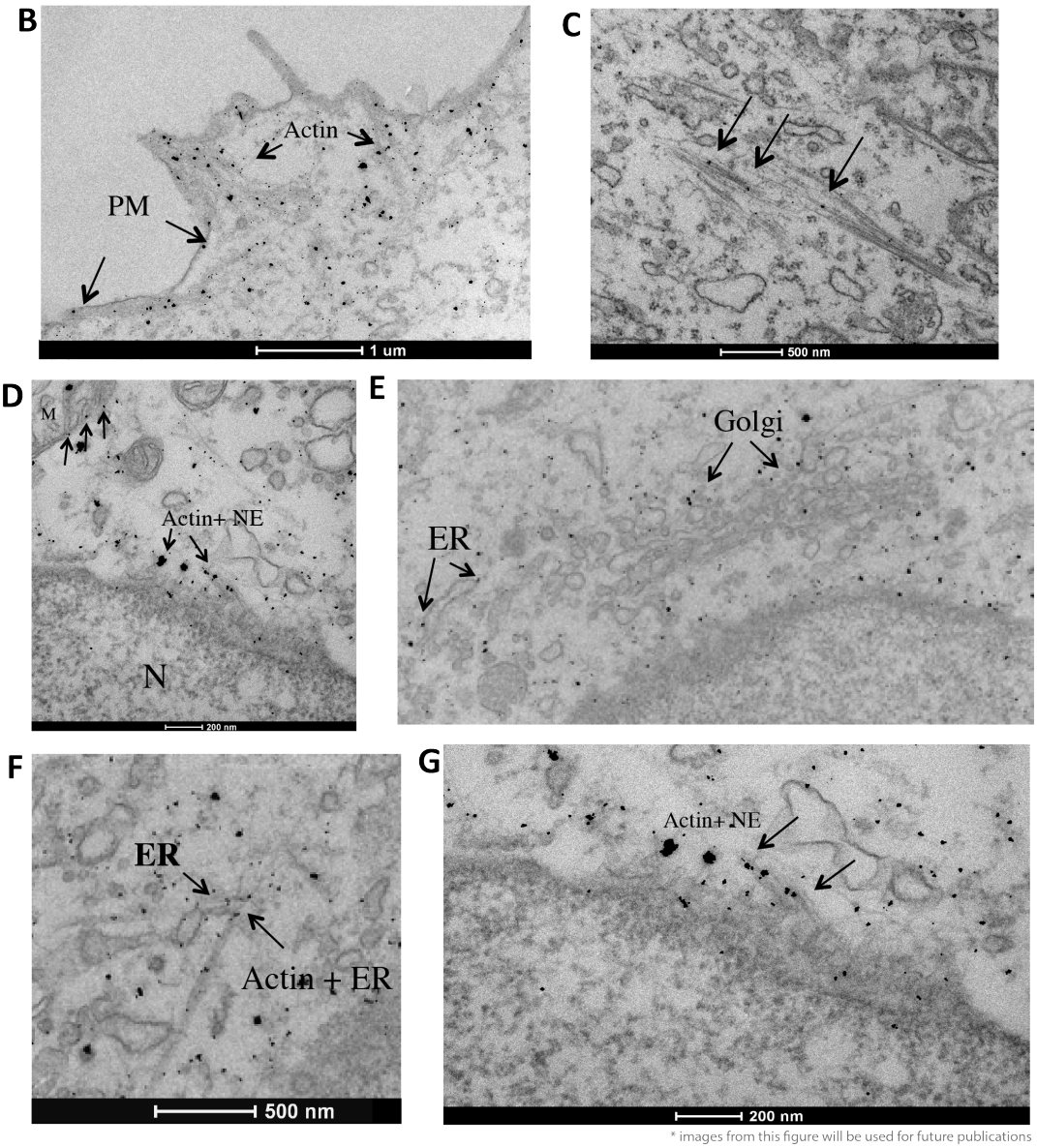

* images from this figure will be used for future publications

Figure 12 – Cellular distribution of ATR

(A) ATR distribution across different organelles of the cells was determined by quantification of ATR nano-gold particles across the cell in exponentially growing HeLa cells (n>10), cells treated with sorbitol (0.5M for 30 min) or cells during prophase of mitosis. (B) In Filopodia ATR is enriched at plasma membranes and actin fiber network. ATR is also enriched in stress fibers (C), perinuclear actin (D) and in ER and Golgi (E,F). (G) At the NE, ATR is present on either side of the membrane and in actin filaments associated with NE.

1.2 Proteomic analysis of ATR interactome.

Encouraged by the sub-cellular distribution of ATR, we performed proteomic analysis of ATR immuno-precpitation (IP) in order to identify potential ATR interactors. First, we immune-precipitated GFP-ATR from U2OS cells stably expressing GFP-ATR plasmid; using anti-GFP conjugated magnetic beads (details in Materials and methods). Prior to proteomic analysis we optimized the conditions for pull-down and confirmed that GFP-ATR is efficiently pulled-down in Mass-Spec samples using western blots and Coomassie staining (sample blot in Figure 15 B, C). We detected 426 interactors including the ATR interacting protein, ATRIP. In order to increase the confidence of data and to eliminate the unspecific interactors, we performed two independent stable isotopes labeling with amino acids in cell culture (SILAC) experiments (strategy in figure 13A), with GFP as unspecific binding control. Candidate list from these three independent proteomic screens were then filtered with stringent thresholds to generate a final interactome list of 479 candidates. First we selected the candidates that appeared in at-least two experiments out of three screens, then we filtered this list by selecting candidates that have least 8-fold enrichment over GFP in at least one SILAC experiment.

Our candidate list of ATR interactome had several interesting candidates from different cellular compartments and regulators of diverse cellular processes. So we utilized online gene ontology (GO) tools from DAVID (david.ncifcrf.gov) for functional annotation clustering (Huang da et al., 2009b, Huang da et al., 2009a). We did GO enrichment analysis on cellular compartments and on biological processes and found that ATR interactors were not only enriched in the nucleus, but were also significantly enriched in several other organelles such as mitochondria, centrosomes and actin cytoskeleton (figure 13B). ATR interactors were enriched for most nuclear processes such as DDR, chromatin remodeling and gene expression, maturation of several RNA species and shuttling of RNA and proteins through the nuclear pore. Interestingly, a significant

proportion of the ATR interactome was involved in cytoskeletal organization and the associated cell mobility (Figure 13C). We then utilized "Revigo" (Supek et al., 2011) online tool to simplify GO terms obtained from DAVID (resulting list size: 0.7, database: Homo sapiens, semantic similarity measure: SimRel). The semantic similarity-based scatterplots of Revigo (Figure 13C) indicated that biological processes enriched in ATR interactome grossly fall into 4 major categories; classical DNA damage response

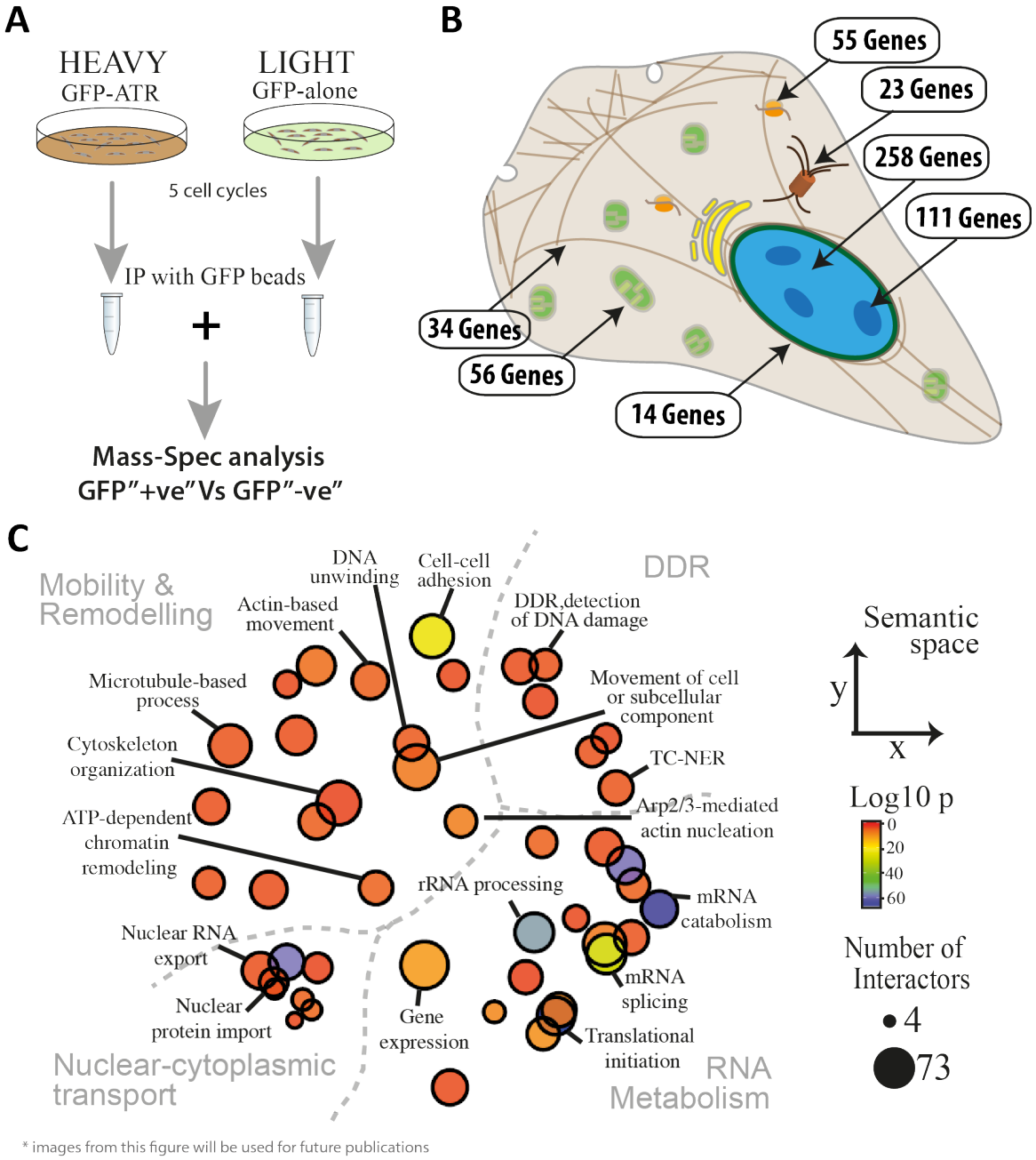

Figure 13 – Proteomic analysis of ATR interactome.
(A) Strategy for SILAC analysis of GFP-ATR. (B) Cellular distribution of ATR interactors. (C) "Biological process" clusters of ATR interactome simplified and visualized in semantic similarity-based scatterplot by Revigo.

regulators, factors involved in RNA metabolism, nuclear transport machinery and mobility and remodeling related processes (Figure 13C).

ATR, is a protein kinase, preferentially phosphorylating serine or threonine residues that are followed by glutamine (SQ/TQ)(Kim et al., 1999). Hence, we analyzed our list of ATR interactors against the online protein phosphorylation database, PhosphoSitePlus (www.phosphosite.org)(Hornbeck et al., 2004). We found more than 97% of the interactors to be positively scored as targets of protein kinases. We then looked for phospshorylation at the ATR consensus site SQ/TQ. We found 55.3% of ATR interactors scoring positive for phosphorylation at SQ or TQ motifs (Figure 14A), while only 29% of the total phospho-proteins (5137/17522) in the PhosphoSitePlus database have reported phosphorylated SQ/TQ motifs, showing that ATR interactors were highly enriched in p-SQ/TQ proteins, which are thus potential direct targets of ATR phosphorylation. We then compared our list with published datasets of potential ATM/ATR substrates; Matsuoka et.al, (Matsuoka et al., 2007) provides ATM/ATR substrates that are phosphorylated upon UV damage, and Olsen et.al, (Olsen et al., 2010) provides S phase specific ATR/ATM substrates. Though our study was DNA damage and cell cycle independent, our ATR interactome showed 15% overlap with Olsen et.al dataset and 10% overlap with Matsuoka et.al (Figure 14A).

We then manually curated ATR interactors into sub-categories of processes that are potentially interesting and not previously studied. We prepared a STRING network (string.embl.de) analysis (Szklarczyk et al., 2017) of each category, highlighting the putative targets of ATR phosphorylation (Figure 14B-G). In the DNA related processes category, we observed 3 major network clusters; histones, chromatin remodelers and DNA damage response proteins including ATRIP (Figure 14B). Topoisomerase II alpha and beta were two most interesting candidates given their overlap with ATR function in controlling topological state of DNA. In addition Topoisomerase IIA and IIB are also potential targets of ATR phosphorylation. ATR and Topoisomerase II are involved in

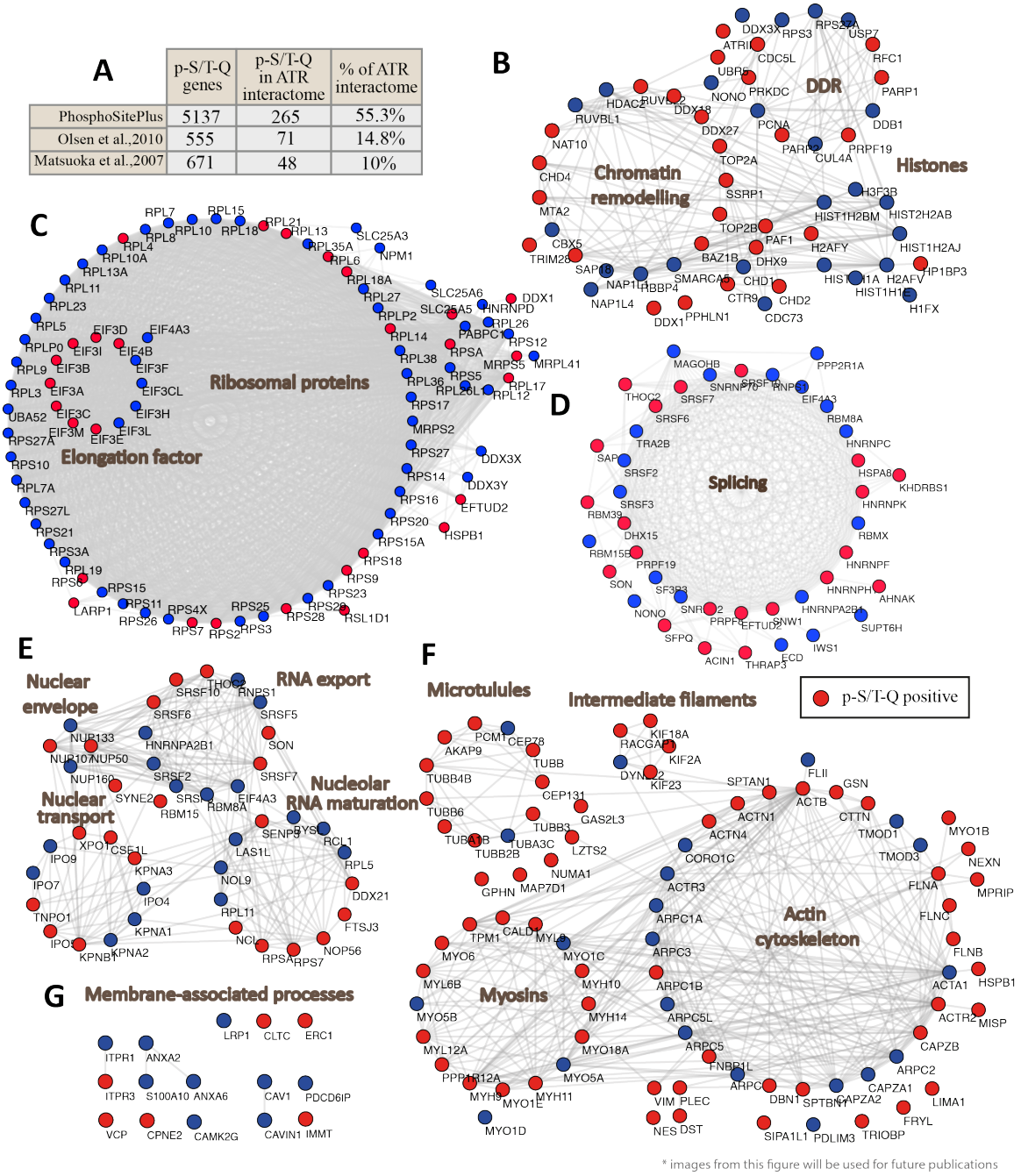

	p-S/T-Q genes	p-S/T-Q in ATR interactome	% of ATR interactome
PhosphoSitePlus	5137	265	55.3%
Olsen et al.,2010	555	71	14.8%
Matsuoka et al.,2007	671	48	10%

Figure 14 - Categorization and network analysis of ATR interactome.
(A) Table comparing ATR interactors with other datasets of ATR/ATM substrates; PhosphoSitePlus, Matsuoka et.al, and Olsen et.al,. STRING networks of ATR interactors in categories (B) DNA related process (C) translation (D) transcription and splicing (E) nuclear envelope related (F) Cytoskeleton regulators and (G) Membrane remodelers.

processes such as chromosome condensation, DNA transcription and replication, indicating that ATR might function as upstream regulator of topoisomerase II.

The most abundant and highly significant category was translation. This category consisted of ribosomal proteins and Eukaryotic translation initiation factors (EIF) (Figure 14C). While few ribosomal proteins were positive for phosphorylation at SQ/TQ sites, a

significant majority of EIF complex members were positive targets of phosphorylation by ATR, suggesting ATR mediated regulation of specific translation pathways. Category of transcription (Figure 14D) was mainly composed of splicing factors, RNA helicases and other regulators of transcription initiation and termination. For the next category we pooled processes associated with nuclear envelope (Figure 14E) comprising of nucleolar RNA maturation, RNA export, nuclear transport and envelope components. Four proteins from nuclear pore complex NUP133, NUP107, NUP50and NUP160, importins, exportins and Nesprin-2, a LINC complex member, were the most interesting candidates from this category (discussed later). Another major sub-category was the cytoskeletal components (Figure 14F). This included proteins of actin cytoskeleton, myosin, microtubules and intermediate filament. Our analysis (Figure 14F) shows that these are not just ATR interactors but are also potential substrates of phosphorylation by ATR. Several isoforms of tubulin, and centrosomal proteins constituted the microtubule network. Interestingly, several of these centrosomal and microtubule components were also involved in mitosis. Myosins and tropomyosins constituted the Myosin network. Actin cytoskeleton regulators formed the largest network of this category with several isoforms of actin, regulators of actin polymerization, and adhesion molecules. ARP2/3 complex, which controls actin polymerization and thereby regulates cell migration, was a potential ATR interactor and phosphorylation target. Other important actin cytoskeleton components include filamins, cofilin, vimentin and several capping proteins. Thus by combining actin fiber localization of ATR and overwhelming number of actin and myosin regulators in ATR interactome, we propose that ATR could regulate actin cytoskeleton, actomyosin contractility and cell migration. We also found several membrane remodelers and endocytosis molecules that did not strictly form a strong network. However considering membrane association and functions of ATR at NE, these proteins could be of significant interest for this study (Figure 14G).

1.3 Stress induced alterations in ATR interactome

Several stress conditions such as replication stress and mechanical stress activate ATR(Kumar et al., 2014, Saldivar et al., 2017). Hence, we decided to focus on proteins that differentially alter their interaction with ATR in a stress dependent manner. We immuno-precipitated GFP-ATR from isotope labeled untreated cells and from cells exposed to replication stress (2mM HU for 4 hours) or osmotic challenge (0.5M Sorbitol for 40 mins) (Figure 15A), and then utilizing quantitative proteomic analysis (SILAC), we quantified proteins which alter their binding with ATR upon these treatments.

We found that 97 proteins have reduced (Figure 15D) and 41 proteins have increased (Figure 15E) binding to ATR (2 fold change) after 4 hours of Hydroxyurea treatment. Functional annotations and clustering revealed that the proteins with reduced affinity towards ATR fall into translation machinery, mainly the Eukaryotic translation initiator factor complex 3 (Eif 3) subunits and splicing factors. Proteins with increased binding towards ATR upon HU treatment are enriched for nuclear RNA metabolism, with several helicases and zinc finger proteins. Based on these findings we can hypothesize that cells undergo replication stress induced ATR mediated alterations of gene expression at both transcriptional and translational stages.

In contrast to the replication stress, osmotic stress resulted in reduced binding of ATR towards nucleic acid binding proteins with increased cytoskeleton interactions (Figure 15F, G). We found that 61 proteins have reduced (Figure 15G) and 37 proteins have increased binding (Figure 15H) to ATR (2 fold change) after sorbitol treatment. However we could not get protein clusters with strong network amongst them, except for the list of reduced proteins upon HU treatment. This could be due to the small number of proteins and the randomness in their distribution or due to technical issues such as the sensitivity of proteomic analysis. Though these results are preliminary and non-conclusive, they encourage further studies towards this direction.

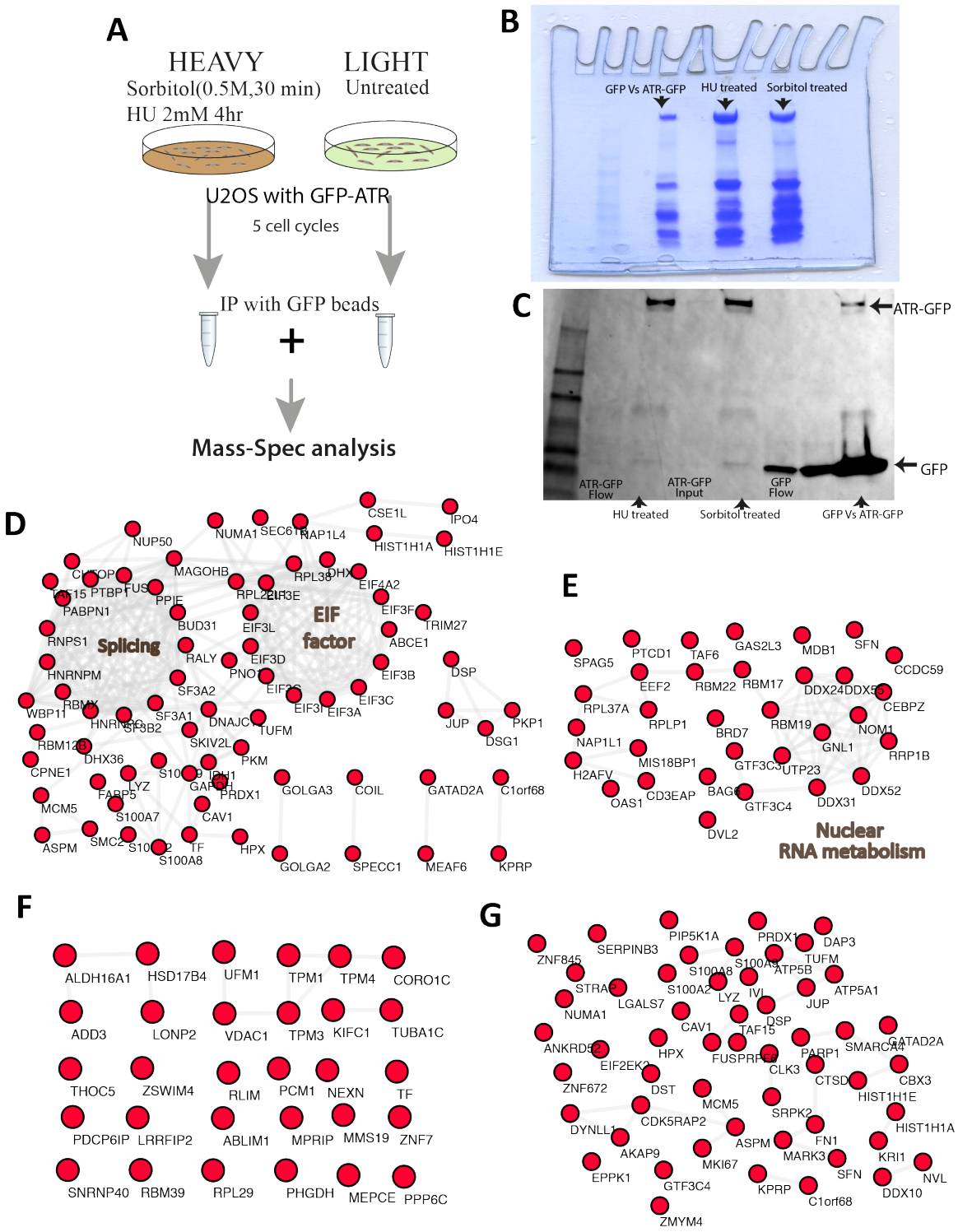

Figure 15 - Stress induced ATR interactome and network analysis.
(A) Strategy for SILAC analysis of ATR-GFP immune-precipitations from HU or sorbitol treated cells. We used approximately 9mg of total cell lysate per condition (B) Coomassie staining of Gel with SILAC samples (C) westernblot validation of IP, with anti- GFP antibody. Arrows pointing towards enriched GFP-ATR and GFP protein. Network analysis of ATR interacting proteins after Hydroxyurea treatment; (D) intreactors with reduced ATR binding and (E) with increased binding. Network analysis of ATR interactors after sorbitol treatment; (F) proteins with increased binding (G) proteins with reduced ATR binding.

1.4 Conclusions.

Our goal was to analyze ATR localization and its interactome in the whole cell. This would serve as a preliminary database for basic understanding of context and provide guideline for studying uncharacterized non-canonical functions of ATR in a cell. Using EM analysis we show that ATR is distributed throughout the cell, enriched in several organelles such as mitochondria and ER and also in actin cytoskeleton and NE. Proteomic analysis derived distribution of ATR interactome also was consistently overlapping with the EM data with high numbers of cytoskeletal proteins and membrane-associated proteins included as ATR interactors. Our data predicts ATR function in several organelles. Recent studies have demonstrated few such roles of ATR including its role in response to membrane stress at the NE (Kumar et al., 2014), antiapoptotic responses in mitochondria(Hilton et al., 2016) and its contribution to cilia growth and function (Stiff et al., 2016). In addition several proteins such as Cofilin and Caveolin1, which according to our data are potential interactors of ATR, have higher phosphorylation status in Seckel cells (Tivey et al., 2013).

Our results also indicate involvement of ATR in several novel cellular processes such as transcription and translation, RNA transport and splicing. Enrichment of ATR in actin cytoskeleton, leading edge of filopodia and in perinuclear actin ring, supported by high number of actin polymerization regulators as ATR substrates strongly indicate the involvement of ATR in cytoskeletal regulation. Based on our data, we conclude that ATR will have several functions in different cellular compartments such as mitochondria, NE, Golgi, centrosomes and plasma membrane, regulating multiple aspects such as gene expression, cytoskeletal organization, nuclear export, RNA metabolism, membrane architecture and migration.

Chapter 2

ATR regulates nuclear envelope integrity

ATR distribution and interactome analysis shed light on several novel functions of ATR that could be further explored. However in this study, we decided to focus on the crosstalk between ATR and NE since it was long-standing interest of our group. According to our findings, fraction of ATR is membrane-associated and its interactome is enriched for proteins involved in NE associated processes. Previous work from our lab demonstrated that ATR could sense and respond to membrane stress stimuli at the NE (Kumar et al., 2014), by relocating into the NE and locally phosphorylating CHK1 kinase at the NE. In *S. cerevisiae,* Mec1 resolves fork collision with transcription machinery near the NE by detethering the RNA from the nuclear pore and relaxing the DNA (Bermejo et al., 2011). In addition, recent works from other groups also show that ATR could be activated by physical and chemical alterations of the NE (Kidiyoor et al., 2016).

Nuclear envelope is a mechano-transducer, it can sense mechanical forces from both nuclear and cytoskeletal part, transform them into chemical signal which later can be exploited by cell to initiate an appropriate stress response (Wang et al., 2009, Isermann and Lammerding, 2013). Since ATR binds to NE and responds to such mechanical stimulus at the NE (Kumar et al., 2014) to prevent any potential threats to genome integrity, we hypothesized that absence of ATR might influence the maintenance of nuclear integrity and homeostasis. We tested this hypothesis by analyzing the NE integrity of ATR depleted cells.

2.1 ATR physically interacts with membranes

ATR is a PIKK kinase with structural homology to lipid kinases of phosphoinositide kinase family. A recent study reported that the FATC domain of ATR could interact with membrane mimetic structures (Sommer et al., 2013). We analyzed the hydropathy profile of ATR using the Kyte-Doolittle algorithm (Kyte and Doolittle, 1982) and the putative membrane associated domains using the SOSUI and WoLF PSORT programs (Mitaku et al., 2002) (wolfpsort.org). A total of eight putative membrane

binding, hydrophobic regions with significant score were distributed across ATR; six in HEAT repeat region and two in c-terminus FAT region (Figure 16A). Kyte-Doolittle algorithm also suggested three regions in HEAT domain as a putative membrane associating regions (Figure 16A).

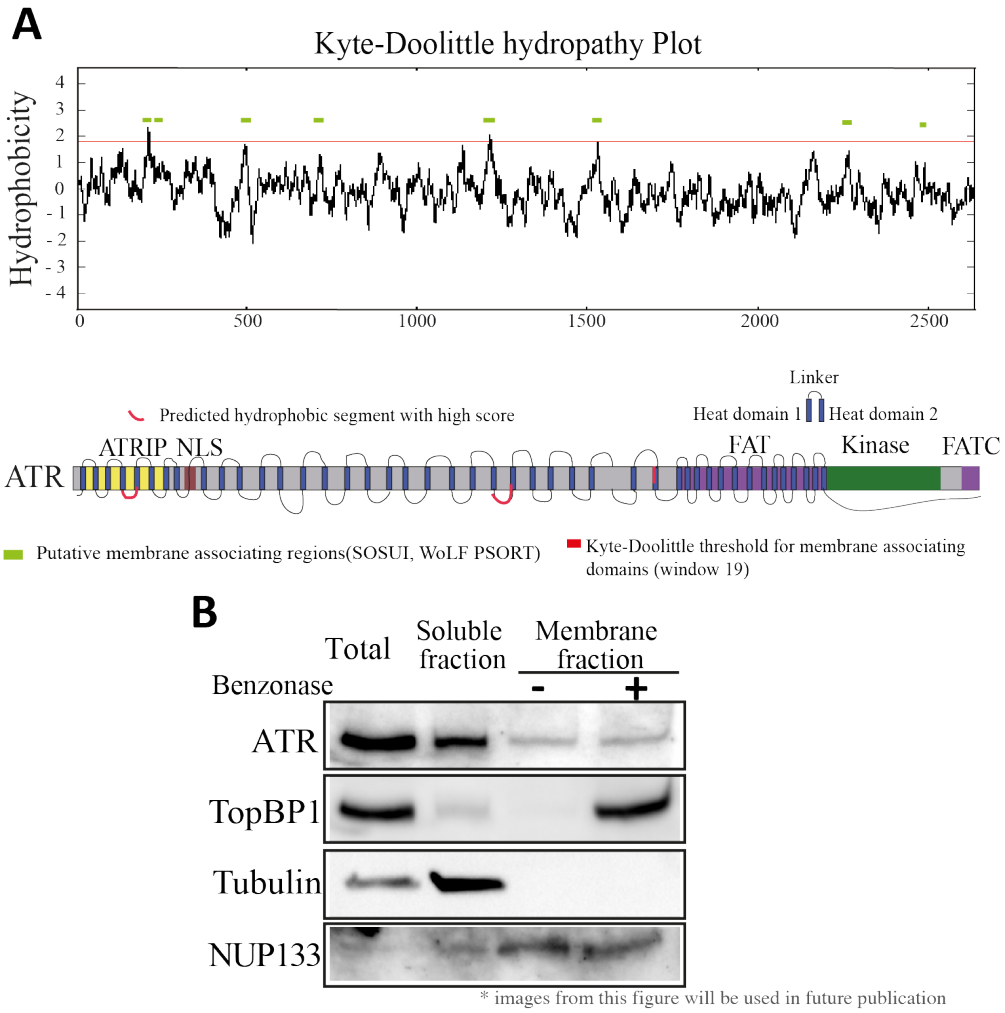

Figure 16- ATR binds to membranes and has several membrane binding domains (A) Hydropathy profile of ATR using the Kyte-Doolittle algorithm and putative membrane associated domains of ATR according to the SOSUI and WoLF PSORT programs. (B) Membrane fractionation of exponentially growing HeLa cells show a fraction of ATR to be membrane bound. Sub-fractionations verified with anti-Tubulin (cytosol specific), anti-NUP133 (NE-specific) and anti-TopBP1 (chromatin binding) antibodies.

We had evidences that ATR can sense mechanical stimuli at the nuclear envelope (Kumar et al., 2014). Our ATR localization analysis indicated that a significant amount of ATR was membrane-bound (Figure 12A). In order to confirm this data we performed

membrane fractionation assay. Using commercial Mem-Per Plus kit we separated the membrane bound proteins from soluble fraction and quantified amount of ATR in each fraction. We found that in exponentially growing HeLa cells 17 % of ATR was associated with membranes (Figure 16B). Fractionation purity was confirmed using anti-Tubulin (cytosol specific), anti-NUP133 (NE-specific) and anti-TopBP1 (chromatin binding) antibodies. Contribution from chromatin contamination in membrane fraction was assesed by treatment with Benzonase nuclease. While major fraction of ATR was present in the soluble fraction, a fraction of ATR was observed in membrane fraction independently of DNA, confirming direct association of ATR with the membranes.

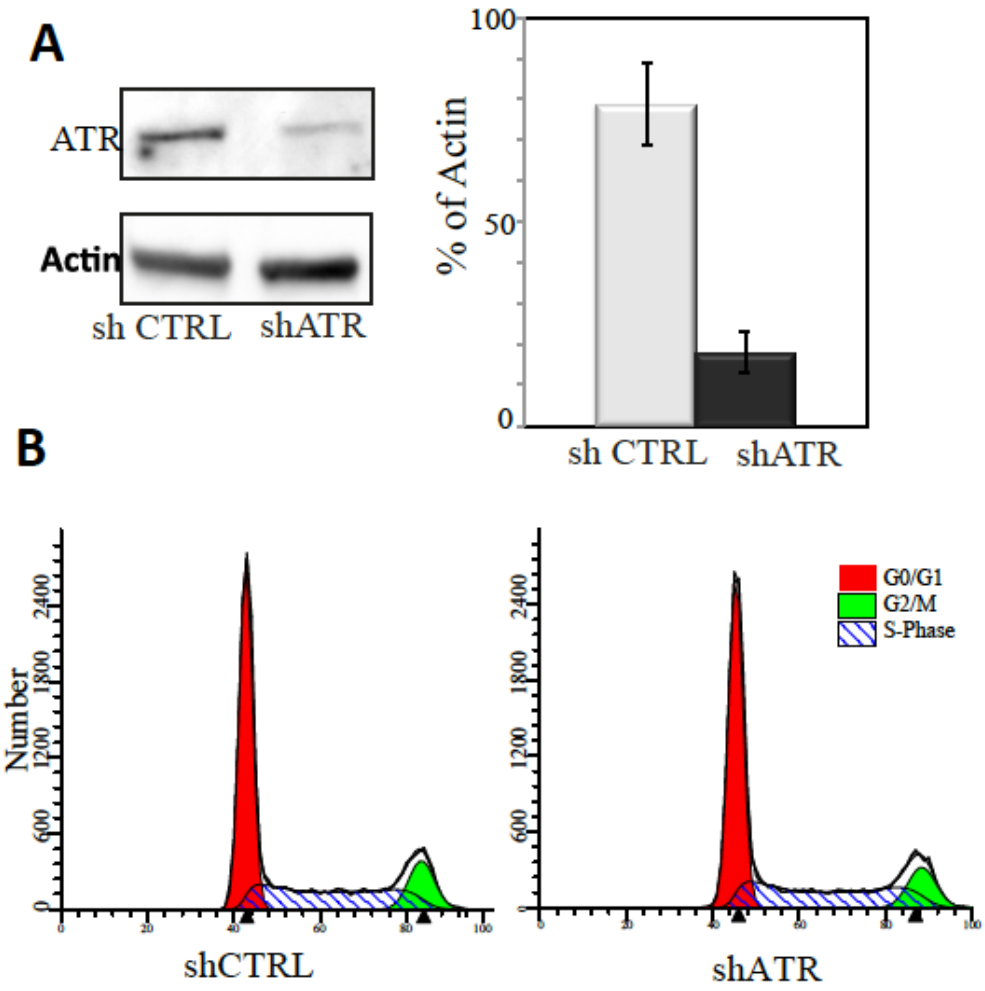

Figure 17 - Knock-Down of ATR with no cell cycle abnormalities
(A) Depletion efficiency of shRNA against ATR in HeLa cells. ATR levels were measured by quantifying anti-ATR antibody signal; actin was used as loading control. (right) Statistics from multiple experiments (n>5) suggesting reproducibility of knockdown. (B) FACS analysis of cell cycle from mock and ATR shRNA treated cells.

2.2 Loss of ATR results in compromised Nuclear envelope architecture

Since ATR coordinates nuclear events with NE, we hypothesized that depletion of ATR from cells would result in a de-regulation of mechanical stress response leading to loss of nuclear integrity. To test this hypothesis, we depleted ATR from HeLa cells using a published efficient shRNA. ATR protein level reduced to 25% compared to control (Figure 17A) as measured by western blotting. Since ATR is an essential kinase, its reduction or depletion could impact cell cycle. We confirmed that our ATR depleted cells, had no obvious abnormalities of cell cycle and growth delays (Figure 17B) by FACS analysis thus implying that 25% of residual ATR protein was sufficient to carry out the essential role of ATR.

As predicted, three days after depletion of ATR, cells displayed compromised nuclear shape (Figure 18A), characterized by invaginations, blebs, multi-nuclei and micronuclei. Performing immunofluorescence (IF) analysis of NE (Lamin B1 antibodies) and DNA (DAPI); followed by manual segregation of nuclei into normal, mild or severely deformed and with micro nuclei categories (Figure 18B) we could clearly observe a significant reduction of normal nuclear morphology in absence of ATR (from 80% to 50%) with an acute increase of cells with deformed nuclear morphology (from 20% to 50%) (Figure 18C). shATR cells had lower nuclear circularity index compared to controls (Figure 18D). ATR depleted cells also exhibited increased number of micronuclei suggesting a loss of appropriate nuclear dynamics during mitosis (Figure 18E). Human *Seckel* fibroblasts were also previously shown to have increased micronuclei (Alderton et al., 2004).

We measured the area of the nucleus (Figure 18F, G) at the central section of the image and detected approximately 20 percent gain in ATR depleted cell nucleus (212.98 ± 7.54 um^2) compared to controls ($177.43\pm3.00um^2$).

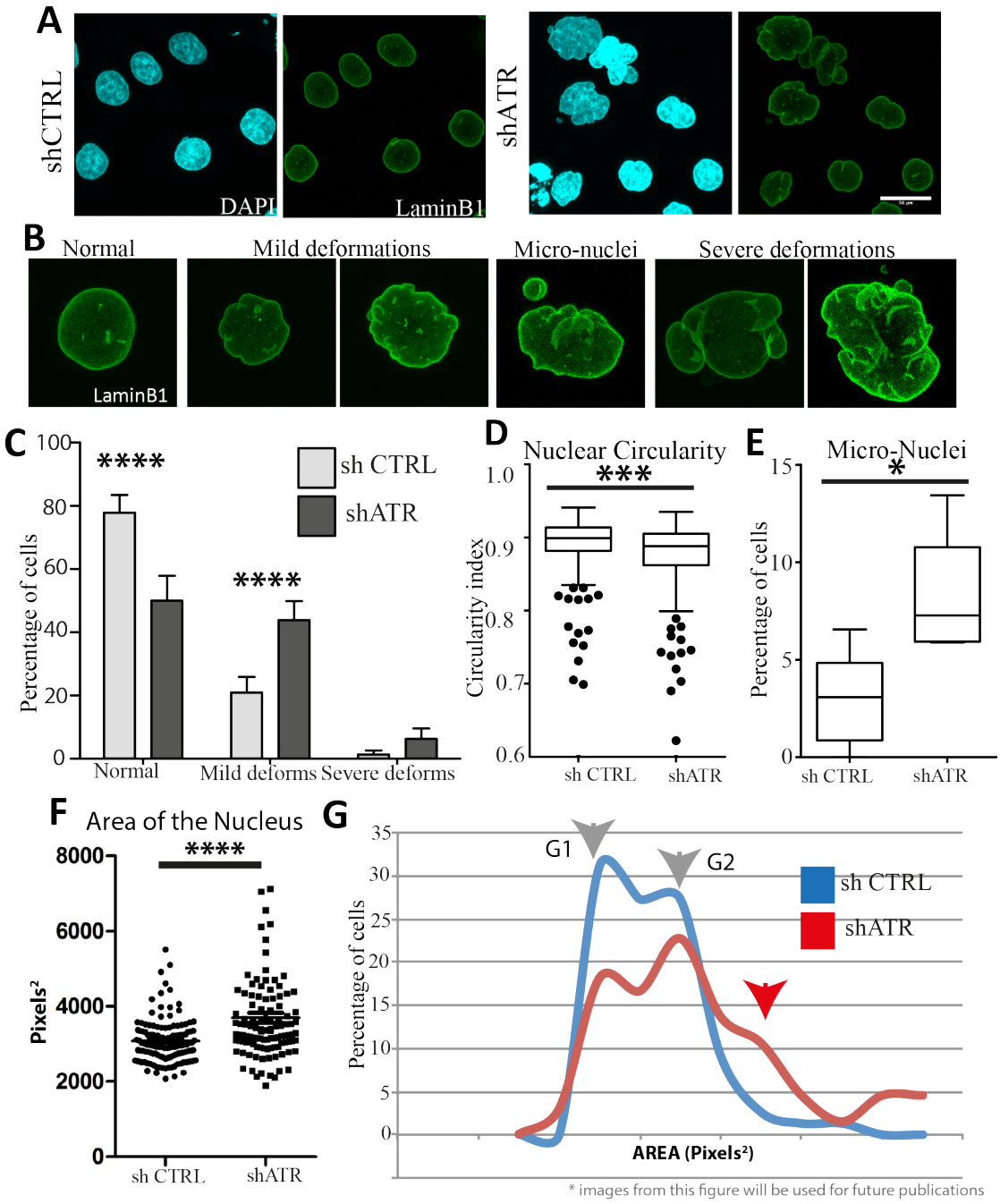

Figure 18 - Knock-Down of ATR results in nuclear shape abnormalities
(A) Depletion of ATR in HeLa cells leads to nuclear shape defects as visualized by LaminB1 staining. (B) Sample images of different nuclear shapes and categories that were considered for quantification. (C) Distribution of nuclear shape alterations in ATR depleted and control cells (n>250). p-values calculated using one-way ANOVA test. (D) Circularity index of nuclei, and (E) micronuclei in control and shATR cells. (F) Dot plot of areas of control (n=117) and shATR cells (n=110). Student t-test performed for calculating p-value. Average area of ATR depleted cell nucleus was 212.98±7.54 um^2 and 177.43±3.00um^2 of controls. (E) Percentage distribution of control and shATR cell nuceli across increasing nuclear area. Brown arrowheads indicate two peaks of G1 and G2 phase respectively. Red arrow indicates the additional peak of shATR cells. (* if 0.01<p<0.05; ** if 0.005<p<0.01; *** if 0.001<p<0.005; **** if p<0.001)

We further analyzed the distribution of cell number with respect to area (Figure 12G). In control cells we could observe a smooth curve with two clear peaks representing G1 and G2 phases of cell cycle. Instead, in shATR cells peaks were shorter and we also found an additional peak at the region of higher area accounting for the increased number of giant nuclei (Figure 18G).

Next, we depleted ATR from U2OS cells (using same shRNA), in order to rule out the contribution of cell type specificity in observed phenotypes. Similar to shATR HeLa cells, U2OS cells exhibited defective nuclear architecture with invaginations, reduced nuclear circularity and increased micronuclei (Figure 19A-D). Consistently, human ATR Seckel fibroblasts also had deformed nuclear morphology, altered circularity index and in addition increased micronuclei (Figure 19E-H), as observed in shATR HeLa and U2OS cells. Usually fibroblasts have elongated nuclear shape (hence lower circularity index), but Seckel fibroblasts had large and more circular nuclei, with invaginations and micronuclei. We then performed similar analysis in primary neurons and mouse embryonic fibroblast (MEF) from humanized Seckel mice(Murga et al., 2009).

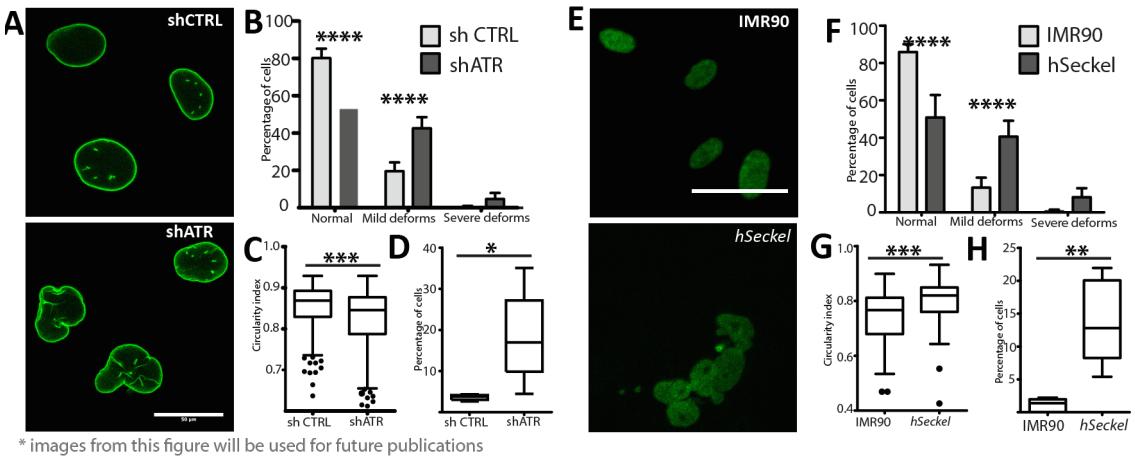

Figure 19 - Seckel fibroblasts and ATR depleted U2OS cells exhibit abnormalities in nuclear morphology (A) shATR U2OS cells (n=330 for control and n=300 for shATR) and (E) Seckel fibroblasts (n=290 for control and n=206 for Seckel) have nuclear shape defects as visualized by LaminB1 staining. (B and F) Quantification of abnormal nuclei in these cell types(C, G) Circularity index of nuclei (D, H) Percentage of cells with Micronuclei. p-values calculated using 2-way ANOVA and student t- test.

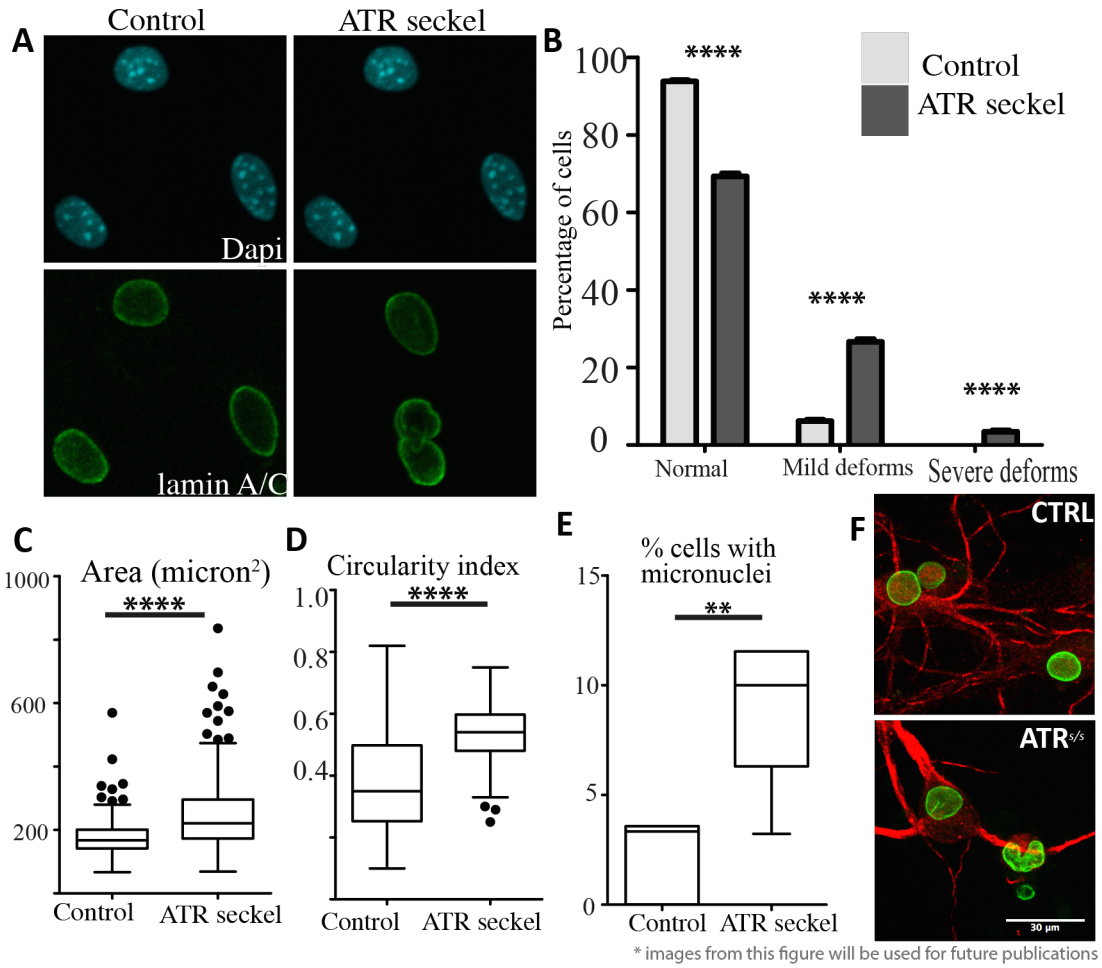

Figure 20 - Neurons and fibroblasts from Seckel mice exhibit nuclear abnormalities (A) Seckel fibroblasts display nuclear shape defects as visualized by LaminB1 staining. (B) Distribution of nuclear shape alterations in Seckel fibroblasts (n=135) and control fibroblasts (n=145). p-values calculated using 2-way ANOVA test. (C) Dot plots of nuclear area of control and Seckel fibroblasts. (D) Circularity index of nuclei, and (E) micronuclei percentage. p-values calculated using student t-test. (F) Representative images of nuclei from primary neurons.

We observed consistent defects in nuclear morphology with increased area and altered circularity index and higher number of micronuclei in both Seckel MEFs (Figure 20A-E), and in primary neurons (Figure 20F) confirming phenotypes of shRNA and Seckel patient cells in another model system.

We then tested if this defective nuclear morphology was reversible. However, the challenge was the lower transfection efficiency of GFP-ATR plasmids combined with the low compatibility of primary cells from Seckel patients or mice for transfection. So we utilized the $ATR^{flox/-}$ cells generated by Cortez et.al. (Cortez et al., 2001). These are

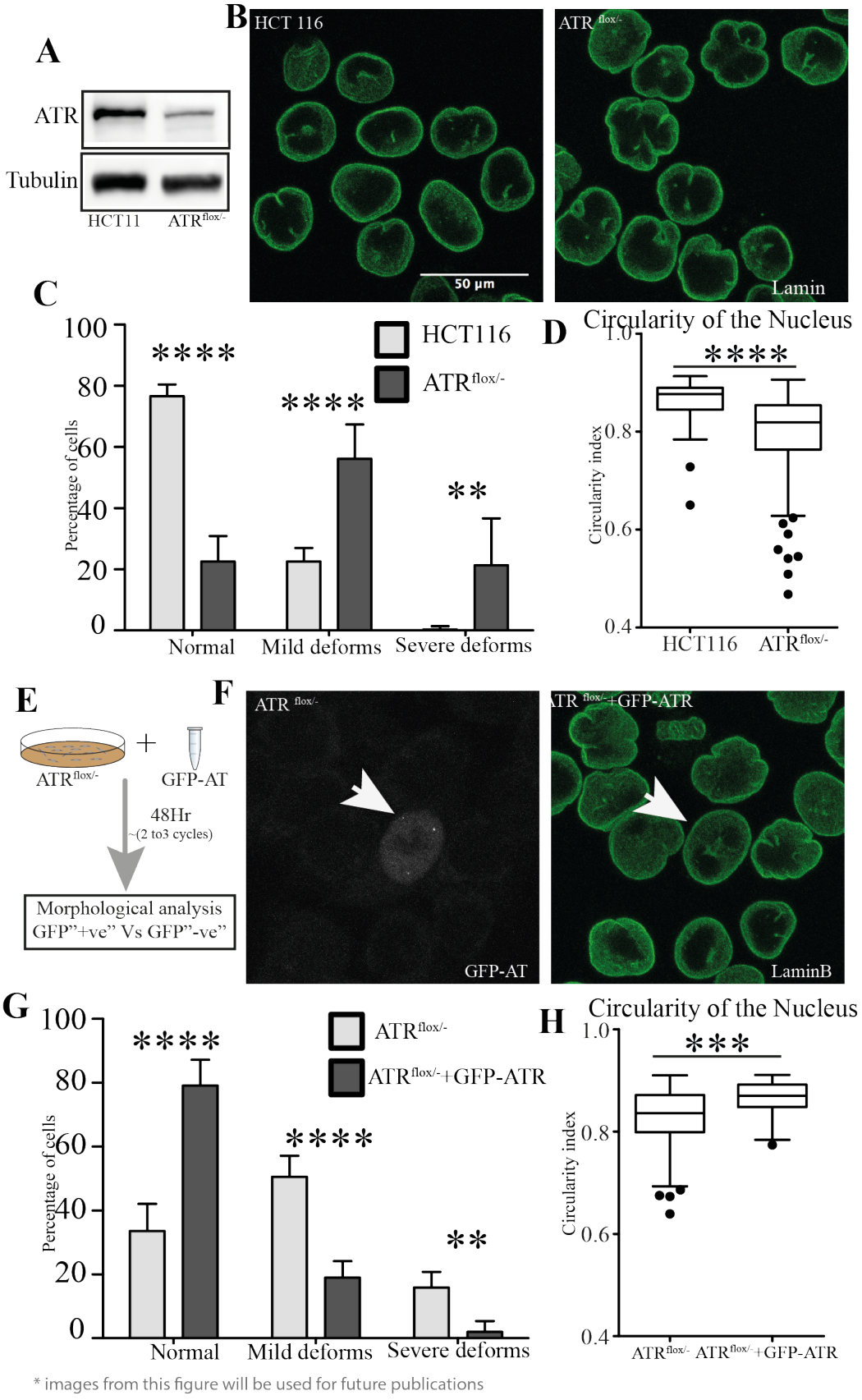

Figure 21- Introducing GFP-ATR rescues the nuclear defects of ATR defective cells. (A) Western-blot of ATR levels in HCT116 and its derivative ATR $^{flox/-}$. (B) Morphological abnormalities in ATR$^{flox/-}$ cells and (C) its analysis. (D) Circularity index. (E) Scheme for rescue experiment. (F) IF image of ATR$^{flox/-}$ cell with restored GFP-ATR (arrow) has normal nuclear shape. (G)Quantification of recued nuclear shape in ATR$^{flox/-}$ cells and (H) restoration of their circularity.

modified HCT116 cells with reduced ATR levels (by approx 80%) compared to original HCT116 cells (Figure 21A). Even in these $ATR^{flox/-}$ cells we observed compromised nuclear morphology similar to shATR cells (Figure 21B, C, D). We transfected $ATR^{flox/-}$ cells with GFP-ATR, fixed them after 48hours and analyzed the GFP positive nuclei by comparing them with non-transfected $ATR^{flox/-}$cells in the same field (Figure 21E, F). Reconstituting ATR in $ATR^{flox/-}$ cells rescued nuclear defects, restored circularity index of the nucleus (Figure 21F, G, H), confirming that the morphological defects in cells lacking ATR are a direct effect of ATR and can be rescued by reconstituting ATR to normal levels.

2.3 ATR maintains chromosomal architecture

Membrane bound ATR was previously reported to regulate the mechanical stress imposed by the topological constrains during replication and condensation (Kumar et al., 2014, Bermejo et al., 2011). We hypothesized that the deformations in shATR cells could be forming due to the inability of the cells to properly respond to such topological stress. So, we performed EM analysis of shATR cells. Control and ATR depleted, exponentially growing, HeLa cells were fixed and carefully analyzed for defects in the perinuclear region. In shATR cells we noticed increased invaginations, micronuclei, higher amount of heterochromatin associated to the NE, nucleoli coated with heterochromatin attached to the NE particularly at the invaginations (Figure 22). Pathological categories of invaginations include type I invaginations where inner membrane alone forms invagination separated from the outer membrane and type II deformations where both membranes form invagination (Malhas et al., 2011). In shATR cells we observed both type I and type II nuclear invaginations (Figure 22A, B). Interestingly, majority of invaginations in shATR cells were associated with chromatin or nucleoli reflecting inadequate topological stress management machinery (Figure 22A, C, D). Previously characterized “nucleolar canal” structures, commonly absent in normal cells (Bourgeois

et al., 1979) were more frequent in shATR cells (Figure 22A, B, D). These structures were hypothesized to regulate rRNA export from the nucleoli to cytoplasm. The increase of nucleolar canals inshATR cells could as well be a consequence of defective rRNA metabolism and export. Type I invaginations were very common in shATR nuclei; in some extreme cases we also observed fragmented inner nuclear membrane attached to nucleoli in the nucleoplasm.

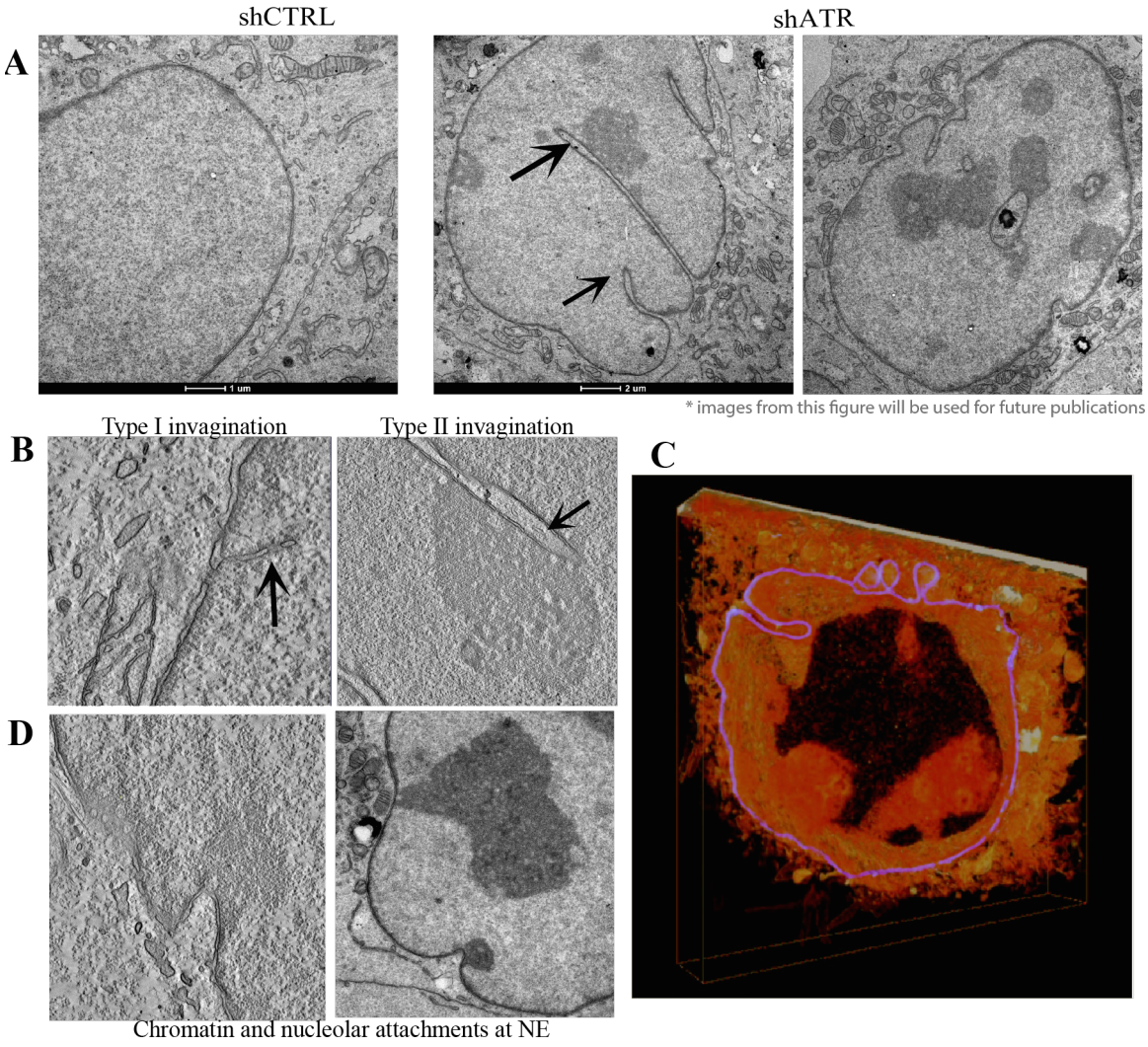

Figure 22 - EM analysis of nuclear abnormalities in ATR depleted cells
(A-D) EM analysis of control and shATR nuclei with defective morphology. (B) Sample nuclei from control and shATR cells. (B) Type I and type II nuclear invaginations are exhibited by shATR nuclei. (C) 3D reconstruction of shATR nuclei section (E) NE associated condensed chromatin and nucleolar attachment to the NE in shATR cells, particularly at the invaginations.

We imposed replication stress by treating cells with HydroxyUrea (HU) to increase the topological stress. The nuclear deformations previously observed in shATR cells were amplified after HU treatment resulting in more severely deformed nuclei with almost all the nucleoli attached to NE (Figure 23). A previous study also reported similar nuclear deformations in cells overexpressing the kinase dead form of ATR (ATR-kd) and amplification of nuclear deformations upon HU treatment (Cliby et al., 1998).

By combining current study, afore mentioned report (Cliby et al., 1998) and previous work from our group, we suggest that ATR functions as a kinase at the NE regulating membrane architecture even though the kinase activity is not necessary for NE binding of ATR (Kumar et al., 2014).

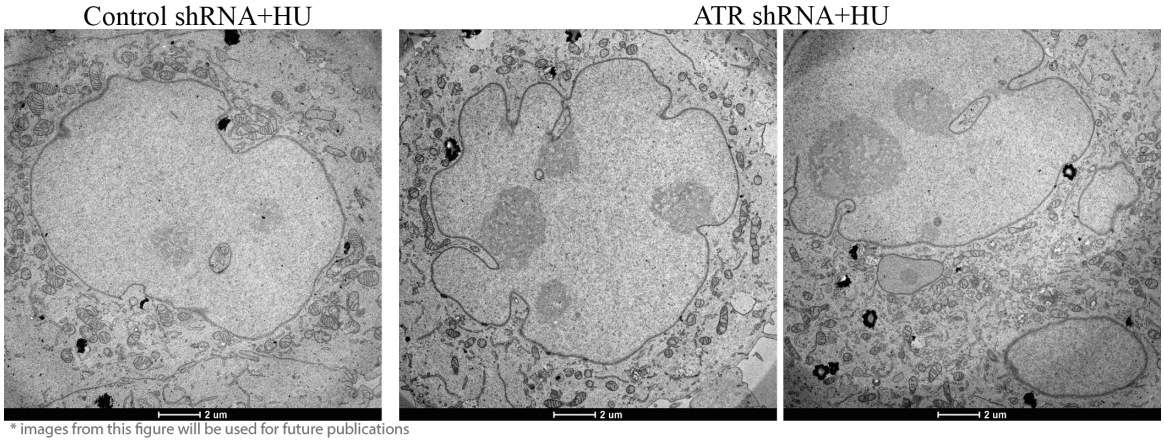

Figure 23 - Replication stress increases nuclear abnormalities in ATR depleted cells
EM analysis of control and shATR nuclei treated with HU (2mM, 16 hours).

Preferential cleaving of decondensed chromatin by DNAse I is classically utilized as an indirect measure of heterochromatin level in cells. To confirm our EM observations of NE attached heterochromatin we utilized this *in-situ* DNase I sensitivity assay (Weintraub and Groudine, 1976). Control and shATR HeLa cells arrested in G1 phase of cell cycle were permeabilized, incubated with DNAse I (50U/ml) for 20 minutes at room temperature, fixed and stained with DAPI. Average area of shCTRL was reduced to 80% of its initial size (Figure 24), while shATR cells were more resistant to DNAse treatment

reducing their size by retaining approximately 95% of its nuclear size. This simple but elegant assay clearly demonstrated the increase of condensed DNA in absence of ATR.

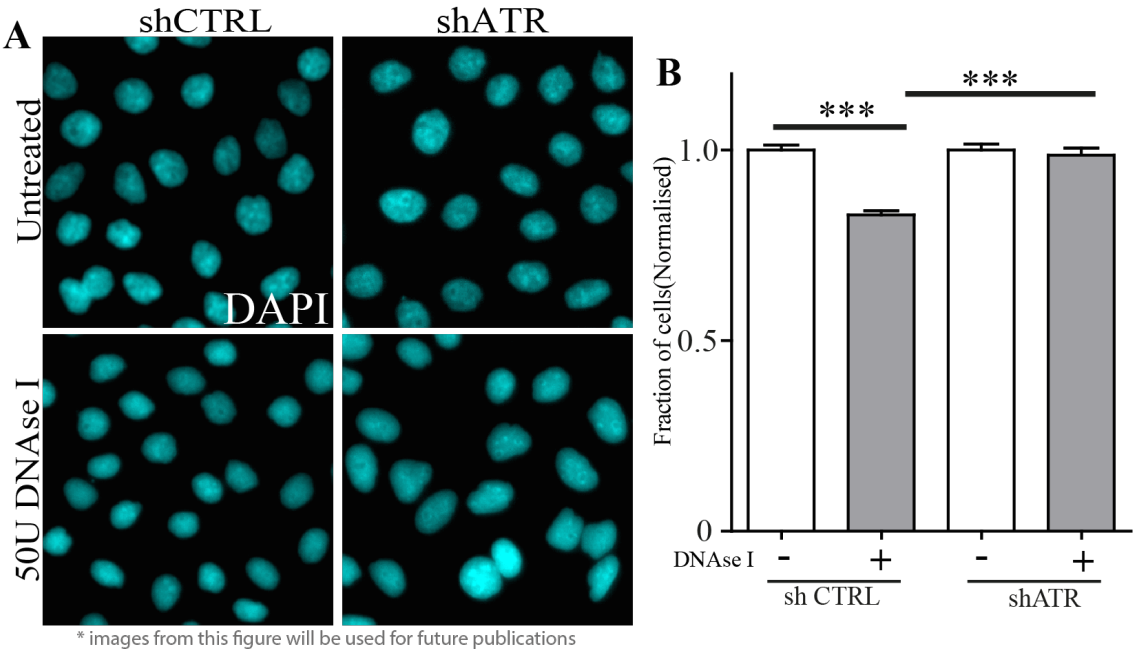

Figure 24 - DNAseI assay indicating higher heterochromatin levels in shATR cells
shATR cells are less susceptible to DNAse I cleavage compared to controls as measured by the reduction in nuclear area (n>100). (A) Example images and (B) quantification.

To further confirm the observation we analyzed the level of heterochromatin landmark, H3K9 tri-methylation in ATR defective cells. First we stained and quantified H3K9Me3 intensity in primary fibroblasts from Seckel mice. We observed a significant increase (approx. 35% gain) in H3K9Me3 signal intensity (Figure 25A, B). We then confirmed this also in shATR U2OS cells, using both Western blot and Immuno-fluorescence. We noticed an increase of about 20% signal intensity of H3K9Me3 in cells lacking ATR (Figure 25C, D, E). These two independent techniques argue that cells lacking ATR have a slight increase of condensed chromatin, in-line with the observations from EM analysis thus suggesting that ATR depleted cells have only higher levels of heterochromatin associated to the NE, without much increase of heterochromatin.

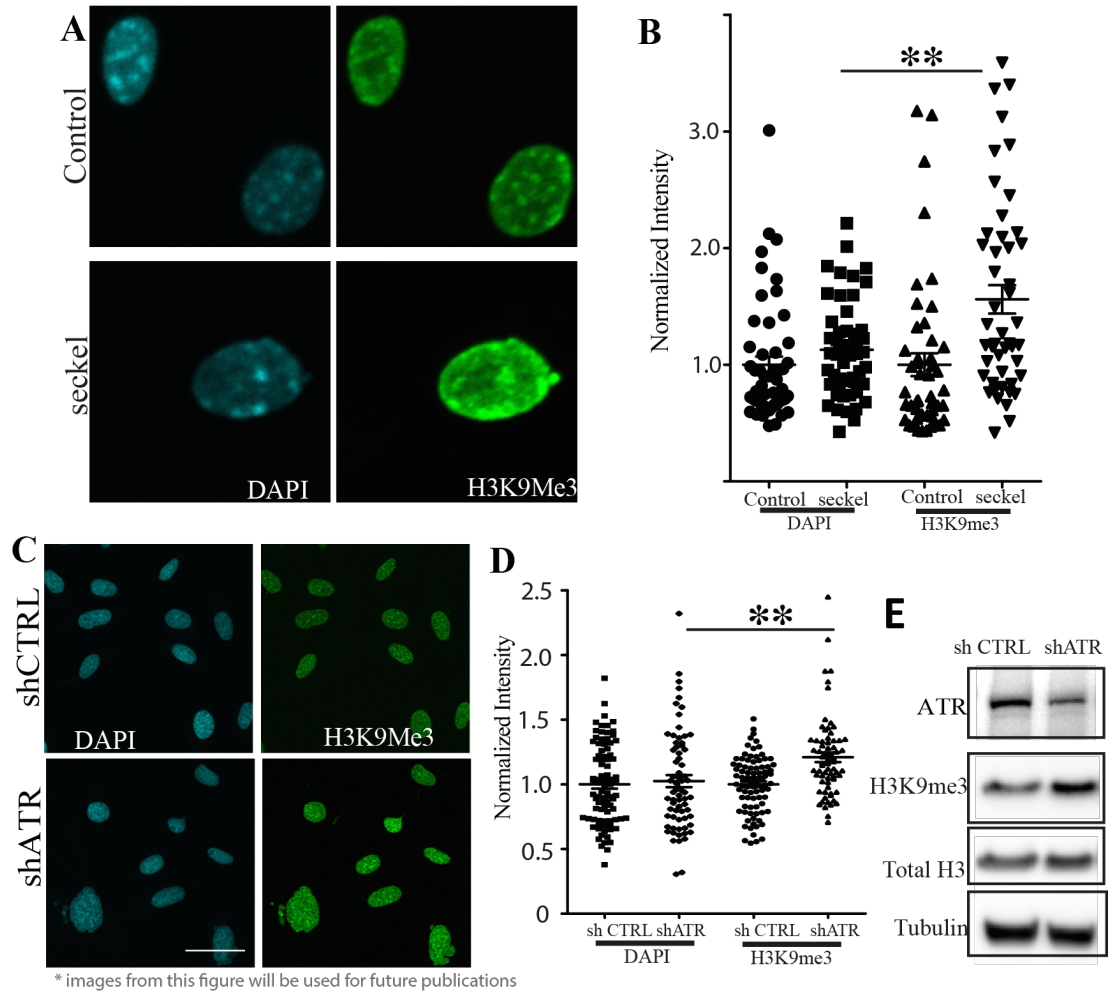

Figure 25 – Cells lacking ATR have higher heterochromatin.
(A) H3K9Me3 staining of control and Seckel cell nuclei (n>50), and (C) of control and shATR nuclei (n>80). (B, D) Normalised signal intensity of H3K9 tri-methylation. H3K9me3 signal is normalized to respective mean DAPI intensity. p-value calculated using one-way ANOVA(E)Western blot analysis of H3K9me3 in shATR and control cells.

Checkpoint kinase I (Chk1), is a well-characterized downstream target of ATR signaling pathway(Awasthi et al., 2015). It was also phosphorylated by ATR at the NE in response to mechanical stress(Kumar et al., 2014). Hence, we decided to test the contribution of Chk1 to the observed phenotype of ATR depleted cells. We analyzed the nucleus of Chk1 depleted HeLa cells (siRNA) using EM. Even-though there we could observe an increase in number of deformed nuclei; we failed to observe any increase in condensed chromatin or nucleoli associated to NE (Figure 26A). Addition of HU to Chk1 depleted cells also did not mimic the effect of ATR depletion (Figure 26B). Hence we conclude that ATR directly regulates NE dynamics without the involvement of canonical

ATR/Chk1 signaling pathway. However, ATR/Chk1 signaling pathway is activated only if NE experiences severe mechanical stress (Kumar et al., 2014). The nuclear morphological defects of Chk1 deficient cells could be due to the altered level of ATR activation in absence of Chk1 (Syljuasen et al., 2005).

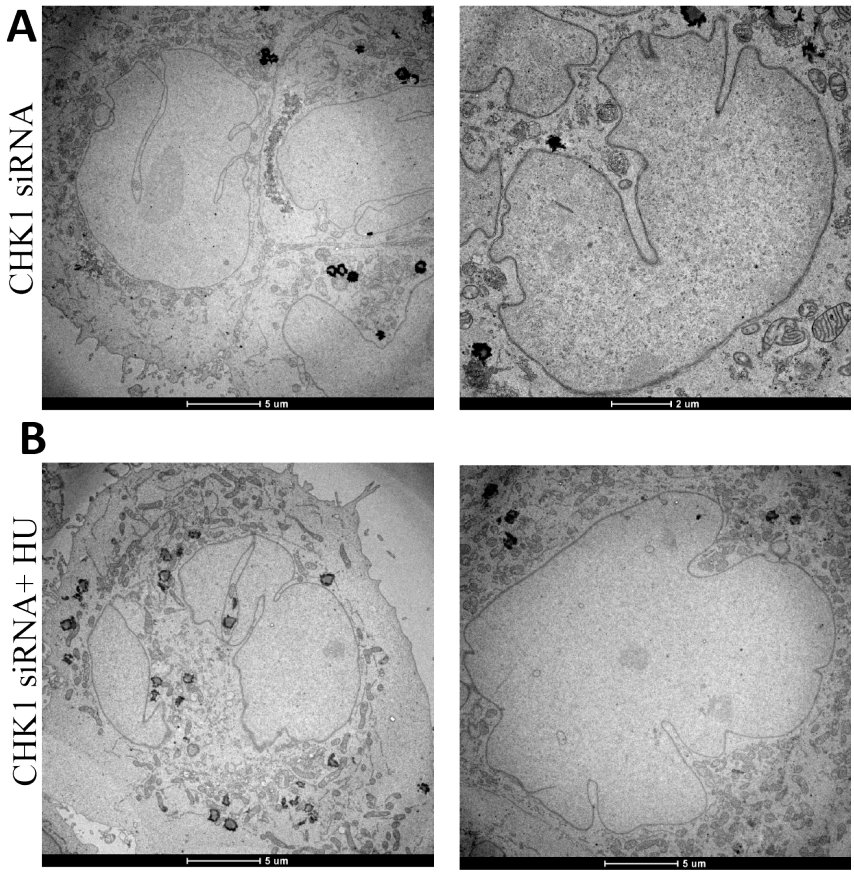

Figure 26 - EM analysis of nuclear abnormalities in Chk1 depleted cells
(A) siRNA mediated depletion of Chk1 also results in abnormal nuclei, and (B) also when treated with HU. However, there are no nucleoli or heterochromatin attached to NE.

2.4 ATR depletion phenotypes are lamin independent

Defective nuclear morphologies are a common hallmark of laminopathy and Progeroid cells and majority of these laminopathies are caused by mutations in lamins particularly LMNA gene (Osmanagic-Myers et al., 2015, Gordon et al., 2014). ATR–knockout mice and humanized Seckel mouse develop progeroid phenotypes and exhibit premature aging phenotype (Murga et al., 2009, Ruzankina et al., 2007) similar to progeria patients (Gordon et al., 2014), suggesting that lamin could be the primary player of shATR nuclear abnormalities. Therefore, we examined LMNA mRNA and protein levels, and localization in ATR depleted cells.

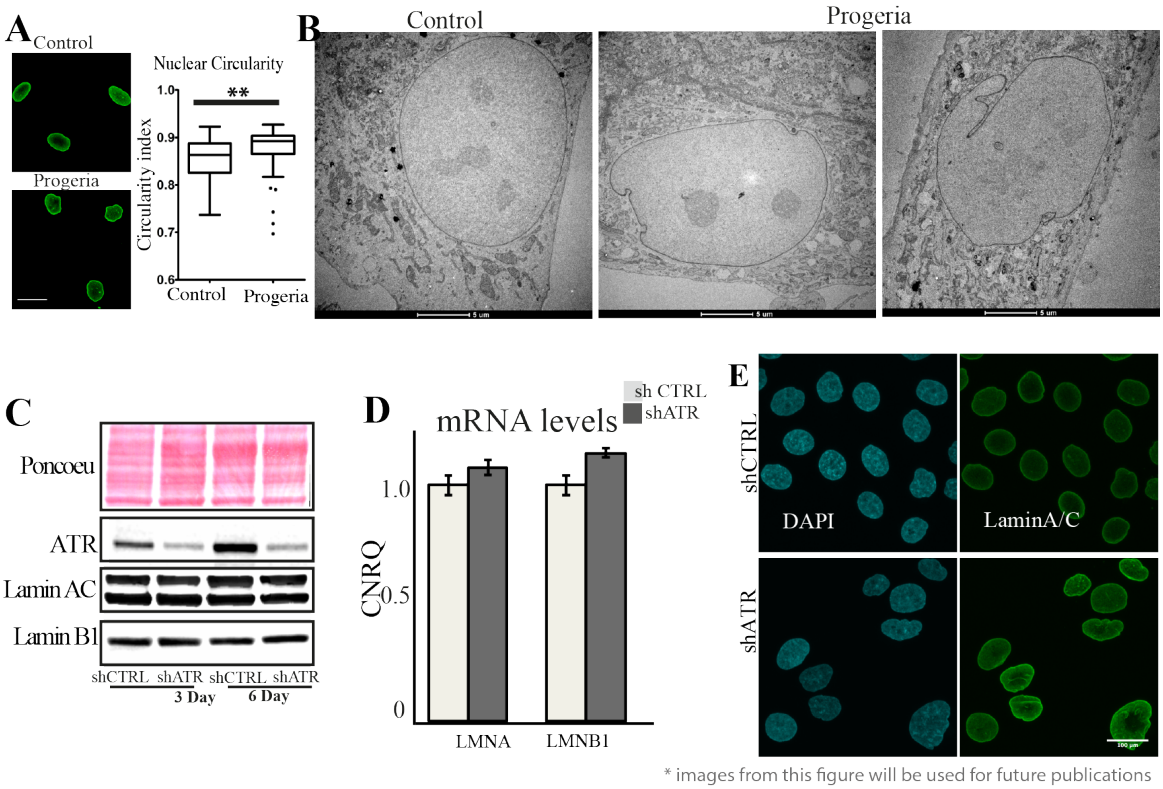

Figure 27- Nuclear abnormalities of shATR cells are not caused by lamins
(A) Nuclear shape defects of progeria visualized with lamin staining and increase in circularity index (n=90 and 81 respectively) (B) Primary fibroblasts from progeria patients with defective nuclear morphology, did not exhibit condensed chromatin or nucleolus attached to NE (C-E) Lamins show no significant change in the (C) protein level (western-Blot analysis) (D) in mRNA level (qPCR analysis) and in (E) cellular localization (IF analysis).

We noticed no obvious changes in protein levels or localization of lamin A/C in absence of ATR; in addition, we also checked for Lamin B1 alterations but could not detect any obvious defects (Figure 27C, D, E). We failed to detect any significant changes in LMNA and LMNB1 mRNA levels, though there was a slight insignificant increase in mRNA levels. We also analyzed the nucleus of progeria patient fibroblasts to score for similarities in invaginations. As reported previously we observe type II nuclear invaginations in progria fibroblasts (Figure 27A, B), progeria nuclei had no type I invaginations and no heterochromatin or nucleoli attached to NE, which are common phenomenon in ATR depleted nuclei (compare Figure 22A to Figure 27B). Loss of ATR leads to higher heterochromatin association to the NE, unlike in laminopathies where both loss of LMNA and accumulation of its mutant form progerin at the NE, detaches

chromatins from the NE (Sullivan et al., 1999, Goldman et al., 2004). It is also interesting to note that ATR Seckel mice develop progeroid phenotypes(Murga et al., 2009) much earlier in development compared to LMNA-/- mice (Sullivan et al., 1999). Hence, ATR depletion results in morphological defects of the nucleus that are progeroid-like but are not caused by alteration of lamins.

2.5 Conclusions

Our data indicate that ATR binds to membranes, particularly to NE and stimuli like mechanical stress at the NE can increase this interaction. At the NE ATR regulates nuclear morphology, chromosomal architecture and co-ordinates nuclear dynamics. Loss of ATR leads to collapse of nuclear morphology, characterized by deformed nuclear shape, pathological invaginations of nuclear membranes, compromised chromosomal architecture with heterochromatins and nucleoli attached to the NE and increased micronuclei. We further demonstrate that nuclear defects in shATR cells are independent of Lamins and canonical ATR/Chk1 pathway. Though ATR mice models and cellular depletion of ATR display progeroid like phenotypes (Murga et al., 2009, Ruzankina et al., 2007), closer analysis reveals that shATR cells exhibit completely different morphological features compared to progeria. Taking these observations together, we can conclude that ATR regulates nuclear and chromosomal architecture at the NE and morphological defects in ATR depleted cells are resulting from mishandling of nuclear dynamics at the NE in absence of ATR.

Chapter 3

ATR regulates mechanical properties and membrane stability of nuclear envelope

Nuclear envelope regulates several essential aspects like chromosomal organization, transcription, replication, DNA repair and thereby influencing cellular fate, cellular homeostasis and cell migration (Bell and Lammerding, 2016, Zuleger et al., 2011). Nuclear shape is vital for cell movement and maintenance of cell plasticity. Majority of the laminopathies and progeroid cells have fragile nuclei with defective mechanical properties, inefficient mechanotransduction and abnormal nucleocytoskeletal coupling (Dutta et al., 2016, Verstraeten et al., 2008). Different diseases have different cellular and nuclear stiffness based on the mutations that they carry. Dilated cardiomyopathy (DCM) with loss of LMNA has reduced stiffness (Gupta et al., 2010), while Hutchinson–Gilford progeria syndrome (HGPS) patient cells have stiffer cell nucleus (Verstraeten et al., 2008). However, all these patient cells, have impaired mechanosensing and are incapable of adapting to mechanical stress conditions. ATR knockout models develop progeroid syndrome (Murga et al., 2009, Ruzankina et al., 2007) and ATR depleted cells exhibit nuclear abnormalities similar to progeroid cells (this study). Since defective nuclear morphology in laminopathies are coupled with changes in mechanical properties of NE, defective mechanosensing and inpaired mechanotransduction, we hypothesized ATR depleted cells to have similar defects as well. Therefore, we measured the mechanical properties of shATR cell and the nucleus.

3.1 ATR depleted cells have softer nuclei

Cellular elasticity and viscosity are prominent parameters for defining mechanical properties of a cell. Cellular elasticity is defined as its ability to recover a deformation. Several techniques have been developed to measure the elasticity of a cell, including micropipette aspiration, optical tweezers, magnetic bead microrheometry and atomic force microscopy (AFM). We tested the rigidity of the ATR depleted cells using AFM. In brief, the system optically measures the deflection of the cantilever, when the cantilever

tip encounters cell surface. A force-indentation curve is generated by AFM measurements, composed of deflection readings during the approach, compression and decompression of cantilever tip into the cellular surface(Yallapu et al., 2015, Lekka, 2016). Young's modulus or elastic modulus of the cell is derived from this force plot. Higher Young's modulus correlates with stiffer objects, as higher forces are required to indent the object. Cells lacking ATR had a significantly reduced elastic modulus compared to control suggesting much softer cellular structure (Figure 28A), suggesting ATR depleted cells are softer than their control counterparts. Cell elasticity is depends on several components such as the cytoskeleton, membrane rigidity and the organelles including the nucleus. Even-though nucleus is stiffer organelle than cytoplasm (Guilak et al., 2000, Caille et al., 2002), it is not sufficient to conclude this to be the main source of cellular elasticity since cytoskeletal components, particularly actin networks is known to contribute significantly to cell elasticity (Haga et al., 2000).

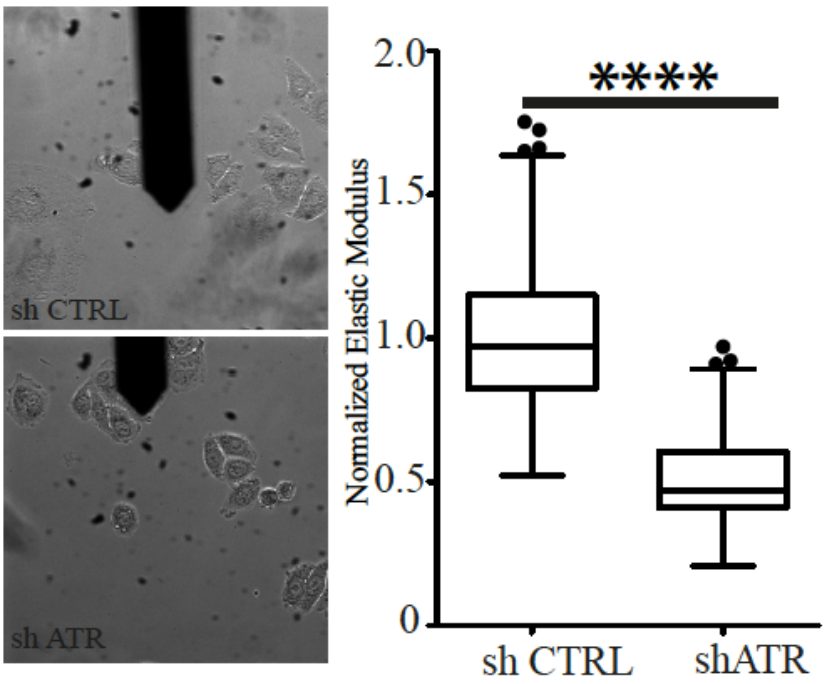

Figure 28- shATR cells are softer than controls
Example image showing cell and AFM cantilever. Elastic modulus measured by AFM and normalized to average of control (n>100). Student ttest performed for p-value.

In our measurements we carefully placed the cantilever tip on the nuclear region of the cell, in order to amplify the nuclear contributions, but to rule out the contribution of cytoskeleton on the overall softness of shATR cells, we measured the stiffness of isolated nuclei. Consistent with cellular elasticity measurements, isolated nuclei of shATR cells were softer compared to controls (Figure 29A, B), confirming that the softness of shATR cells is because of softer nuclei. Interestingly we also noticed that shATR nuclei had higher frequency of aberrant force plots (Figure 29C, D).

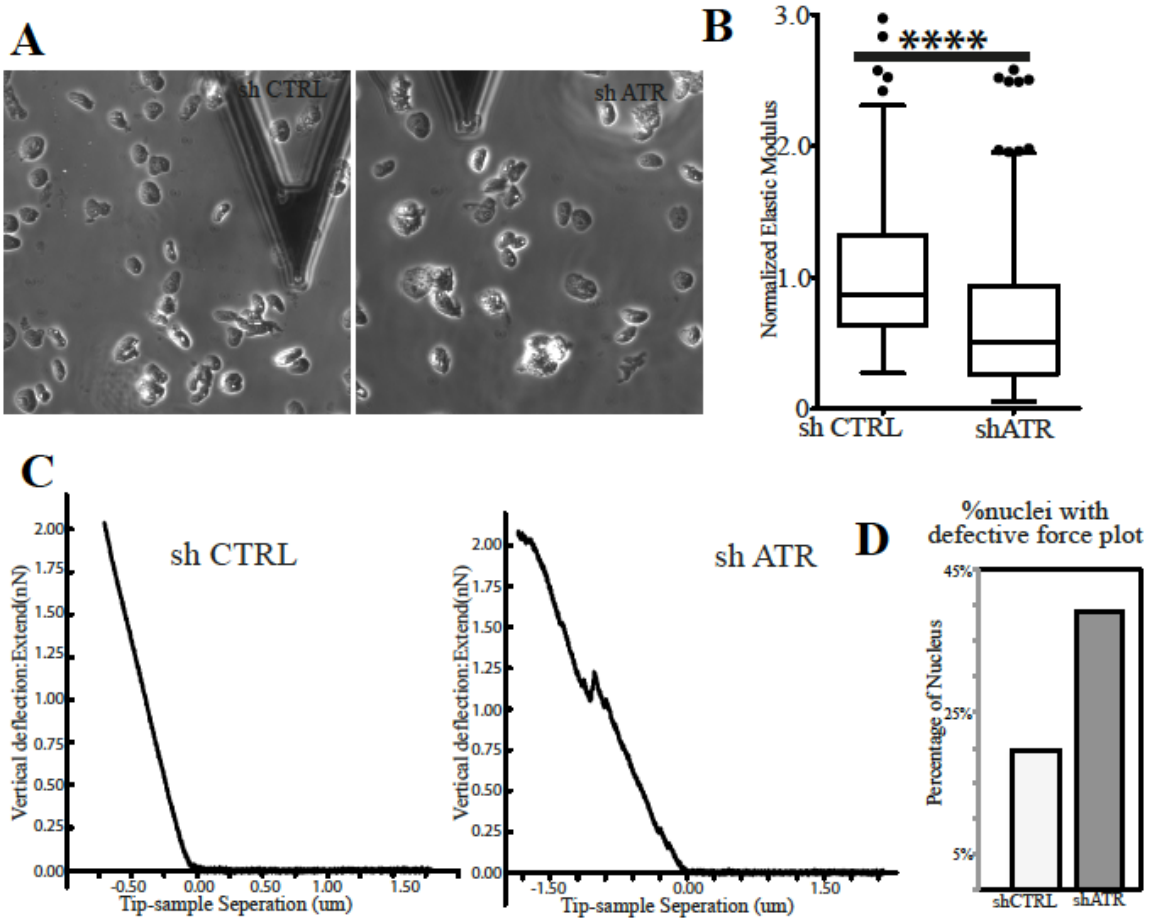

Figure 29- shATR cells have softer nuclei with abnormal composition.
(A) Example image showing isolated nuclei from control and shATR with AFM cantilever. (B) Elastic modulus of nuclei measured by AFM normalized to average of control (n>100). (C) Typical force plots observed in control nuclei and abberent forceplots of shATR nuclei. (D) Quantifications indicating that increased shATR nuclei exhibit abnormal force plot.Student ttest performed for p-value.

The increase was from 20% in controls to 50% in shATR consistent with the percentage of deformed nuclei in ATR depleted cells (Figure 18C). Two major components that regulate the nuclear elasticity are NE or lamins and chromatins, the load-bearing component of the nucleus (Mazumder and Shivashankar, 2010, Dahl et al., 2005). Our observations show that ATR depleted cells have defects in both of this components. Compromised nuclear integrity and uneven distribution of heterochromatin could lead to nuclear collapse during nuclear compression by the cantilever and this could be the reason for increased number of abnormal force plots in ATR depleted cells.

3.2 ATR interacts with nesprin-2 at the NE

Nucleus maintains its equilibrium by coordinating internal events such as transcription and replication with the external environmental cues. Nuclear envelope is vital for maintaining this nuclear steady state, since it serves as a mechanosensor, communicating with nuclear components as well as the cytoskeleton. Components of NE such as nuclear pores, the LINC (linker of the nucleus and cytoskeleton) complex, emerin and lamins, mediate mechanotransduction at the NE and are essential maintaining nuclear integrity. In a functional NE, mechanical signal from external environment can cause epigenetic regulations, chromosomal rearrangements and transcription activation and physical alterations in the nucleus could induce cytoskeletal arrangements. Loss of these components could lead to pathologies such as progeria, cardiomyopathy and muscular dystrophy. ATR depleted cells, also develop nuclear abnormalities indicating a compromised nuclear integrity as a result of mismanagement of topological stress, evident by appearance of heterochromatin and nucleoli attached to the NE. However, a normal NE is capable of resolving such invaginations by modulating nuclecytoskeletal forces.

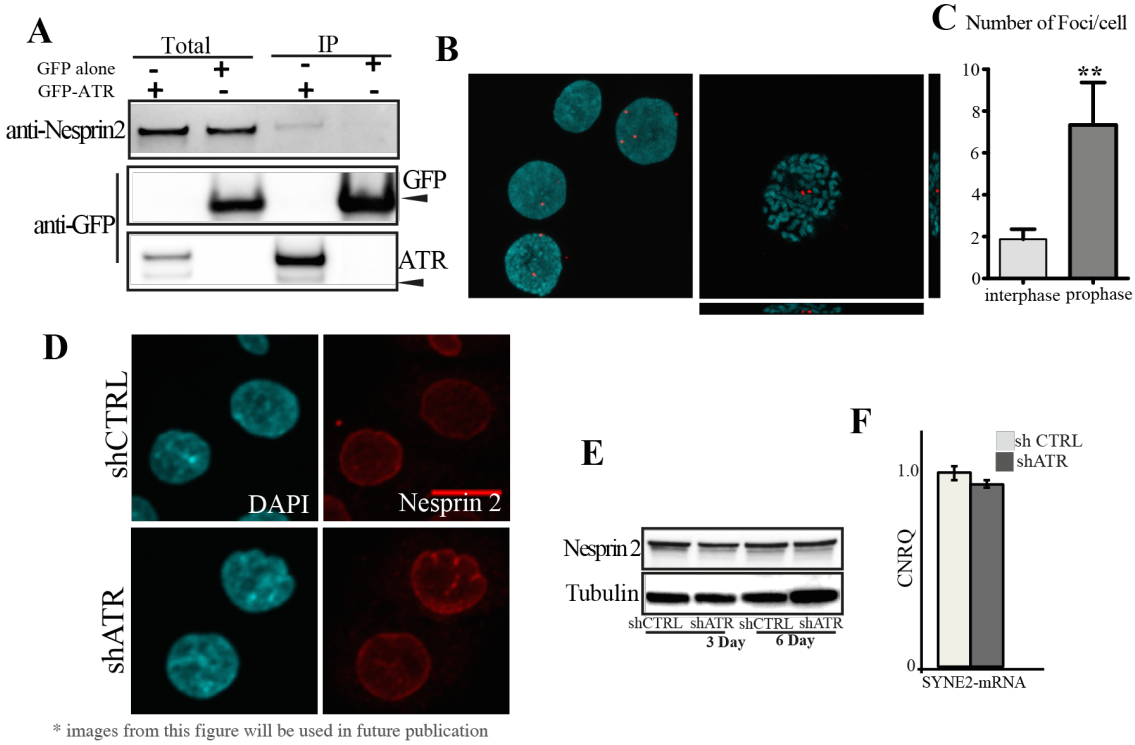

Figure 30 - ATR interacts with nesprin-2 at the nuclear envelope.
(A) Western blot analysis of GFP-ATR immuno-precipitation. Interaction with nesprin is confirmed by blotting for nesprin 2, GFP alone was used as a negative control, pull down validated by antiGFP bands of GFP alone and ATR-GFP (B) Proximity ligation assay of ATR and nesprin-2. Right image shows a section of image with XZ and YZ views. (C) Number of PLA foci per cell (n>10). (D) Confocal stack of shATR and control nuclei stained with nesprin 2. (E) Western blots showing protein levels of nesprin do not alter in shATR cells. (F) mRNA levels of nesprin-2 remain similar to controls and shATR HeLa cells.

ATR depleted cells have defective nuclear morphology along with compromised chromosomal architecture. Since the defects are unlikely to be caused by lamins, we focused on ATR interaction with nesprin-2 (Figure 14E). Nesprin -2 is a member of LINC (Linker of Nucleoskeleton and Cytoskeleton) complex. The LINC complexes are composed of SUN (Sad1 and UNC-84) proteins (SUN1 and SUN2) and KASH (Klarsicht, ANC-1, and Syne Homology) proteins (nesprin1, 2 and 3). The LINC complex with SUN in the inner nuclear membrane and KASH protein on the outer nuclear membrane connects nuclear lamina with the cytoskeleton.

We found Nesprin-2 to be an interactor of ATR in our proteomics screens (figure 14E). Nesprin-2 is a outer nuclear membrane protein containing C-terminal KASH

domain for binding to SUN2 at the NE and N-terminal actin binding domain for connecting to cytoskeleton (Meinke and Schirmer, 2015). Interestingly, NE bound ATR was also localized to outer nuclear membranes and perinuclear actin fibers. Keratinocytes depleted of nesprin-2 show similar nuclear defects as ATR (Luke et al., 2008) and nesprin-2 knockout murine cardiomyocytes had heterochromatin dense regions attached to NE (Banerjee et al., 2014). Nesprin-2 has several potential ATR phosphorylation sites and is phosphorylated in s-phase of cell cycle (Olsen et al., 2010) as well as during mitosis. Therefore we decided to further characterize the ATR and nesprin-2 interaction. We confirmed the interaction by immune-precipitating GFP-ATR and blotting for nesprin-2 (Figure 30A). Then we performed proximity ligation assay (PLA), to gain insights into the localization of ATR and nesprin-2 interaction. PLA is a advanced immunofluorescence technology used to confirm and quantify protein-protein interactions with single molecule resolution. We observed majority of foci formation around the nuclear periphery (Figure 30B), suggesting that the interaction was perinuclear. In some cells we also noticed one in the cytoplasm, could be localized to centrosomes. However, further experiments are required for confirming this. In an interphase cell we could observe foci counts of zero to four averaging to two foci per cell. Interestingly, the foci number was significantly higher in cells undergoing mitosis (Figure 30C). This suggests that the ATR-nesprin2 interaction is dynamic in nature and could vary depending on the membrane tension or mechanical forces at the NE. We then analyzed the status of nesprin-2 in ATR depleted cells. HeLa cells lacking ATR had no obvious defects in nesprin-2 localization (Figure 30D). ATR depletion did not affect the protein level or mRNA stability of nesprin-2 (Figure 30E, F). Considering that the interaction between ATR and nesprin-2 is very weak according to western blot (compare nesprin-2 levels in input to IP in Figure 30A), and PLA analysis (Figure 30B) and stress induced (Figure 30C), it is unlikely that disruption of such weak interaction could influence the stability of one protein, in this case nesprin-2.

3.3 Loss of ATR impairs nucleocytoskeleton connections and NE tension

Nuclear shape and its anchorage to the cytoskeleton are essential components of cell function and homeostasis. Nucleocytoskeletal coupling ensures faithful transfer of forces from the cytoskeleton onto the nucleus. Since ATR interacts with nesprin-2 at the NE and ATR depleted cells show defective nuclear dynamics, we hypothesized that the nuclear cytoskeletal connections (via LINC) in shATR will also be compromised. We utilized a recently reported mini-nesprin-2G FRET tension sensor (Arsenovic et al., 2016), a tension sensor that directly measures mechanical tension applied to the LINC complex, for measuring the tension at the nuclear envelope in ATR depleted cells. This sensor consists of a fluorophore and chromophore attached before the actin binding domain and the KASH domain, separated by linear-elastic spring of spectrin repeats (Figure 31A). Cytoskeletal tension stretches the sensor, increasing the distance between the fluorophore and chromophore, reducing the FRET, while Nesprin-2G sensor not

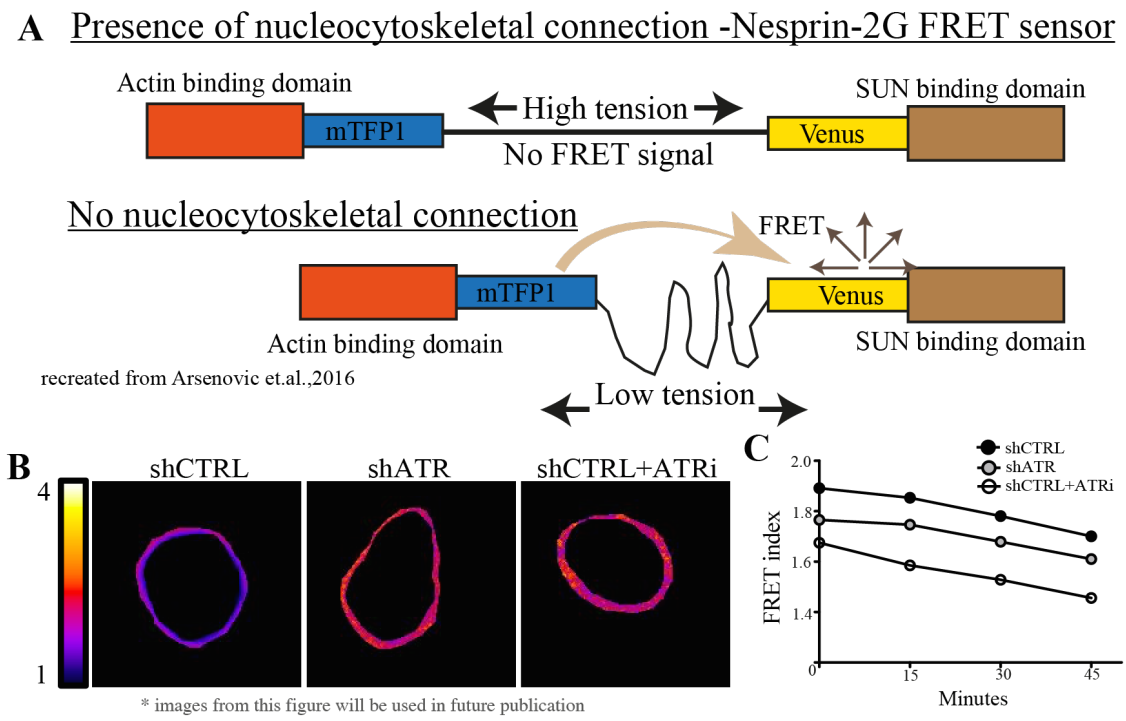

Figure 31 - Defective ATR reduces nesprin-2 mediated nuclear envelope tension
(A) Nesprin-2G tension sensor working scheme. (B) Examples of shCTRL, shATR and shCTRL cells in presence of ATR inhibitor (1 to 2 hours, n>20). (C) Quantification of FRET index over a period of 1 hour.

bound to cytoskeleton is relaxed with fluorophore and chromophore in close proximity to generate FRET signal. Hence, FRET is inversely proportional to force. We measured the membrane tension exerted by cytoskeleton at the NE in cells with or without ATR, using this FRET- sensor of Nesprin-2G. We micro-injected the control and shATR HeLa cells with the Sensor plasmid to ensure uniform expression of sensor, and focused on the equatorial section of the nuclei as suggested in the Arsenovic et.al.,(Arsenovic et al., 2016) We performed time-lapse up to 1 hour, until the signal started to bleach. We compared the FRET signal of control cells with the control cells treated with ATR inhibitor or depleted of ATR. Cells defective for ATR, through inhibition or depletion, exhibited an increased FRET signal at the NE that implying reduced membrane tension (Figure 31). This clearly demonstrates that ATR regulates membrane mechanics and responds to mechanical alternations of the nuclear envelope.

3.4 Conclusions

In this section we conclude that ATR regulates mechanical properties of NE. ATR depleted cells have defective nuclear mechanics along with defective nuclear morphology. shATR cells are much softer, mainly due to their soft nuclei, these fragile shATR nuclei fail to keep up with mechanical assaults and collapse under stress. We introduce a new role of ATR in maintaining NE homeostasis by regulating chromatin association at the inner part of NE and cytoskeletal connections at the outer compartment of NE. We also discovered a novel, stress induced, dynamic interaction between ATR and nesprin-2 at the NE. ATR depletion or inhibition uncouples nucleocytoskeletal connections resulting in lower membrane tensions at the NE.

Chapter 4

ATR facilitates cell migration and metastasis

Cell migration is a complex process involving coordination of several cellular compartments including cytoskeleton, nucleus, Golgi and centrosomes. During migration cytoskeletal alterations lead to cell polarization and elongation, followed by reorientation of Golgi, centrosomes and nucleus in the direction of migration (Liu et al., 2016), which is then followed by the actomyosin network-mediated dragging and pushing of nucleus along the actin filaments. Nuclear integrity is a prerequisite for 2D and 3D migration since factors such as size, stiffness of the nucleus, morphology and chromatin architecture can pose challenge for cell migration. Loss of Lamins or accumulation of their mutant forms hinders the migration ability of cell (Verstraeten et al., 2008, Houben et al., 2009). Loss of LINC complex leads to failed force transmission from the cytoskeleton to nucleus resulting in defective nuclear positioning and cell migration(Yu et al., 2011). In addition, condensed chromatin and migration-induced global chromatin condensation (Gerlitz and Bustin, 2010, Gerlitz and Bustin, 2011), could alter nuclear stiffness, which in turn also contribute to migration defects. ATR interactor nesprin-2 regulates nuclear membrane architecture(Luke et al., 2008) and mediates centrosome association and nuclear positioning in migration and neurogenesis (Zhang et al., 2009). Cells lacking Nesprin-2 show defective nuclear morphology, defective wound healing ability (Rashmi et al., 2012) and alter migration in 3D(Jayo et al., 2016, Thomas et al., 2015).

ATR depleted cells have defective nuclear morphology, mechanical properties and impaired nuclear cytoskeletal connections. So, we reasoned that the cells lacking ATR would have migration defects as well. Therefore, we tested the migration ability of ATR defective cells in several migration paradigms including single cell migration and collective migration though wound healing. Interstitial migration through narrow pores pose much severe challenge to the nucleus demanding it to adapt into deformed morphology, unstable mechanical microenvironment and increased membrane stress. NE components such as lamins, surrounding perinuclear actin and efficient repair pathways of NE and DNA are all reported to be essential during such migrations (Raab et al., 2016,

Denais et al., 2016, Lammerding and Wolf, 2016, Skau et al., 2016). We reasoned that intrinsic tendency of ATR-defective nuclei to collapse in response to mechanical stress should make cells unable to efficiently migrate through narrow pores. We tested fate of ATR depleted cells in the *in-vitro* 3D migration inside constrictions and their ability to survive the journey through the circulatory system and efficiently invade host organs. We also analyzed *in-vivo* migration of ATR depleted neurons in a developing mouse brain.

4.1 Cells migrate slower in absence of ATR

To test the role of ATR in migration we first performed the time-lapse of control and Seckel immortalized fibroblasts, and quantified their velocity by manual tracking. Seckel cells were moving less with lower mean velocity compared to controls in similar conditions (Figure 32).

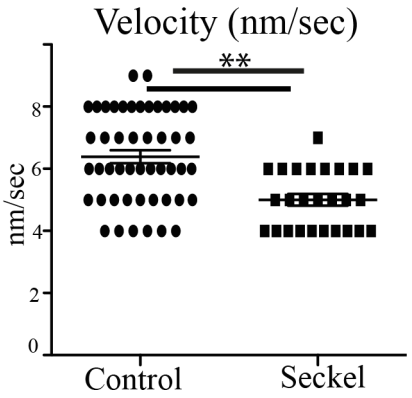

Figure 32 - ATR Seckel fibroblasts migrate less on culture dish.
Immortalized control and Seckel mouse embryonic fibroblasts imaged and tracked for 24 hours. Graph shows mean velocities of control ans Seckel MEFs. (Control n= 48; Seckel n=27). Student t-test, performed ($p<0.001$).

We analyzed the migration of U2OS cells on 2D micro patterned lines of 10-micron thickness, in presence or absence of ATR inhibitor. Cells are treated with DMSO or ATR inhibitor (AZ20 -1uM) for 1 hour, then trypsinised and loaded on (with DMSO or ATR inh) to the glass coverslips with fibronectin coated lines of 10 micron thickness. After 3 hours incubation for cells to settle down, 24 hour time-lapse image acquisition was set with 10 min time interval between images. Images were then analyzed using a

macro on imageJ. Cells treated with ATR inhibitor showed a reduced velocity of migration and covered lower distance (Figure 33). ATR inhibitor treated cells also were changing directions more frequently and were also less persistent compared to controls (Figure 33A, B).

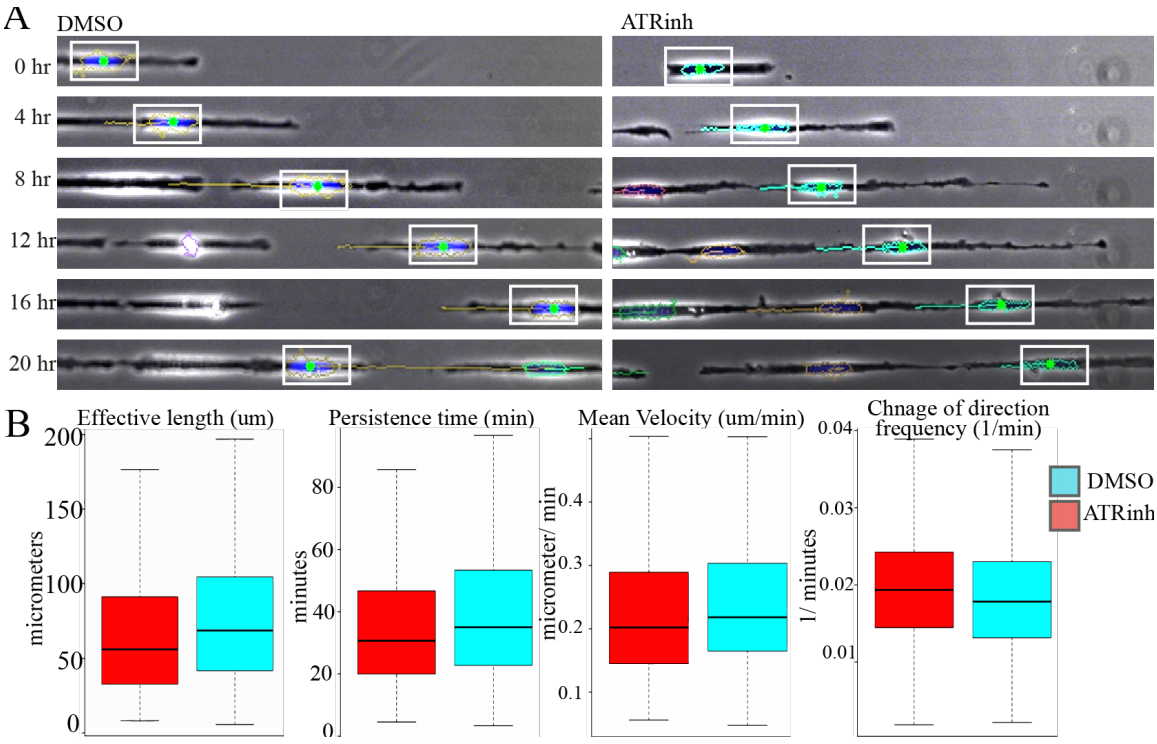

Figure 33 - ATR inhibitor affects cell migration in unidirectional migration assay. (A) Examples of time-lapse image of DMSO and ATR inhibitor (AZ20-1uM) treated U2OS cells, with the tracking. (B) Quantifications of effective length, persistent time, mean velocity and the frequency of direction change (n>100).

We then test the effect of ATR inhibitors in wound healing assay. 6 well dishes of 100 percent confluence, growth arrested, immortalized primary MEF's, were scratched with sharp pipette tip to generate wound. Cells were incubated with DMSO or ATR inhibitor (ETP46464; 2uM) one hour prior to the wound formation, and inhibitors are kept through the entire duration of the experiment. We noticed that cells treated with ATR inhibitor were slower in closing the gap of their wound (Figure 34A). By measuring the speed of area coverage we found that ATR inhibitor dampens the migration speed of

the cell (Figure 34B). Similar results were also observed in ATR depleted U2OS cells (Kidiyoor et al., unpublished).

Cells treated with ATR inhibitor exhibit arrest during G1 to S phase transition, inducing delay in cell division, which might in-turn impact the wound closing ability of ATR inhibitor treated cells. Therefore, to rule out the contribution of cell cycle in observed phenotype, we treated the cells with mild replication stress by treating them with aphidicolin (0.2mM). We compared the speed of wound closure ability of DMSO treated cells with the ATR inhibitor treated and aphidicolin treated cells (Figure 34C). Though aphidicolin treated cells, exhibited delay in wound closure time, it was significantly milder than that of ATR inhibited cells, suggesting that the observed effect in ATR inhibited cells is not just due to the cell cycle defects of cells.

We performed similar analysis using immortalized Seckel MEFs, to rule out the off target effects of ATR inhibitor in the observed phenotype. We observed that Seckel cells were significantly slower than controls. Interestingly, Seckel cells treated with ATR inhibitor were migrating even slower than both untreated Seckel and controls treated with ATR inhibitor (Figure 34D). Seckel cells are hypomorphic mutants of ATR, with small amount of residual ATR left in them for survival, however treating them with ATRi would result in complete loss of functional ATR, challenging cell fitness and survival, this could be the reason why Seckel cells have severely slow migration speed. Therefore, we conclude that cells lacking ATR are defective in wound closure ability. We also note that absence of ATR does not inhibit the migration or wound healing, only reduces the speed, indicating that ATR is not the essential component of migration or wound healing but is a facilitator for efficient cell migration.

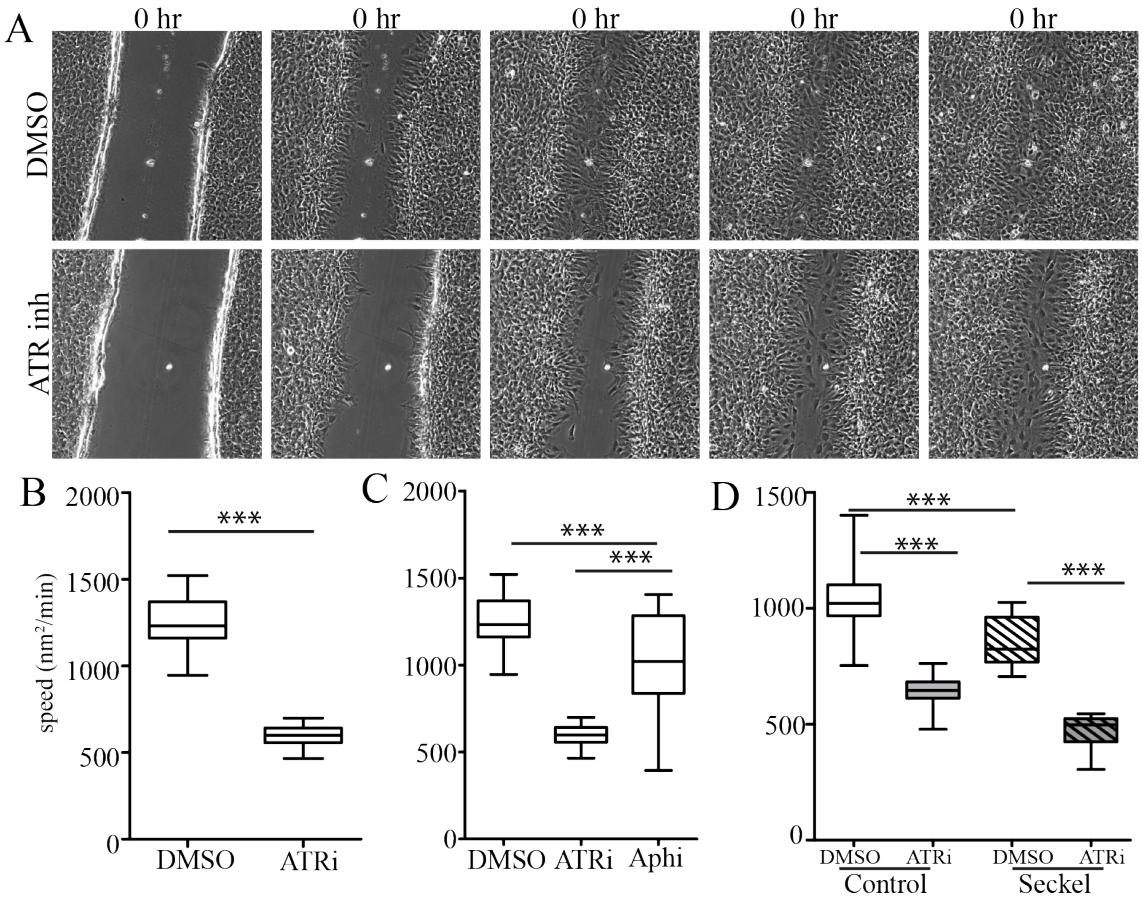

Figure 34 - ATR delays wound closure.
(A) Examples of time-lapse image of DMSO and ATR inhibitor (ETP46464-2uM) treated MEF's cell wound healing, (B) Quantification of wound closure speed in control an ATR inhibitor treated cells (n>30), and (C) in presence of aphidicolin (0.2mM). (D) Wound closure speed of control and Seckel MEF's in presence of ATR inhibitor or DMSO. Student t-test and one-way ANOVA tests were used to calculate statistical significance.

4.2 Loss of ATR leads to defective interstitial migration in constriction

Since ATR-defective cells have compromised NE dynamics, we investigated their fate while undergoing migration through narrow constrictions on micro patterned 3D channels. We used the channels with 4 micron-wide and 15 micron-long artificial constrictions (Raab et al., 2016, Skau et al., 2016) (Figure 35A). During such migration nuclei experience mechanical stress that causes nuclear ruptures consequently leading DNA damage. Cell survival under these conditions depends upon nuclear membrane repair and DNA repair efficiency (Raab et al., 2016).

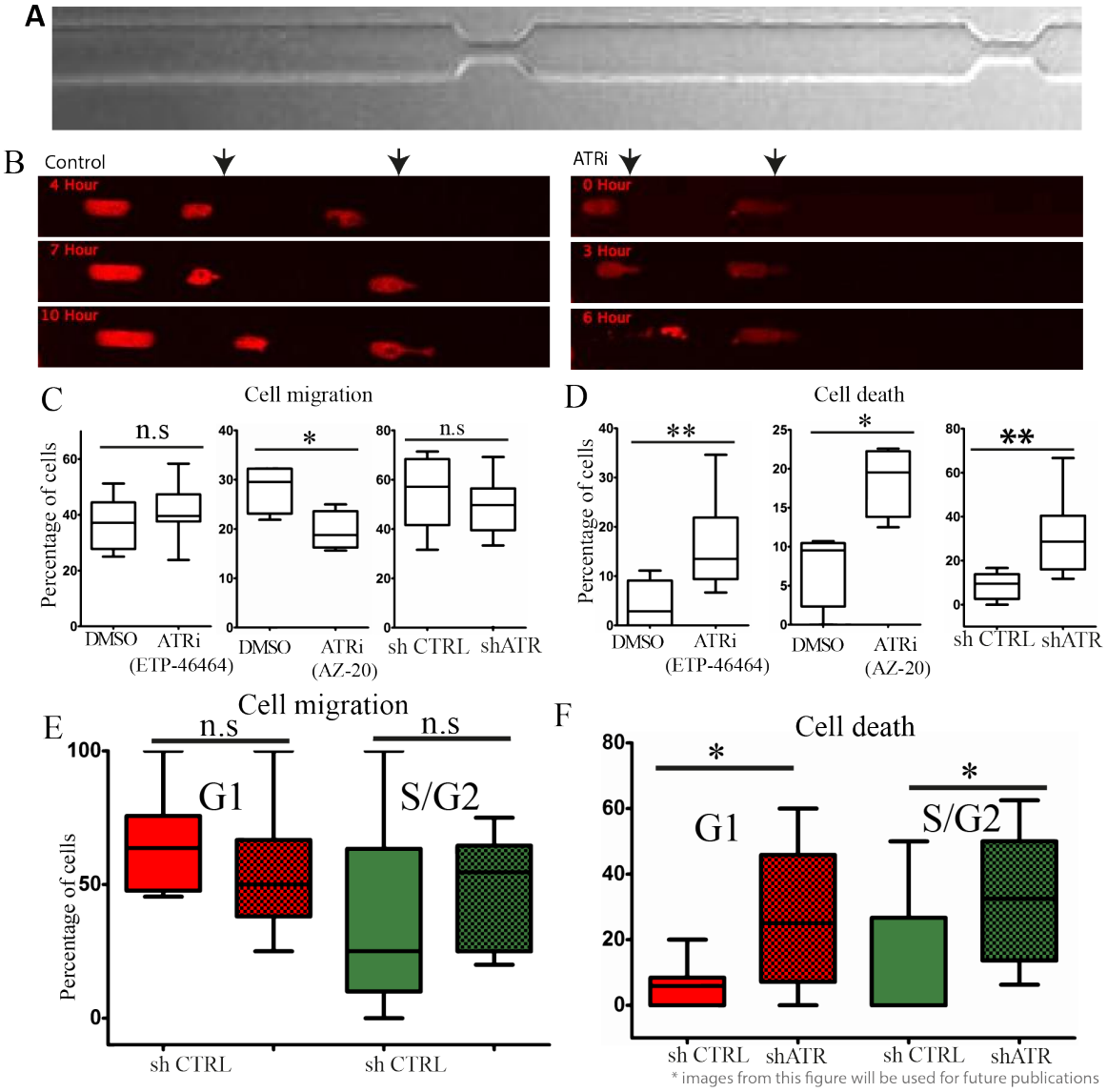

Figure 35 – Absence of ATR leads to cell death during interstitial migration.

(A) Examples of Channel with constrictions used in the experiment. (B) Time-lapse images of DMSO and ATR inhibitor (ETP46464-2uM) treated HeLa cells labeled with H2B-mCherry migrating through the channel. Arrow heads indicate the beginning point of constriction on the channel (C-D) Quantifications of HeLa cell migration, treated with shRNA and two ATR inhibitors with their respective controls. (C) Quantification of percentage cells passing the constriction with respect to the total cells that reaches constriction during the experimental period. (D) Quantification of cell death percentage at the constriction with respect to the total cells reaching the constriction (n>100 cells). (E) Quantifications of constructional migration of U2OS FUCCi cells depleted of ATR or controls. Red represents G1 phase and green S and G2 phases of cell cycle; (E) percentage of cells passing through the constriction (F) Percentage of cell death during migration. Student t-test and one-way ANOVA were used to calculate significance (* if $0.01<p<0.05$; ** if $0.005<p<0.01$; *** if $0.001<p<0.005$; **** if $p<0.001$)

We tested the ability of HeLa cells depleted of ATR or in presence of ATR inhibitor to survive during 3D migration (Figure 35B, C, D). As predicted both ATR

depletion and ATR inhibition using two different inhibitors, almost doubled the cell death (around 10% in controls to 20% in absence of ATR) at the constrictions compared to their respective controls (Figure 35D). However this lack of ATR did not affect the inherent ability of the cells to migrate, as we could not see any significant reduction in number of cells successfully passing through the channel (Figure 35C). We only observe a minor non-significant reduction of percentage of cells passing (7 to 8%) in absence of ATR except for ATR inhibitor AZ-20 treatment, where this difference was statistically significant. This indicates that ATR does not inhibit the ability of cells to squeeze their nuclei through narrow pores; but only assists nuclei to preserve their integrity against constriction-induced mechanical assaults. From these observations we conclude that absence of ATR renders cell nuclei more fragile for interstitial migration through narrow pores leading to increased mortality rate.

We then analyzed if there is any cell cycle specificity amongst the apoptotic cells in absence of ATR. In our experimental conditions ATR depletion using shRNA did not induce any cell cycle arrests. However, one cannot exclude the fact that replication stress combined with mechanical stress would lead to increased cell death of late S and G2 phase cells. We took advantage of the FUCCI (fluorescence ubiquitination cell cycle indicator) cell cycle indicator to mark the cell cycle. FUCCI marks different cell cycles with different fluorescent colors; G1 in red, G1 to S transition in yellow and S and G2 in green. Control or shATR infected U2OS cells stably expressing FUCCI plasmids were loaded on to the channels and were analyzed for their migration defects. Cells from all phases of cell cycle entered the constrictions and S/G2 cells had longer passage time due to their larger nuclei. We observed no obvious biasness towards a particular cell cycle in shATR cells; instead we observed overall increase of mortality rate in all cell cycle phases without any major effect on migration (Figure 35E, F). Similar effects were also

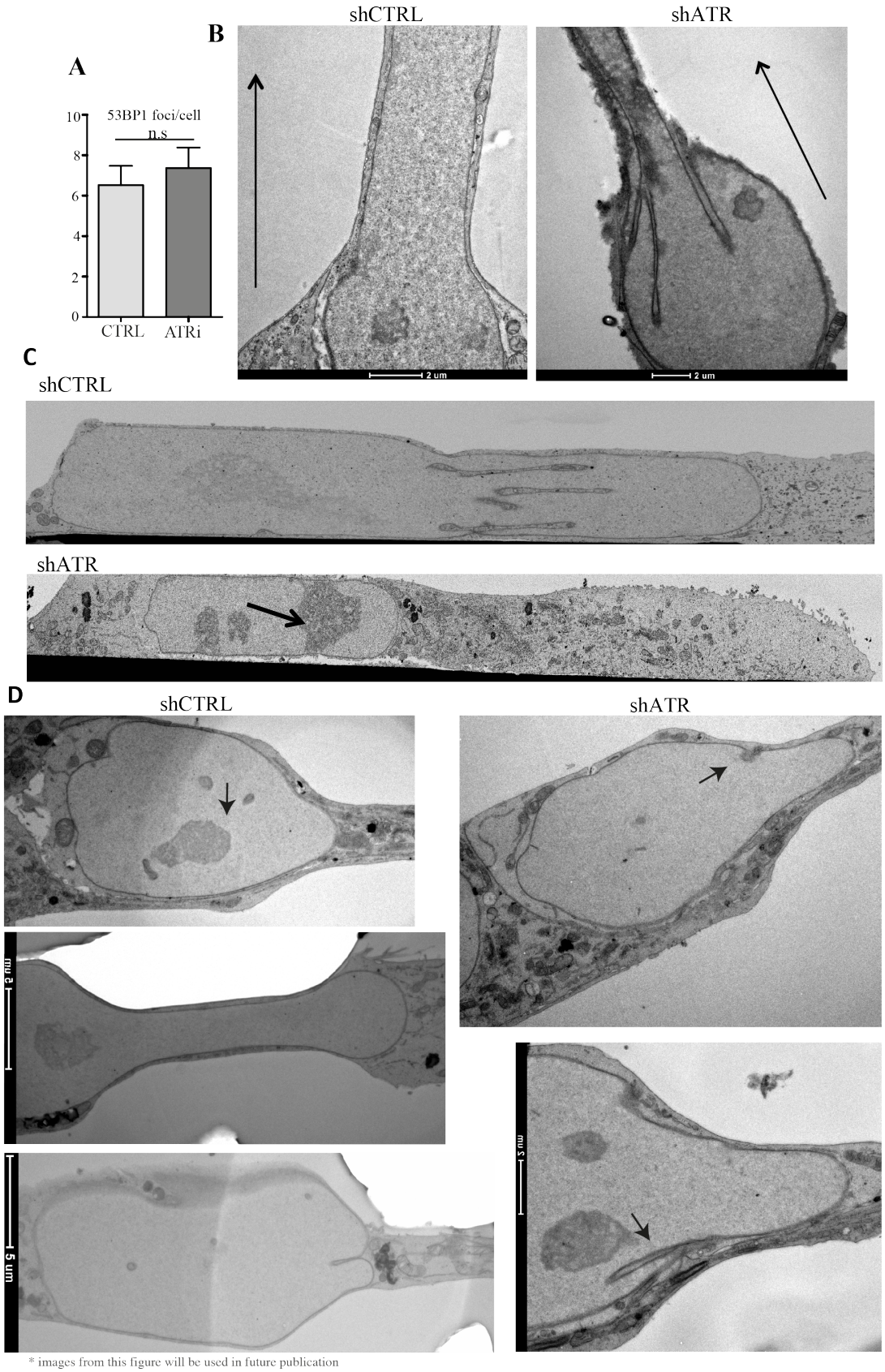

* images from this figure will be used in future publication

Figure 36 – shATR cell death during interstitial migration is caused by defective nuclear integrity.

(A) Maximum 53BP1-GFP foci per cell in RPE1 cells migrating into the 1.5 micron channel (n>15). (B-D) EM images of control and shATR cells migrating through constriction;(B) top view (C) side-view (D) Top view of control nuclei and shATR nuclei with abnormal morphologies. Long arrowheads in (B) indicate the direction of migration and small arrowheads in (C) and (D) indicate invaginations and nucleoli associated to NE

observed in yellow cells, however due to lower cell number we did not include them in the analysis. Hence we conclude that nuclear fragility towards mechanical stress in absence of ATR is cell cycle independent.

4.3 Fragile nuclear membrane leads to cell death in ATR depleted cells

Cell migration through constriction exerts mechanical stress to the nucleus, leading to membrane ruptures and DNA damage. Intact nuclear integrity, stable NE, perinuclear cytoskeleton and efficient membrane and DNA repair machinery are all needed for a cell to successfully pass through the constriction. Reports have demonstrated that loss of Lamins, Formin 2 (FMN2) mediated perinuclear cytoskeleton, membrane repair protein ESCRT III and DDR protein ATM compromises migration efficiency (Raab et al., 2016, Skau et al., 2016, Bell and Lammerding, 2016). We reasoned that defect in one or more such component in shATR cells causes cell death. So we quantified the DNA damage by counting foci of 53BP1-GFP, a DNA repair reporter in migrating cells. We utilized the H-tert RPE1 cells stably expressing 53BP1-GFP. Since RPE-1 cells are have smaller cell size, we analyzed their migration in channels with constrictions of 1.5 micron in presence or absence of ATR inhibitor. Using ImageJ, we counted the maximum number of DNA foci that cells accumulate whilst passing through the constriction (Figure 36A). ATR inhibited cells generated on average 7 foci per cell (7.36 ±0.73) with respect to 6.5 foci per cell in controls (6.52 ±0.94). This indicated that the fragility in ATR depleted cells are not resulting from their increased genomic instability or higher damage accumulated in DNA. This data was consistent with the previous report indicating that DNA damage foci (marked by γH2AX) formed during invasion assay are ATM dependent and independent of ATR (Skau et al., 2016).

From previous experiment we could infer that DNA damage is not the major contributor of cell death in shATR cells or ATR inhibitor treated cells. Since we know that ATR depletion renders nuclei fragile and incompetent for adapting to mechanical

assaults, we analyzed the nuclei of ATR depleted HeLa cells while migrating through narrow pores (Figure 36B, C, D and figure 30) by EM. Control cell nuclei migrating through narrow pores had a smooth and continuous NE structure, consistent chromosomal density and nucleoli situated at the center of the nucleus without any association to NE (Figure 36C, D and figure 37A).

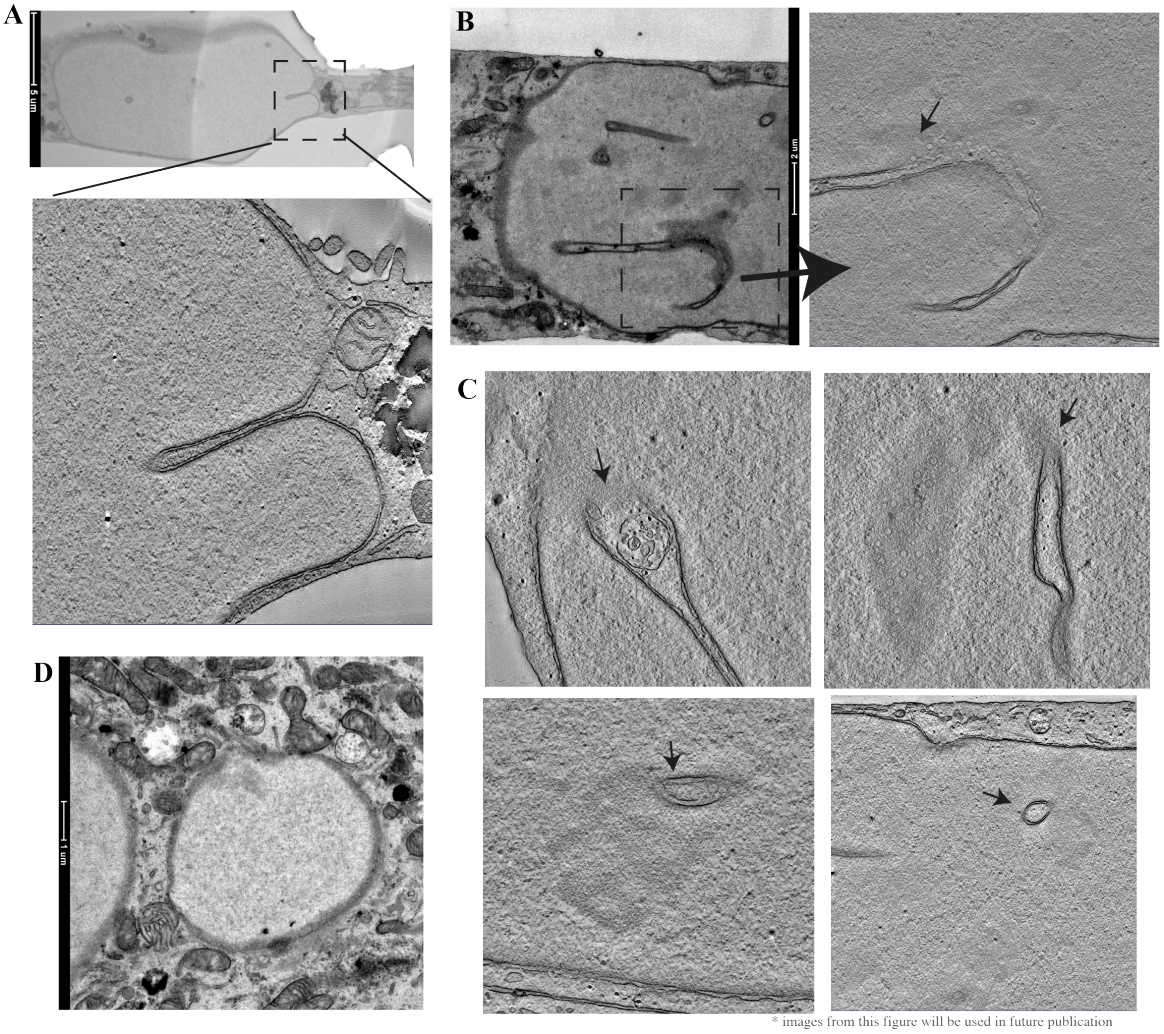

Figure 37 – Compromised nuclear and chromosomal architecture are obstacles for efficient interstitial migration in absence of ATR
(A) EM images of control nuclei entering constriction with zoom in of invagination at the leading edge. (B) shATR nuclei in constriction with zoom in of invagination. (C) Nuclear abnormalities of shATR nuclei in channels invagination, nucleoli and heterochromatin attachment to NE, and (D) micronuclei.

Even, when they generated nuclear membrane invaginations they were more organized and oriented in the direction of cell migration (Figure 36C). We observed in only one case formation of one invagination at the leading edge in parallel to the direction of migration

(Figure 37A). In contrast, ATR depleted cells had highly disorganized membrane architecture with ruffles, long and disoriented invaginations and micronuclei with damaged membrane in the constrictions (Figure 36B, C, D and Figure 37B, C, D). Nucleoli and heterochromatin associated to the nuclear envelope were very evident (Figure 36C, Figure 37C). Presence of such structures transforms into a physical obstacle for the movement of nuclei demanding the cell to exert higher amount of forces to the nuclei in order to push through the constriction. Higher forces will lead to higher NE ruptures. Considering the NE of shATR cells are incapable of dealing with membrane tension, higher forces at the NE would result in much higher membrane damage and even nuclear collapse. To test this we decided to focus on the NE composition at the leading edge of control and shATR cells migrating through the constrictions (Figure 38). In line with our hypothesis, we observed higher amount of membrane damage in shATR cells compared to controls (Figure 37A). In the leading edge of the control nuclei, majority of the damage was on the external membrane of the bilayer (Figure 38B, green color), with few narrow ruptures of the inner membrane (Figure 38B, yellow color). In complete contrast to controls, shATR nuclei had severe damages of inner nuclear membrane (Figure 38B, C yellow color). We observed an overall increase in size of the ruptures in shATR nuceli representing higher nuclear damage. We also observed heterochromatin bound to broken membranes indicating collapse of genomic organization machinery (Figure 38B, red color). We counted the number of breaks, and compared the ratio between the inner and outer nuclear membrane ruptures (Figure 38E). In controls the average ratio was approximately 5, suggesting that for every 5 outer membrane ruptures, there is single damage in the inner membrane. However, in shATR cells this ratio was reduced to 2, indicating a fragility of inner membrane in shATR cells. We also analyzed ta section of nuclear membrane from the posterior section of shATR nuclei, but did not observe any nuclear ruptures (Figure 38D). This indicates that the damage in the front is resulting from the mechanical forces; ruling out the argument that shATR cells possess

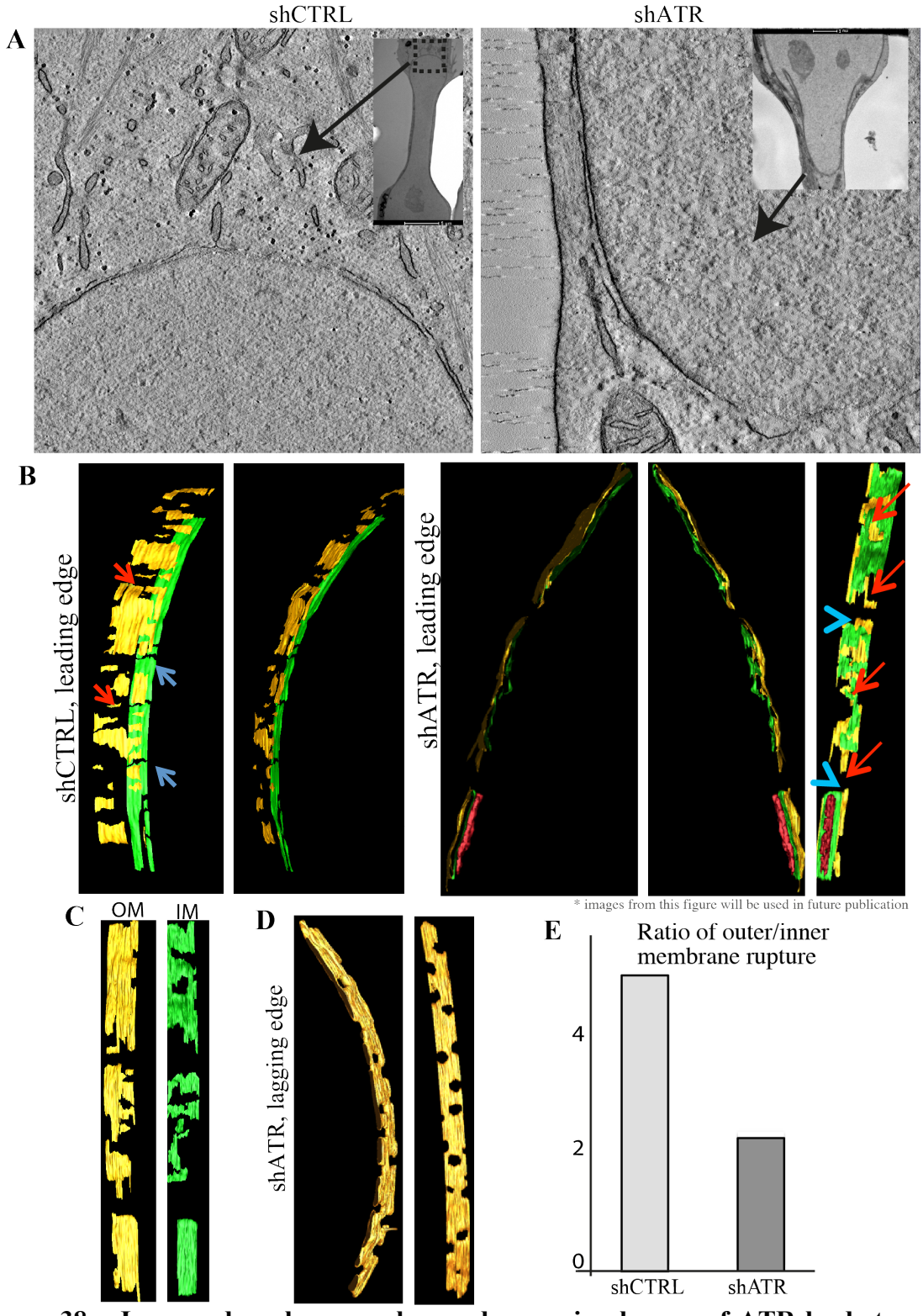

Figure 38 – Increased nuclear membrane damage in absence of ATR leads to cell death during interstitial migration.

(A) EM images of front leading edge of NE from control and shATR nuclei (B-D) 3D reconstruction of nuclear membrane section from cells migrating through constrictions. Yellow represents outer nuclear membrane and green represents inner nuclear membrane, red labels Heterochromatin (B) Reconstructions of Leading edge (front) from shCTRL nuclei and from a shATR nuclei. Red arrow indicates inner membrane ruptures and green arrow for outer membrane damage. (C) 3D reconstruction of inner (IM) and outer membrane (OM) from shATR nuclei. (B) Leading edge. (C) posterior section (lagging edge) of shATR nuclei (D) Ratio of outer membrane ruptures to inner membrane ruptures of control and shATR cells respectively.

damaged nuclear membrane in general (Figure 38D). In summary, we can conclude that nuclei of cells lacking ATR are incapable of dealing with the mechanical stress imposed on them during nuclear squeezing in 3D migration through pores leading to severe membrane damage and in some cases cell death

4.4 Role of ATR in neuronal migration during development

Cell migration plays a critical role during development; defects and delays in migration of progenitor cells might lead to defective organogenesis. We were interested to analyze the neuronal migration, since the pathological features of Seckel patients are associated with brain development. Interestingly, knockout mice of ATR interactor nesprin-2 exhibited

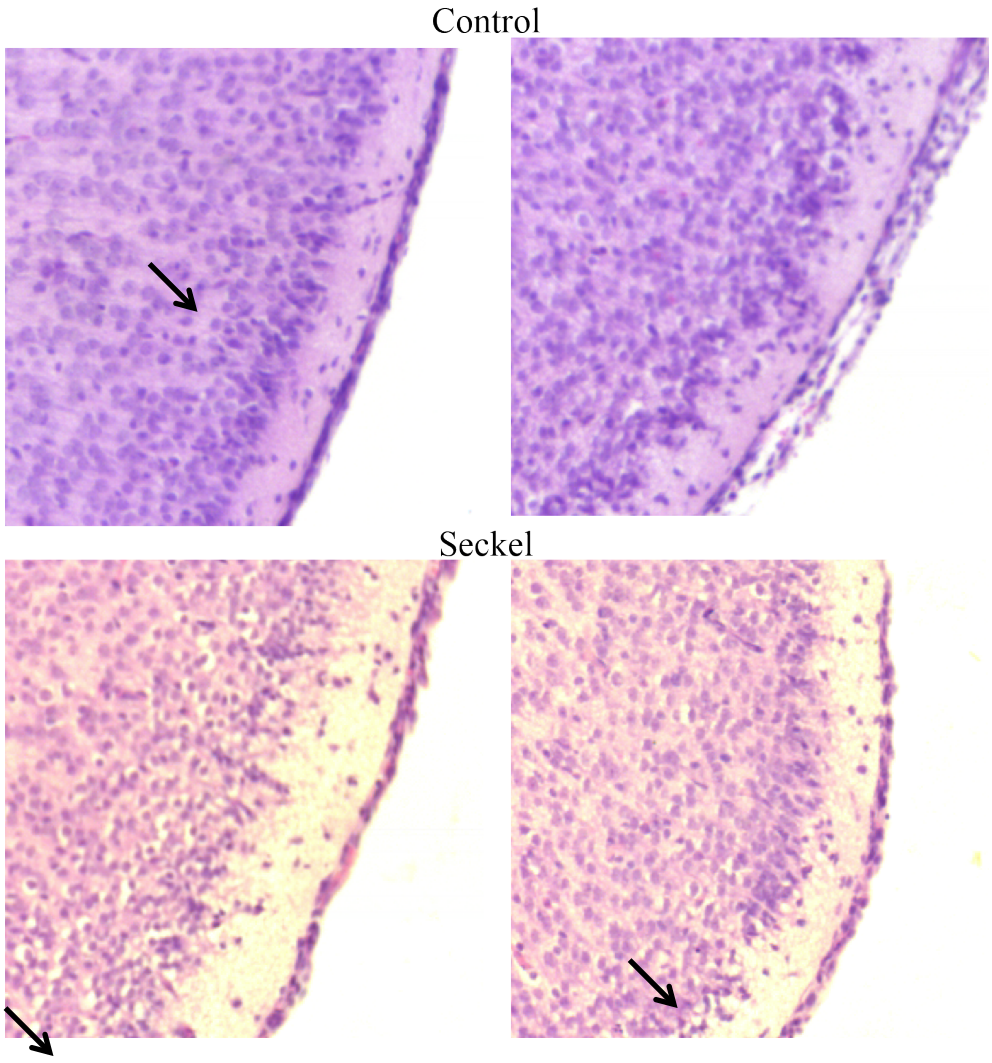

Figure 39 – ATR contributes to neuronal migration during development.
Brain sections from 5 day old control and ATR Seckel mice. Arrow indicates lower neuronal density at the peripheral layer of Seckel brains.

defective neuronal migration and learning disabilities (Zhang et al., 2009). ATR Seckel mice have severe defects in brain development (Murga et al., 2009). While majority of this problems are attributed to neuronal apoptosis due to genomic instability, we hypothesized that loss of nuclear integrity in absence of ATR could also contribute to certain extent by hindering neuronal migration and neurogenesis. We analyzed the consequences of ATR depletion *in-vivo* in neurons and noticed that it dampens neuronal migration in developing mouse brain. (Data not shown; Kidiyoor et.al., unpublished). We then performed the pathological analysis of brain sections from control and Seckel mice (figure 39). Consistent with the previous reports we noticed a deformed brain structure, with lower density of neurons. Focusing on the periphery of cortex region we found fewer neurons on the top or peripheral layers of the section, with higher number in the internal regions (Figure 39). This suggests that other than neuronal apoptosis ATR Seckel mice also suffer neuronal migration defects during development.

4.5 ATR facilitates tumor migration and metastasis.

ATR is traditionally a tumor suppressor gene and inhibitors targeting kinase activity are actively perceived as anti-cancer drug in therapeutics (Manic et al., 2015). In contrary, our results imply that ATR supports tumor cell survival in interstitial migration. In addition, recent studies reported that higher levels of ATR were associated with severe phenotypes and more invasive cancers (Abdel-Fatah et al., 2015, Abdel-Fatah et al., 2014). Hence, we hypothesized ATR might have a dual role in tumorogenisis; primarily as a barrier against tumor by maintaining genomic stability and secondly as a facilitator of tumor progression by supporting cell survival in extreme micro-environmental alterations. In order to test the requirement of ATR in metastasis and invasion we performed modified in-vivo tail vein injection assay (Zeidman et al., 1950). Equal number of control and ATR depleted HeLa cells labeled with a vital dye were injected into the tail-vein of immune compromised mice, the lungs were dissected from these mice at 2 and 48 hour

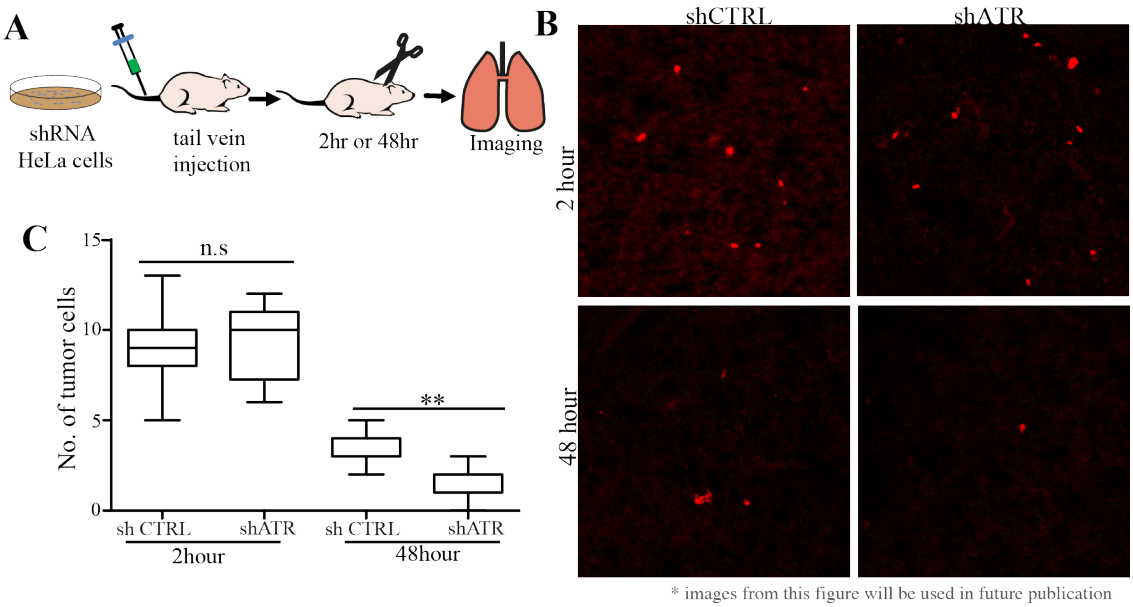

Figure 40 – ATR facilitates tumor metastasis.
(A) Scheme depicting the in-vivo homing assay strategy. Control and shATR HeLa cells labeled with vital dye were injected into the tail vein of immune-compromised mice. Sections of Lung were collected after 2 and 48 hours respectively. (B) Representative images of mice lungs with labeled HeLa cells residing on them. (C) Number of control or shATR HeLa cells / field in mice lungs at 2 hour and 48 hour respectively. p-values calculated using one way ANOVA test (** if 0.005<p<0.01)

respectively and quantification of injected cells in lung surface (scheme in Figure 40A). Fraction of cells injected was also plated on dishes during the same period (48hr) for monitoring growth and to confirm level of ATR depletion in absence of selection. Equal number of cells reached the lung at 2 hours after injection for shATR and controls, confirming identical preparations and injection. However, there was a significant reduction of fluorescent positive shATR cells in the lung 48 hours after injection compared to controls (Figure 40B, C). The general reduction in number of cells homing in lung surface 48 hours after injection (Figure 40B, C Control cells), with respect to number of cells reaching lung (2hour after injection) is due to death of majority of circulating cells with only a minor fraction successfully forming secondary tumor (Zeidman et al., 1950). However, upon depleting ATR tumor cells become hypersensitive and fail to survive the journey through the circulatory system, suggesting a role of ATR in tumor progression and metastasis.

4.6 Conclusions

Extrapolating from the nuclear abnormalities of ATR depleted cells; we hypothesized a potential role of ATR in cell migration via regulating nuclear dynamics. We performed a wide range of migration assays from single cell 2D tracking to in-vivo tumor metastasis in presence or absence of ATR. Our results strongly suggest that ATR is a facilitator of cell migration; it does so by coordinating nuclear dynamics with cell migration. In absence of ATR cells are less persistent and slower in migration and wound closure. During 3D migration through constrictions ATR maintains nuclear integrity by balancing mechanical forces acting on the NE, hence alleviating the chances of nuclear collapse. ATR also facilitates neuronal migration during development. *In-vivo,* cancer cells with reduced ATR fail to survive the circulation and efficiently invade host organs. Therefore, we propose that ATR has dual role in tumorogenisis, as a tumor suppressor by maintaining genomic stability and as a facilitator of tumor progression by supporting cell survival in extreme mechano-environmental alterations.

Discussion

ATR is a guardian of cellular homeostasis

PIKK kinases are evolutionarily conserved giant unconventional protein kinases. They regulate variety of cellular functions and are involved in several stress responses including DNA damage, replication and topological stress, hypoxia, mitochondrial stress, osmotic stress and nutrient starvation (Baretic and Williams, 2014, Lempiainen and Halazonetis, 2009). PIKK share a common structure and mechanism of activation. A peculiar characteristic of PIKK is that they can regulate various processes in different cellular compartments, activated by a diverse range of independent stress stimuli. mTOR by forming 2 complexes, TORC1 and TORC2, contributes to autophagy, hypoxia osmotic stress, nutrient signaling and even DNA damage (Reiling and Sabatini, 2006). ATM, ATR and DNA-PK are PIKK members known for their role in DNA damage repair. In addition to this, DNA-PK is involved in DNA damage induced structural changes of Golgi (Farber-Katz et al., 2014), influences tumor metastasis by regulating cytoskeletal components such as vimentin (Kotula et al., 2013) and modulates the secretome of cancer cells (Kotula et al., 2015). ATM is activated upon DNA damage, oxidative stress, membrane receptor and nutrient starvation. Alongside, maintaining genome integrity ATM contributes towards mitochondrial homeostasis, glucose homeostasis, neural firing and insulin-mediated signaling (Ambrose and Gatti, 2013). ATR is involved in nuclear homeostasis, nucleolar stress responses and mitochondrial apoptotic signal regulation (Kidiyoor et al., 2016). In comparison to ATM, very little is known about the DDR independent roles of ATR. Though several recent articles demonstrated the importance of DNA damage independent role of ATR, a concrete understanding of such roles and their relevance at the organismal level are yet to be fully explored. Therefore, we decided to characterize ATR in a cellular context by quantifying its distribution across the cell and by identifying potential interactors in different cellular compartments.

Our analysis provided several interesting insights into potential ATR processes including transcription, translation, RNA metabolism and export, and maintenance of various organelles such as nucleoli, centrosomes, mitochondria and Golgi. Few interesting ones are listed below.

i. ATR maintains organelle integrity and cytoskeletal organization.

By EM analysis of ATR depleted cells, we observed defects in several cellular compartments other than nuclei. We noticed defects in morphology of Golgi; compromised mitochondrial morphology with higher amount of fused mitochondria and large nucleoli in shATR cells. We also observed increased actin stress fibers and signs of compromised actinomyosin thread-milling, correlating with the previous report that shows increased stress-fibers in Seckel patient fibroblasts (Tivey et al., 2013). One could utilize our ATR interactome dataset to predict the deregulated proteins or pathways of specific organelle that leads to the observed phenotype in absence of ATR. For example, we found Golgin A2, as an interactor and potential phosphorylation target of ATR. Golgin A2, is important for dispersion of Golgi membranes during mitosis. Hence, one could hypothesize that morphological defects of golgi in shATR cells are a consequence of deregulated of Golgin A2. ATR localizes to centrosomes and contributes towards centrosome duplication, cilia development and functioning (Stiff et al., 2016, Valdes-Sanchez et al., 2013, Kidiyoor et al., 2016). Our ATR interactome list constituted 23 centrosomal proteins, involved in centrosome assembly and function, stress-induced ciliogenesis, and kinetochore assembly, providing potential targets of ATR in centrosome maintenance.

ii Mitosis

Our proteomic screen for ATR interactors identified several proteins involved in mitosis, including microtubules, kinetochore proteins, nuclear envelope components and centrosomal proteins and Golgi fragmentation regulator Golgin A2. Mitosin (Cenp-F), is

a potential ATR interactor and phosphorylation target that localizes to the NE during early prophase like ATR (Kumar et al., 2014). At the prophase NE, it coordinates with NUP133 and LINC complex members to ensure the proper tethering of centrosomes into the NE and then assists microtubule attachment to kinetochores (Vergnolle and Taylor, 2007, Bolhy et al., 2011). These proteins are also involved in proper and timely nuclear envelope breakdown (NEBD) and its removal from DNA. Deleting some of these proteins delays mitosis, similar to the phenotype of seckel or ATR inhibited cells (Kumar et al., 2014). In addition, higher proportion Seckel cells exhibit higher supernumerary centrosomes leading to increased multipolar cell divisions, aneuploidy and mitotic catastrophe (Alderton et al., 2006). Put together, we suggest that cells ATR undergo faulty mitosis and that few of the several mitotic phenotypes observed in seckel patients and shATR cells could be resulting from defective mitosis.

iii. Transcription and translation

ATR localizes to the nucleoli and responds to nucleolar stress (Kidiyoor et al., 2016). Studies with upregulated TopBP1 show that active ATR at the nucleoli are capable of shutting down rRNA synthesis (Sokka et al., 2015). Our ATR intreractome list is enriched for nucleolar proteins involved in rRNA synthesis and rRNA export machinery at the NE, suggesting a participation of ATR in rRNA metabolism. ATR interactome also contains several RNA helicases, polymerases, splicing factor, transcription regulators and RNA export proteins, some of which are differentially interacting with ATR in a stress dependent manner.

Our interactome data was enriched with translation related proteins. One most interesting candidate of this list is the eIF3 complex. The eIF3 complex is composed of 13 subunits and all the 13 of them were detected as ATR interactors, and 8 out of 13 are to be potential phosphorylation target of ATR. eIF3 complex functions in all stages of transcription initiation, and is deregulated in several cancers(Hershey, 2015). Studies

show that it functions as a scaffold for docking mTOR at the active translation site, in mTOR mediated translational regulation pathway (Peterson and Sabatini, 2005), suggesting that it is able to bind PIKKs. Another study shows that ATR is involved in replication- dependent histone mRNP translational switch from an actively translating mode to an mRNA degrading mode. ATR does so by hyper-phosphorylating UPF1, which leads to release of eIF3 complex from the translation site (Choe et al., 2014). Our preliminary data together the available literature strongly suggests a role of ATR in regulating protein synthesis.

ATR at the nuclear envelope

ATR localizes to the NE and can be activated by altering physical and chemical composition (Kidiyoor et al., 2016). Here we show that a fraction of ATR in membrane bound, in particular at the NE, localized on inner and outer nuclear periphery. Previous work from our group, reported that ATR relocalizes at the NE and at nucleoli in response to mechanical stimuli (Kumar et al., 2014) to coordinate the membrane stress response, eliminating any potential treats to the DNA. Accordingly, cells depleted of ATR exhibited NE invaginations and micronuclei due to their inability to coordinate NE and nucleolar dynamics in response to mechanical stress.

The NE constantly experiences mechanical forces originating internally by topological constrains of chromatin or by external stimuli on the cytoskeleton (Isermann and Lammerding, 2013). Aberrant replication and transcription mediated topological stress at the NE, RNA export, chromatin movements and chromatin condensation are all the main causes of mechanical stress at the NE from the inside (Bozler et al., 2015, Bermejo et al., 2012); forces generated during cytoskeletal rearrangements and forces generated by interference of external objects such as pores during migration constitute as the main sources of mechanical stress a the NE. NE maintains its steady state by balancing the forces acting inwards with the forces acting outwards. Disturbing this

steady state of NE by manipulating forces from either side leads to damaging consequences. Cells with defective lamins, with impaired nucleus to cytoskeleton connections and with decondensed chromatin (HDAC inhibitor) all show an increased nuclear invaginations (Drozdz and Vaux, 2017).

Majority of the forces on the NE, particularly the ones originating from the topological constrains, act transiently at the NE without inducing any structural alterations to the NE. In a normal scenario, membrane stress generated from the topological constraints at the NE recruits ATR to the NE (Bermejo et al., 2012, Kumar et al., 2014). Once activated, ATR recruits several other response proteins such as Chk1 and type II topoisomerases, and modulates nuclear pore proteins, and LINC complex proteins. ATR restores the NE equilibrium by facilitating detachment of chromatin from the NE and by strengthening LINC mediated nuclear connections with the perinuclear cytoskeleton (Figure 41). Though the exact mechanism of ATR mediated stress response is unclear, based on our observations we propose a mechanism of ATR mediated membrane stress response and discuss the key proteins potentially involved and their role in this process.

Nesprin-2 is a member of LINC complexes, regulating nuclear membrane architecture (Luke et al., 2008), centrosome association during migration and mitosis (Zhang et al., 2009). Nesprin-2 is a potential ATR target proposed to be phosphorylated during S-phase of cell cycle by ATR/ATM (Olsen et al., 2010). We also note that, other members of the LINC complexes might also be regulated by ATR. Seckel fibroblasts exhibit four-fold reduction in phosphorylation of SUN2 (Ser-12), a Nesprin-2 inner membrane binding protein (Stokes et al., 2007). SUN proteins also contribute towards NEBD (Turgay et al., 2014).

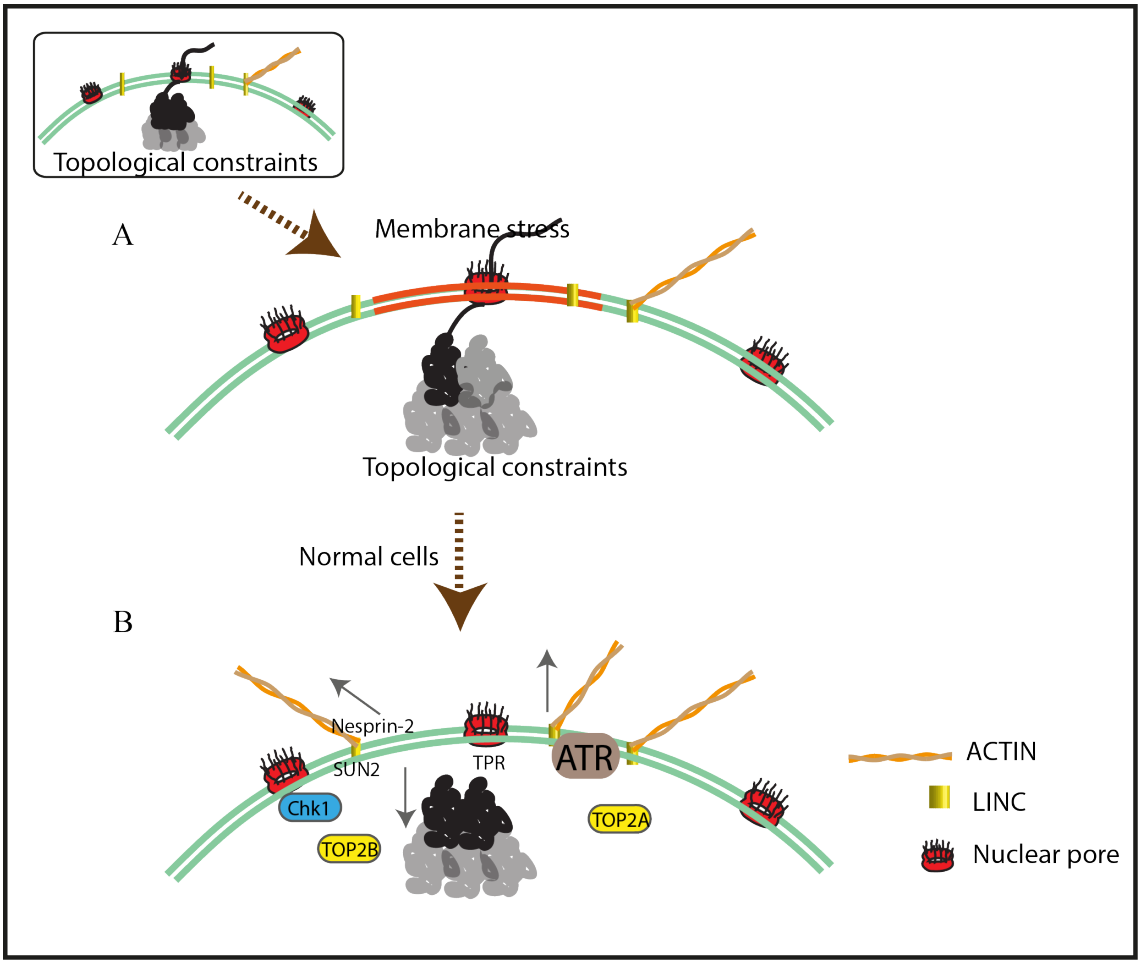

Figure 41 – ATR mediated maintenance of nuclear envelope integrity.
(A, inlet) Scheme depicting RNA export as an example of nuclear process, which might (A) induce mechanical stress at the NE by exerting inward pulling force. (B) In response to the membrane stress, ATR is recruited to the NE. Active ATR mediated stress response modulates DNA topology regulators such as topoisomerases and repair kinases such as checkpoint kinases and nuclear components including LINC and nuclear pore complex proteins, ultimately restoring the NE to its steady state, by detethering chromatin from the NE and by reinforcing nucleocytoskeltal connections.

Type II DNA topoisomerases regulate DNA topology, chromosome condensation and chromatid segregation. Topoisomerase IIα is essential for faithful segregation of daughter chromosomes. Topoisomerase Iiβ is essential for opening heterochromatins and facilitating transcription of genes regulating differentiation(Heng and Le, 2010). Similar to Seckel patients mutations in topoisomerase IIB cause developmental delay, intellectual disability and microcephaly (Lam et al., 2017). Both type II topoisomerases are ATR interactors and have several potential phosphorylation sites. Olsen et al., suggests that they are phosphorylated during S-phase of cell cycle by ATR/ATM (Olsen et al., 2010).

We propose that ATR regulates the fate of NE attached chromatin by differentially modulating phosphorylation status of both type II topoisomerases in a stress dependent manner. Interestingly, ATR, nepsrin-2 and topoisomerase II all contribute towards neuronal migration, brain development, and their knockouts exhibit learning disability (Zhang et al., 2009, Heng and Le, 2010).

TPR is a component of the inner nuclear pore involved in protein and RNA export as well as gene gating. Though TPR does not appear in our screens as ATR interactor, several screens identified TPR to be phosphorylated by ATR/ATM upon DNA damage (Matsuoka et al., 2007). In *S. cerevisiae* $Mec1^{ATR}$ phosphorylates Mlp1, yeast ortholog of TPR, in order to resolve fork collision with transcription machinery near the NE (Bermejo et al., 2011). We believe that similar regulations of TPR by ATR in mammalian cells are highly plausible considering their highly conserved functionalities at the nuclear pore.

In summary we propose that in response to mechanical stress at the NE ATR phosphorylates Chk1 to preserve genome stability (Kumar et al., 2014); phosphorylates nucleoporins to resolve complications pertaining to nuclear export and RNA transport (Bermejo et al., 2012); counteracts force induced NE deformations. ATR does this by detethering topological constrains from the NE through differentially regulating topoisomerases and by reinforcing connections between nucleus and cytoskeleton via regulating nuclear proteins such as LINC complex, Thereby restoring nuclear integrity and alleviating mechanical stress induced NE collapse and consequential genome instability.

Though majority of topology induced membrane stress are resolved immediately, some of the unresolved forces could generate type II nuclear membrane invaginations by pulling in the nuclear membrane. However, such events occur more frequently in absence of ATR due to compromised nuclear mechanics and chromosomal architecture (Figure 42A). ATR depleted cells fail to efficiently carry out NEBD and undergo faulty mitosis with chromatins still bound to lamins (Kumar et al., 2014). This leads to micronuclei

formation and interferes with NE reassembly in daughter cells. These nuclei inefficiently respond to mechanical forces resulting in increased nuclear collapse. They also exhibit defective nuclear cytoskeletal connections significantly attenuating the outer nuclear membrane tension. Aberrant replication, transcription, RNA export and other deregulated nuclear functions in absence of ATR additively increase topological stress. Hence in contrast to outer membrane, inner nuclear membrane experiences higher stress due to higher topological constrains. This unique combination of hypo tensed the outer nuclear membrane and hyper tensed inner membrane makes NE unstable leading to frequent NE collapse and increasing the chances of invagination formation. At brief, aberrant mitosis, weak cytoskeletal connection, inefficient stress response at the NE lead to accumulation of invaginations in ATR depleted cells.

Transient NE ruptures are rare in normal cells on a culture dish, ranging from zero to 10% depending on cell type (Shah et al., 2017), but more frequent in cancer cells and cells with compromised NE integrity (De Vos et al., 2011, Vargas et al., 2012). ATR deletion leads to fragile nuclei and compromised NE integrity, rendering them more prone to spontaneous NE ruptures. We could also assume that the invaginations are more prone to such ruptures as they experience higher mechanical stress. It is well known that that invaginations characterized as nucleoplasmic reticulum are also calcium storage centers, which can locally release calcium into the nucleus, independently from the cytoplasmic calcium levels(Oliveira et al., 2014, Drozdz and Vaux, 2017). Spontaneous NE ruptures at these invaginations disrupt the structure resulting in local release of this stored calcium into the nucleus. Similar to plasma membrane repair, this increased spike of calcium would function as a membrane damage signal initiating repair process (Figure 42B) (Jimenez et al., 2014, Hurley, 2015). The endosomal-sorting complex required for transport (ESCRT) complex III is the major complex that is implicated in nuclear membrane repair and reassembly. After cytokinesis, ESCRT III is involved in daughter

cell nuclear envelope assembly, spindle disassembly and NE sealing (Vietri et al., 2015, Olmos et al., 2015). ESCRT III also seals transient NE ruptures occurring during interstitial migration through narrow pores (Raab et al., 2016). ESCRT III repair can adopt two mechanisms depending on the size of the gap. One mechanism is the patching model, involved for repair of membranes smaller than 100nm (Jimenez et al., 2014) and the other model involves tension reduction by the delivery of additional membrane at the damage site (McNeil and Steinhardt, 2003), requiring fusion of phospholipid bodies to fuse with NE. In case of ruptures below 100nm size in the shATR nuclear invaginations, the uneven force distribution between inner and outer membranes pose a challenge for repairing by synchronously pinching the two membranes together. Hence, forcing the system to repair the bilayer individually (Figure 42).

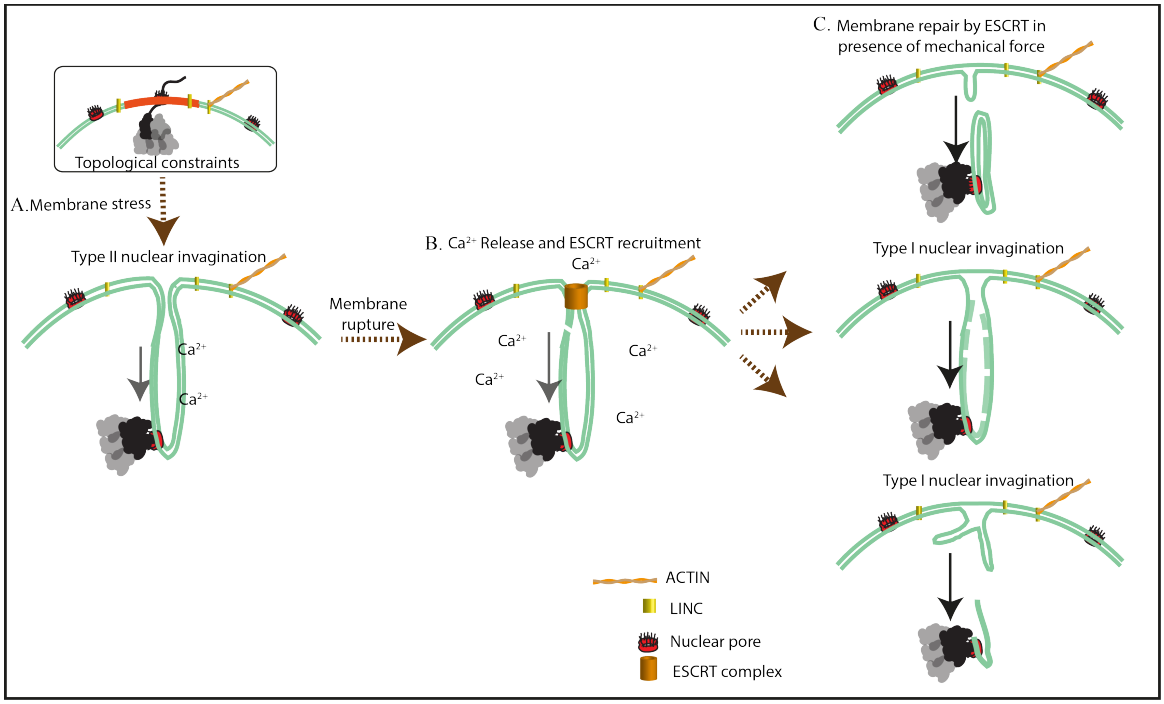

Figure 42 – Formation of NE abnormalities in absence of ATR
(A, inlet) Scheme depicting RNA export induced mechanical stress at the NE by exerting inward pulling force. (A) Defective response to the membrane stress in absence of ATR lead to formation of type II invaginations. (B) This invaginations are the storage center of calcium and their fragility can cause spontaneous ruptures consequently resulting in calcium release and recruitment of ESCRT for repair (C) Repair of membrane bilayer individually leads to more NE abnormalities.

Similarly, the biasness in the availability of the free membrane bodies pushes the repair machinery to repair the bilayer individually, in case of wounds larger than 100nm. In addition we also noticed that the size of gaps might vary between the inner and outer membranes of NE, indicating a possibility that they might be repaired individually utilizing different mechanisms. Based upon the differences in forces experienced by each membranes, mechanism of repair and the time consumed to repair, membrane resealing at invaginations might lead to several possibilities including formation of type I invaginations, pinching out both membranes or just inner nuclear membrane from the NE in continued presence of topological forces (Figure 42C).

In summary, we conclude that ATR regulates nuclear integrity by regulating NE dynamics. It does so by regulating several aspects around the NE; ATR maintains nuclear morphology and optimal membrane tension, ATR counteracts mechanical force imbalances at the NE, ATR coordinates nuclear events with nuclear and cell migration and most importantly ATR guards NE genome from mechanical assaults. Therefore the nuclear phenotypes observed in ATR depleted cells represent a collective inefficiency of all the above-mentioned components in absence of the master regulator ATR, rather than originating from a single cause.

References

Abdel-Fatah, T. M., Arora, A., Moseley, P., Coveney, C., Perry, C., Johnson, K., Kent, C., Ball, G., Chan, S. & Madhusudan, S. (2014). ATM, ATR and DNA-PKcs expressions correlate to adverse clinical outcomes in epithelial ovarian cancers. *BBA Clin,* 2**,** 10-7.

Abdel-Fatah, T. M., Middleton, F. K., Arora, A., Agarwal, D., Chen, T., Moseley, P. M., Perry, C., Doherty, R., Chan, S., Green, A. R., Rakha, E., Ball, G., Ellis, I. O., Curtin, N. J. & Madhusudan, S. (2015). Untangling the ATR-CHEK1 network for prognostication, prediction and therapeutic target validation in breast cancer. *Mol Oncol,* 9**,** 569-85.

Aguilera, A. & Gomez-Gonzalez, B. (2008). Genome instability: a mechanistic view of its causes and consequences. *Nat Rev Genet,* 9**,** 204-17.

Alderton, G. K., Galbiati, L., Griffith, E., Surinya, K. H., Neitzel, H., Jackson, A. P., Jeggo, P. A. & O'driscoll, M. (2006). Regulation of mitotic entry by microcephalin and its overlap with ATR signalling. *Nat Cell Biol,* 8**,** 725-33.

Alderton, G. K., Joenje, H., Varon, R., Borglum, A. D., Jeggo, P. A. & O'driscoll, M. (2004). Seckel syndrome exhibits cellular features demonstrating defects in the ATR-signalling pathway. *Hum Mol Genet,* 13**,** 3127-38.

Ambrose, M. & Gatti, R. A. (2013). Pathogenesis of ataxia-telangiectasia: the next generation of ATM functions. *Blood,* 121**,** 4036-45.

Andersen, J. S., Lam, Y. W., Leung, A. K., Ong, S. E., Lyon, C. E., Lamond, A. I. & Mann, M. (2005). Nucleolar proteome dynamics. *Nature,* 433**,** 77-83.

Arsenovic, P. T., Ramachandran, I., Bathula, K., Zhu, R., Narang, J. D., Noll, N. A., Lemmon, C. A., Gundersen, G. G. & Conway, D. E. (2016). Nesprin-2G, a Component of the Nuclear LINC Complex, Is Subject to Myosin-Dependent Tension. *Biophys J,* 110**,** 34-43.

Awasthi, P., Foiani, M. & Kumar, A. (2015). ATM and ATR signaling at a glance. *J Cell Sci,* 128**,** 4255-62.

Banerjee, I., Zhang, J., Moore-Morris, T., Pfeiffer, E., Buchholz, K. S., Liu, A., Ouyang, K., Stroud, M. J., Gerace, L., Evans, S. M., Mcculloch, A. & Chen, J. (2014). Targeted ablation of nesprin 1 and nesprin 2 from murine myocardium results in cardiomyopathy, altered nuclear morphology and inhibition of the biomechanical gene response. *PLoS Genet,* 10**,** e1004114.

Baretic, D. & Williams, R. L. (2014). PIKKs--the solenoid nest where partners and kinases meet. *Curr Opin Struct Biol,* 29**,** 134-42.

Bell, E. S. & Lammerding, J. (2016). Causes and consequences of nuclear envelope alterations in tumour progression. *Eur J Cell Biol,* 95**,** 449-464.

Bentley, N. J., Holtzman, D. A., Flaggs, G., Keegan, K. S., Demaggio, A., Ford, J. C., Hoekstra, M. & Carr, A. M. (1996). The Schizosaccharomyces pombe rad3 checkpoint gene. *EMBO J,* 15**,** 6641-51.

Bermejo, R., Capra, T., Jossen, R., Colosio, A., Frattini, C., Carotenuto, W., Cocito, A., Doksani, Y., Klein, H., Gomez-Gonzalez, B., Aguilera, A., Katou, Y., Shirahige, K. & Foiani, M. (2011). The replication checkpoint protects fork stability by releasing transcribed genes from nuclear pores. *Cell,* 146**,** 233-46.

Bermejo, R., Kumar, A. & Foiani, M. (2012). Preserving the genome by regulating chromatin association with the nuclear envelope. *Trends Cell Biol,* 22**,** 465-73.

Beveridge, R. D., Staples, C. J., Patil, A. A., Myers, K. N., Maslen, S., Skehel, J. M., Boulton, S. J. & Collis, S. J. (2014). The leukemia-associated Rho guanine

nucleotide exchange factor LARG is required for efficient replication stress signaling. *Cell Cycle,* 13**,** 3450-9.
Beznoussenko, G. V., Dolgikh, V. V., Seliverstova, E. V., Semenov, P. B., Tokarev, Y. S., Trucco, A., Micaroni, M., Di Giandomenico, D., Auinger, P., Senderskiy, I. V., Skarlato, S. O., Snigirevskaya, E. S., Komissarchik, Y. Y., Pavelka, M., De Matteis, M. A., Luini, A., Sokolova, Y. Y. & Mironov, A. A. (2007). Analogs of the Golgi complex in microsporidia: structure and avesicular mechanisms of function. *J Cell Sci,* 120**,** 1288-98.
Beznoussenko, G. V., Ragnini-Wilson, A., Wilson, C. & Mironov, A. A. (2016). Three-dimensional and immune electron microscopic analysis of the secretory pathway in Saccharomyces cerevisiae. *Histochem Cell Biol,* 146**,** 515-527.
Bolhy, S., Bouhlel, I., Dultz, E., Nayak, T., Zuccolo, M., Gatti, X., Vallee, R., Ellenberg, J. & Doye, V. (2011). A Nup133-dependent NPC-anchored network tethers centrosomes to the nuclear envelope in prophase. *J Cell Biol,* 192**,** 855-71.
Bourgeois, C. A., Hemon, D. & Bouteille, M. (1979). Structural relationship between the nucleolus and the nuclear envelope. *J Ultrastruct Res,* 68**,** 328-40.
Bozler, J., Nguyen, H. Q., Rogers, G. C. & Bosco, G. (2015). Condensins exert force on chromatin-nuclear envelope tethers to mediate nucleoplasmic reticulum formation in Drosophila melanogaster. *G3 (Bethesda),* 5**,** 341-52.
Brown, E. J. & Baltimore, D. (2000). ATR disruption leads to chromosomal fragmentation and early embryonic lethality. *Genes Dev,* 14**,** 397-402.
Caille, N., Thoumine, O., Tardy, Y. & Meister, J. J. (2002). Contribution of the nucleus to the mechanical properties of endothelial cells. *J Biomech,* 35**,** 177-87.
Chandris, P., Giannouli, C. C., Panayotou, G. & Kletsas, D. (2010). Compromise in mRNA processing machinery in senescent human fibroblasts: implications for a novel potential role of Phospho-ATR (ser428). *Biogerontology,* 11**,** 421-36.
Choe, J., Ahn, S. H. & Kim, Y. K. (2014). The mRNP remodeling mediated by UPF1 promotes rapid degradation of replication-dependent histone mRNA. *Nucleic Acids Res,* 42**,** 9334-49.
Cimprich, K. A. & Cortez, D. (2008). ATR: an essential regulator of genome integrity. *Nat Rev Mol Cell Biol,* 9**,** 616-27.
Cliby, W. A., Roberts, C. J., Cimprich, K. A., Stringer, C. M., Lamb, J. R., Schreiber, S. L. & Friend, S. H. (1998). Overexpression of a kinase-inactive ATR protein causes sensitivity to DNA-damaging agents and defects in cell cycle checkpoints. *EMBO J,* 17**,** 159-69.
Conduit, P. T., Wainman, A. & Raff, J. W. (2015). Centrosome function and assembly in animal cells. *Nat Rev Mol Cell Biol,* 16**,** 611-24.
Cortez, D., Guntuku, S., Qin, J. & Elledge, S. J. (2001). ATR and ATRIP: partners in checkpoint signaling. *Science,* 294**,** 1713-6.
Cox, J. & Mann, M. (2008). MaxQuant enables high peptide identification rates, individualized p.p.b.-range mass accuracies and proteome-wide protein quantification. *Nat Biotechnol,* 26**,** 1367-72.
Dahl, K. N., Engler, A. J., Pajerowski, J. D. & Discher, D. E. (2005). Power-law rheology of isolated nuclei with deformation mapping of nuclear substructures. *Biophys J,* 89**,** 2855-64.
Dahl, K. N., Ribeiro, A. J. & Lammerding, J. (2008). Nuclear shape, mechanics, and mechanotransduction. *Circ Res,* 102**,** 1307-18.
Dasilva, L. F., Pillon, S., Genereaux, J., Davey, M. J., Gloor, G. B., Karagiannis, J. & Brandl, C. J. (2013). The C-terminal residues of Saccharomyces cerevisiae Mec1 are required for its localization, stability, and function. *G3 (Bethesda),* 3**,** 1661-74.

Dauer, W. T. & Worman, H. J. (2009). The nuclear envelope as a signaling node in development and disease. *Dev Cell,* 17**,** 626-38.

De Klein, A., Muijtjens, M., Van Os, R., Verhoeven, Y., Smit, B., Carr, A. M., Lehmann, A. R. & Hoeijmakers, J. H. (2000). Targeted disruption of the cell-cycle checkpoint gene ATR leads to early embryonic lethality in mice. *Curr Biol,* 10**,** 479-82.

De Noronha, C. M., Sherman, M. P., Lin, H. W., Cavrois, M. V., Moir, R. D., Goldman, R. D. & Greene, W. C. (2001). Dynamic disruptions in nuclear envelope architecture and integrity induced by HIV-1 Vpr. *Science,* 294**,** 1105-8.

De Vos, W. H., Houben, F., Kamps, M., Malhas, A., Verheyen, F., Cox, J., Manders, E. M., Verstraeten, V. L., Van Steensel, M. A., Marcelis, C. L., Van Den Wijngaard, A., Vaux, D. J., Ramaekers, F. C. & Broers, J. L. (2011). Repetitive disruptions of the nuclear envelope invoke temporary loss of cellular compartmentalization in laminopathies. *Hum Mol Genet,* 20**,** 4175-86.

Denais, C. M., Gilbert, R. M., Isermann, P., Mcgregor, A. L., Te Lindert, M., Weigelin, B., Davidson, P. M., Friedl, P., Wolf, K. & Lammerding, J. (2016). Nuclear envelope rupture and repair during cancer cell migration. *Science,* 352**,** 353-8.

Drozdz, M. M. & Vaux, D. J. (2017). Shared mechanisms in physiological and pathological nucleoplasmic reticulum formation. *Nucleus,* 8**,** 34-45.

Dutta, S., Bhattacharyya, M. & Sengupta, K. (2016). Implications and Assessment of the Elastic Behavior of Lamins in Laminopathies. *Cells,* 5.

Ericson, E., Wennberg Huldt, C., Stromstedt, M. & Brodin, P. (2015). A novel role of the checkpoint kinase ATR in leptin signaling. *Mol Cell Endocrinol,* 412**,** 257-64.

Farber-Katz, S. E., Dippold, H. C., Buschman, M. D., Peterman, M. C., Xing, M., Noakes, C. J., Tat, J., Ng, M. M., Rahajeng, J., Cowan, D. M., Fuchs, G. J., Zhou, H. & Field, S. J. (2014). DNA damage triggers Golgi dispersal via DNA-PK and GOLPH3. *Cell,* 156**,** 413-27.

Gerlitz, G. & Bustin, M. (2010). Efficient cell migration requires global chromatin condensation. *J Cell Sci,* 123**,** 2207-17.

Gerlitz, G. & Bustin, M. (2011). The role of chromatin structure in cell migration. *Trends Cell Biol,* 21**,** 6-11.

Goldman, R. D., Shumaker, D. K., Erdos, M. R., Eriksson, M., Goldman, A. E., Gordon, L. B., Gruenbaum, Y., Khuon, S., Mendez, M., Varga, R. & Collins, F. S. (2004). Accumulation of mutant lamin A causes progressive changes in nuclear architecture in Hutchinson-Gilford progeria syndrome. *Proc Natl Acad Sci U S A,* 101**,** 8963-8.

Gordon, L. B., Rothman, F. G., Lopez-Otin, C. & Misteli, T. (2014). Progeria: a paradigm for translational medicine. *Cell,* 156**,** 400-7.

Griffith, E., Walker, S., Martin, C. A., Vagnarelli, P., Stiff, T., Vernay, B., Al Sanna, N., Saggar, A., Hamel, B., Earnshaw, W. C., Jeggo, P. A., Jackson, A. P. & O'driscoll, M. (2008). Mutations in pericentrin cause Seckel syndrome with defective ATR-dependent DNA damage signaling. *Nat Genet,* 40**,** 232-6.

Guilak, F., Tedrow, J. R. & Burgkart, R. (2000). Viscoelastic properties of the cell nucleus. *Biochem Biophys Res Commun,* 269**,** 781-6.

Gupta, P., Bilinska, Z. T., Sylvius, N., Boudreau, E., Veinot, J. P., Labib, S., Bolongo, P. M., Hamza, A., Jackson, T., Ploski, R., Walski, M., Grzybowski, J., Walczak, E., Religa, G., Fidzianska, A. & Tesson, F. (2010). Genetic and ultrastructural studies in dilated cardiomyopathy patients: a large deletion in the lamin A/C gene is associated with cardiomyocyte nuclear envelope disruption. *Basic Res Cardiol,* 105**,** 365-77.

Haahr, P., Hoffmann, S., Tollenaere, M. A., Ho, T., Toledo, L. I., Mann, M., Bekker-Jensen, S., Raschle, M. & Mailand, N. (2016). Activation of the ATR kinase by the RPA-binding protein ETAA1. *Nat Cell Biol,* 18**,** 1196-1207.

Haga, H., Sasaki, S., Kawabata, K., Ito, E., Ushiki, T. & Sambongi, T. (2000). Elasticity mapping of living fibroblasts by AFM and immunofluorescence observation of the cytoskeleton. *Ultramicroscopy,* 82**,** 253-8.

Halazonetis, T. D., Gorgoulis, V. G. & Bartek, J. (2008). An oncogene-induced DNA damage model for cancer development. *Science,* 319**,** 1352-5.

Hanahan, D. & Weinberg, R. A. (2011). Hallmarks of cancer: the next generation. *Cell,* 144**,** 646-74.

Heng, X. & Le, W. D. (2010). The function of DNA topoisomerase IIbeta in neuronal development. *Neurosci Bull,* 26**,** 411-6.

Hershey, J. W. (2015). The role of eIF3 and its individual subunits in cancer. *Biochim Biophys Acta,* 1849**,** 792-800.

Hilton, B. A., Li, Z., Musich, P. R., Wang, H., Cartwright, B. M., Serrano, M., Zhou, X. Z., Lu, K. P. & Zou, Y. (2015). ATR Plays a Direct Antiapoptotic Role at Mitochondria, which Is Regulated by Prolyl Isomerase Pin1. *Mol Cell,* 60**,** 35-46.

Hilton, B. A., Li, Z., Musich, P. R., Wang, H., Cartwright, B. M., Serrano, M., Zhou, X. Z., Lu, K. P. & Zou, Y. (2016). ATR Plays a Direct Antiapoptotic Role at Mitochondria, which Is Regulated by Prolyl Isomerase Pin1. *Mol Cell,* 61**,** 487.

Hoeijmakers, J. H. (2009). DNA damage, aging, and cancer. *N Engl J Med,* 361**,** 1475-85.

Hornbeck, P. V., Chabra, I., Kornhauser, J. M., Skrzypek, E. & Zhang, B. (2004). PhosphoSite: A bioinformatics resource dedicated to physiological protein phosphorylation. *Proteomics,* 4**,** 1551-61.

Houben, F., Willems, C. H., Declercq, I. L., Hochstenbach, K., Kamps, M. A., Snoeckx, L. H., Ramaekers, F. C. & Broers, J. L. (2009). Disturbed nuclear orientation and cellular migration in A-type lamin deficient cells. *Biochim Biophys Acta,* 1793**,** 312-24.

Huang Da, W., Sherman, B. T. & Lempicki, R. A. (2009a). Bioinformatics enrichment tools: paths toward the comprehensive functional analysis of large gene lists. *Nucleic Acids Res,* 37**,** 1-13.

Huang Da, W., Sherman, B. T. & Lempicki, R. A. (2009b). Systematic and integrative analysis of large gene lists using DAVID bioinformatics resources. *Nat Protoc,* 4**,** 44-57.

Hurley, J. H. (2015). ESCRTs are everywhere. *EMBO J,* 34**,** 2398-407.

Irianto, J., Swift, J., Martins, R. P., Mcphail, G. D., Knight, M. M., Discher, D. E. & Lee, D. A. (2013). Osmotic challenge drives rapid and reversible chromatin condensation in chondrocytes. *Biophys J,* 104**,** 759-69.

Irianto, J., Xia, Y., Pfeifer, C. R., Athirasala, A., Ji, J., Alvey, C., Tewari, M., Bennett, R. R., Harding, S. M., Liu, A. J., Greenberg, R. A. & Discher, D. E. (2017). DNA Damage Follows Repair Factor Depletion and Portends Genome Variation in Cancer Cells after Pore Migration. *Curr Biol,* 27**,** 210-223.

Isermann, P. & Lammerding, J. (2013). Nuclear mechanics and mechanotransduction in health and disease. *Curr Biol,* 23**,** R1113-21.

Jacquot, G., Le Rouzic, E., David, A., Mazzolini, J., Bouchet, J., Bouaziz, S., Niedergang, F., Pancino, G. & Benichou, S. (2007). Localization of HIV-1 Vpr to the nuclear envelope: impact on Vpr functions and virus replication in macrophages. *Retrovirology,* 4**,** 84.

Jayo, A., Malboubi, M., Antoku, S., Chang, W., Ortiz-Zapater, E., Groen, C., Pfisterer, K., Tootle, T., Charras, G., Gundersen, G. G. & Parsons, M. (2016). Fascin Regulates Nuclear Movement and Deformation in Migrating Cells. *Dev Cell,* 38**,** 371-83.

Jimenez, A. J., Maiuri, P., Lafaurie-Janvore, J., Divoux, S., Piel, M. & Perez, F. (2014). ESCRT machinery is required for plasma membrane repair. *Science,* 343**,** 1247136.

Kidiyoor, G. R., Kumar, A. & Foiani, M. (2016). ATR-mediated regulation of nuclear and cellular plasticity. *DNA Repair (Amst),* 44**,** 143-150.

Kiger, A. A., Baum, B., Jones, S., Jones, M. R., Coulson, A., Echeverri, C. & Perrimon, N. (2003). A functional genomic analysis of cell morphology using RNA interference. *J Biol,* 2**,** 27.

Kim, S. T., Lim, D. S., Canman, C. E. & Kastan, M. B. (1999). Substrate specificities and identification of putative substrates of ATM kinase family members. *J Biol Chem,* 274**,** 37538-43.

Klingseisen, A. & Jackson, A. P. (2011). Mechanisms and pathways of growth failure in primordial dwarfism. *Genes Dev,* 25**,** 2011-24.

Kotula, E., Berthault, N., Agrario, C., Lienafa, M. C., Simon, A., Dingli, F., Loew, D., Sibut, V., Saule, S. & Dutreix, M. (2015). DNA-PKcs plays role in cancer metastasis through regulation of secreted proteins involved in migration and invasion. *Cell Cycle,* 14**,** 1961-72.

Kotula, E., Faigle, W., Berthault, N., Dingli, F., Loew, D., Sun, J. S., Dutreix, M. & Quanz, M. (2013). DNA-PK target identification reveals novel links between DNA repair signaling and cytoskeletal regulation. *PLoS One,* 8**,** e80313.

Kovacic, J. C., Moreno, P., Hachinski, V., Nabel, E. G. & Fuster, V. (2011). Cellular senescence, vascular disease, and aging: Part 1 of a 2-part review. *Circulation,* 123**,** 1650-60.

Kumagai, A., Lee, J., Yoo, H. Y. & Dunphy, W. G. (2006). TopBP1 activates the ATR-ATRIP complex. *Cell,* 124**,** 943-55.

Kumar, A., Mazzanti, M., Mistrik, M., Kosar, M., Beznoussenko, G. V., Mironov, A. A., Garre, M., Parazzoli, D., Shivashankar, G. V., Scita, G., Bartek, J. & Foiani, M. (2014). ATR mediates a checkpoint at the nuclear envelope in response to mechanical stress. *Cell,* 158**,** 633-46.

Kweon, H. S., Beznoussenko, G. V., Micaroni, M., Polishchuk, R. S., Trucco, A., Martella, O., Di Giandomenico, D., Marra, P., Fusella, A., Di Pentima, A., Berger, E. G., Geerts, W. J., Koster, A. J., Burger, K. N., Luini, A. & Mironov, A. A. (2004). Golgi enzymes are enriched in perforated zones of golgi cisternae but are depleted in COPI vesicles. *Mol Biol Cell,* 15**,** 4710-24.

Kyte, J. & Doolittle, R. F. (1982). A simple method for displaying the hydropathic character of a protein. *J Mol Biol,* 157**,** 105-32.

Lam, C. W., Yeung, W. L. & Law, C. Y. (2017). Global developmental delay and intellectual disability associated with a de novo TOP2B mutation. *Clin Chim Acta,* 469**,** 63-68.

Lammerding, J. & Wolf, K. (2016). Nuclear envelope rupture: Actin fibers are putting the squeeze on the nucleus. *J Cell Biol,* 215**,** 5-8.

Larsen, D. H. & Stucki, M. (2015). Nucleolar responses to DNA double-strand breaks. *Nucleic Acids Res*.

Lee, Y., Katyal, S., Downing, S. M., Zhao, J., Russell, H. R. & Mckinnon, P. J. (2012). Neurogenesis requires TopBP1 to prevent catastrophic replicative DNA damage in early progenitors. *Nat Neurosci,* 15**,** 819-26.

Lekka, M. (2016). Discrimination Between Normal and Cancerous Cells Using AFM. *Bionanoscience,* 6**,** 65-80.

Lempiainen, H. & Halazonetis, T. D. (2009). Emerging common themes in regulation of PIKKs and PI3Ks. *EMBO J,* 28**,** 3067-73.
Li, J., Han, Y. R., Plummer, M. R. & Herrup, K. (2009). Cytoplasmic ATM in neurons modulates synaptic function. *Curr Biol,* 19**,** 2091-6.
Li, Q. S., Lee, G. Y., Ong, C. N. & Lim, C. T. (2008). AFM indentation study of breast cancer cells. *Biochem Biophys Res Commun,* 374**,** 609-13.
Liu, L., Luo, Q., Sun, J. & Song, G. (2016). Nucleus and nucleus-cytoskeleton connections in 3D cell migration. *Exp Cell Res,* 348**,** 56-65.
Liu, S., Shiotani, B., Lahiri, M., Marechal, A., Tse, A., Leung, C. C., Glover, J. N., Yang, X. H. & Zou, L. (2011). ATR autophosphorylation as a molecular switch for checkpoint activation. *Mol Cell,* 43**,** 192-202.
Loeb, L. A. (1991). Mutator phenotype may be required for multistage carcinogenesis. *Cancer Res,* 51**,** 3075-9.
Lopez-Contreras, A. J., Specks, J., Barlow, J. H., Ambrogio, C., Desler, C., Vikingsson, S., Rodrigo-Perez, S., Green, H., Rasmussen, L. J., Murga, M., Nussenzweig, A. & Fernandez-Capetillo, O. (2015). Increased Rrm2 gene dosage reduces fragile site breakage and prolongs survival of ATR mutant mice. *Genes Dev,* 29**,** 690-5.
Lopez-Otin, C., Blasco, M. A., Partridge, L., Serrano, M. & Kroemer, G. (2013). The hallmarks of aging. *Cell,* 153**,** 1194-217.
Lucocq, J. M., Habermann, A., Watt, S., Backer, J. M., Mayhew, T. M. & Griffiths, G. (2004). A rapid method for assessing the distribution of gold labeling on thin sections. *J Histochem Cytochem,* 52**,** 991-1000.
Luke, Y., Zaim, H., Karakesisoglou, I., Jaeger, V. M., Sellin, L., Lu, W., Schneider, M., Neumann, S., Beijer, A., Munck, M., Padmakumar, V. C., Gloy, J., Walz, G. & Noegel, A. A. (2008). Nesprin-2 Giant (NUANCE) maintains nuclear envelope architecture and composition in skin. *J Cell Sci,* 121**,** 1887-98.
Macurek, L., Benada, J., Mullers, E., Halim, V. A., Krejcikova, K., Burdova, K., Pechackova, S., Hodny, Z., Lindqvist, A., Medema, R. H. & Bartek, J. (2013). Downregulation of Wip1 phosphatase modulates the cellular threshold of DNA damage signaling in mitosis. *Cell Cycle,* 12**,** 251-62.
Maiuri, P., Rupprecht, J. F., Wieser, S., Ruprecht, V., Benichou, O., Carpi, N., Coppey, M., De Beco, S., Gov, N., Heisenberg, C. P., Lage Crespo, C., Lautenschlaeger, F., Le Berre, M., Lennon-Dumenil, A. M., Raab, M., Thiam, H. R., Piel, M., Sixt, M. & Voituriez, R. (2015). Actin flows mediate a universal coupling between cell speed and cell persistence. *Cell,* 161**,** 374-86.
Malhas, A., Goulbourne, C. & Vaux, D. J. (2011). The nucleoplasmic reticulum: form and function. *Trends Cell Biol,* 21**,** 362-73.
Manic, G., Obrist, F., Sistigu, A. & Vitale, I. (2015). Trial Watch: Targeting ATM-CHK2 and ATR-CHK1 pathways for anticancer therapy. *Mol Cell Oncol,* 2**,** e1012976.
Marechal, A., Li, J. M., Ji, X. Y., Wu, C. S., Yazinski, S. A., Nguyen, H. D., Liu, S., Jimenez, A. E., Jin, J. & Zou, L. (2014). PRP19 transforms into a sensor of RPA-ssDNA after DNA damage and drives ATR activation via a ubiquitin-mediated circuitry. *Mol Cell,* 53**,** 235-46.
Matsuoka, S., Ballif, B. A., Smogorzewska, A., Mcdonald, E. R., 3rd, Hurov, K. E., Luo, J., Bakalarski, C. E., Zhao, Z., Solimini, N., Lerenthal, Y., Shiloh, Y., Gygi, S. P. & Elledge, S. J. (2007). ATM and ATR substrate analysis reveals extensive protein networks responsive to DNA damage. *Science,* 316**,** 1160-6.
Mazumder, A. & Shivashankar, G. V. (2010). Emergence of a prestressed eukaryotic nucleus during cellular differentiation and development. *J R Soc Interface,* 7 Suppl 3**,** S321-30.

Mckinnon, P. J. (2013). Maintaining genome stability in the nervous system. *Nat Neurosci,* 16**,** 1523-9.
Mcneil, P. L. & Steinhardt, R. A. (2003). Plasma membrane disruption: repair, prevention, adaptation. *Annu Rev Cell Dev Biol,* 19**,** 697-731.
Meinke, P. & Schirmer, E. C. (2015). LINC'ing form and function at the nuclear envelope. *FEBS Lett,* 589**,** 2514-21.
Mironov, A. A., Jr. & Mironov, A. A. (1998). Estimation of subcellular organelle volume from ultrathin sections through centrioles with a discretized version of the vertical rotator. *J Microsc,* 192**,** 29-36.
Mitaku, S., Hirokawa, T. & Tsuji, T. (2002). Amphiphilicity index of polar amino acids as an aid in the characterization of amino acid preference at membrane-water interfaces. *Bioinformatics,* 18**,** 608-16.
Mordes, D. A., Glick, G. G., Zhao, R. & Cortez, D. (2008). TopBP1 activates ATR through ATRIP and a PIKK regulatory domain. *Genes Dev,* 22**,** 1478-89.
Mori, C., Takanami, T. & Higashitani, A. (2008). Maintenance of mitochondrial DNA by the Caenorhabditis elegans ATR checkpoint protein ATL-1. *Genetics,* 180**,** 681-6.
Murga, M., Bunting, S., Montana, M. F., Soria, R., Mulero, F., Canamero, M., Lee, Y., Mckinnon, P. J., Nussenzweig, A. & Fernandez-Capetillo, O. (2009). A mouse model of ATR-Seckel shows embryonic replicative stress and accelerated aging. *Nat Genet,* 41**,** 891-8.
Nam, E. A., Zhao, R., Glick, G. G., Bansbach, C. E., Friedman, D. B. & Cortez, D. (2011). Thr-1989 phosphorylation is a marker of active ataxia telangiectasia-mutated and Rad3-related (ATR) kinase. *J Biol Chem,* 286**,** 28707-14.
Negrini, S., Gorgoulis, V. G. & Halazonetis, T. D. (2010). Genomic instability--an evolving hallmark of cancer. *Nat Rev Mol Cell Biol,* 11**,** 220-8.
Niccoli, T. & Partridge, L. (2012). Ageing as a risk factor for disease. *Curr Biol,* 22**,** R741-52.
Nigg, E. A. & Raff, J. W. (2009). Centrioles, centrosomes, and cilia in health and disease. *Cell,* 139**,** 663-78.
Nikolaishvili-Feinberg, N. & Cordeiro-Stone, M. (2000). Discrimination between translesion synthesis and template switching during bypass replication of thymine dimers in duplex DNA. *J Biol Chem,* 275**,** 30943-50.
O'driscoll, M. (2012). Diseases associated with defective responses to DNA damage. *Cold Spring Harb Perspect Biol,* 4.
O'driscoll, M., Ruiz-Perez, V. L., Woods, C. G., Jeggo, P. A. & Goodship, J. A. (2003). A splicing mutation affecting expression of ataxia-telangiectasia and Rad3-related protein (ATR) results in Seckel syndrome. *Nat Genet,* 33**,** 497-501.
Oliveira, A. G., Guimaraes, E. S., Andrade, L. M., Menezes, G. B. & Fatima Leite, M. (2014). Decoding calcium signaling across the nucleus. *Physiology (Bethesda),* 29**,** 361-8.
Olmos, Y., Hodgson, L., Mantell, J., Verkade, P. & Carlton, J. G. (2015). ESCRT-III controls nuclear envelope reformation. *Nature,* 522**,** 236-9.
Olsen, J. V., Vermeulen, M., Santamaria, A., Kumar, C., Miller, M. L., Jensen, L. J., Gnad, F., Cox, J., Jensen, T. S., Nigg, E. A., Brunak, S. & Mann, M. (2010). Quantitative phosphoproteomics reveals widespread full phosphorylation site occupancy during mitosis. *Sci Signal,* 3**,** ra3.
Osmanagic-Myers, S., Dechat, T. & Foisner, R. (2015). Lamins at the crossroads of mechanosignaling. *Genes Dev,* 29**,** 225-37.
Perez-Castro, A. J. & Freire, R. (2012). Rad9B responds to nucleolar stress through ATR and JNK signalling, and delays the G1-S transition. *J Cell Sci,* 125**,** 1152-64.

Perry, J. & Kleckner, N. (2003). The ATRs, ATMs, and TORs are giant HEAT repeat proteins. *Cell,* 112**,** 151-5.
Peterson, T. R. & Sabatini, D. M. (2005). eIF3: a connecTOR of S6K1 to the translation preinitiation complex. *Mol Cell,* 20**,** 655-7.
Prunuske, A. J. & Ullman, K. S. (2006). The nuclear envelope: form and reformation. *Curr Opin Cell Biol,* 18**,** 108-16.
Raab, M., Gentili, M., De Belly, H., Thiam, H. R., Vargas, P., Jimenez, A. J., Lautenschlaeger, F., Voituriez, R., Lennon-Dumenil, A. M., Manel, N. & Piel, M. (2016). ESCRT III repairs nuclear envelope ruptures during cell migration to limit DNA damage and cell death. *Science,* 352**,** 359-62.
Rashmi, R. N., Eckes, B., Glockner, G., Groth, M., Neumann, S., Gloy, J., Sellin, L., Walz, G., Schneider, M., Karakesisoglou, I., Eichinger, L. & Noegel, A. A. (2012). The nuclear envelope protein Nesprin-2 has roles in cell proliferation and differentiation during wound healing. *Nucleus,* 3**,** 172-86.
Rauch, A., Thiel, C. T., Schindler, D., Wick, U., Crow, Y. J., Ekici, A. B., Van Essen, A. J., Goecke, T. O., Al-Gazali, L., Chrzanowska, K. H., Zweier, C., Brunner, H. G., Becker, K., Curry, C. J., Dallapiccola, B., Devriendt, K., Dorfler, A., Kinning, E., Megarbane, A., Meinecke, P., Semple, R. K., Spranger, S., Toutain, A., Trembath, R. C., Voss, E., Wilson, L., Hennekam, R., De Zegher, F., Dorr, H. G. & Reis, A. (2008). Mutations in the pericentrin (PCNT) gene cause primordial dwarfism. *Science,* 319**,** 816-9.
Reiling, J. H. & Sabatini, D. M. (2006). Stress and mTORture signaling. *Oncogene,* 25**,** 6373-83.
Restuccia, U., Boschetti, E., Fasoli, E., Fortis, F., Guerrier, L., Bachi, A., Kravchuk, A. V. & Righetti, P. G. (2009). pI-based fractionation of serum proteomes versus anion exchange after enhancement of low-abundance proteins by means of peptide libraries. *J Proteomics,* 72**,** 1061-70.
Rocha, S., Garrett, M. D., Campbell, K. J., Schumm, K. & Perkins, N. D. (2005). Regulation of NF-kappaB and p53 through activation of ATR and Chk1 by the ARF tumour suppressor. *EMBO J,* 24**,** 1157-69.
Roobol, A., Roobol, J., Carden, M. J., Bastide, A., Willis, A. E., Dunn, W. B., Goodacre, R. & Smales, C. M. (2011). ATR (ataxia telangiectasia mutated- and Rad3-related kinase) is activated by mild hypothermia in mammalian cells and subsequently activates p53. *Biochem J,* 435**,** 499-508.
Roshal, M., Kim, B., Zhu, Y., Nghiem, P. & Planelles, V. (2003). Activation of the ATR-mediated DNA damage response by the HIV-1 viral protein R. *J Biol Chem,* 278**,** 25879-86.
Ruzankina, Y., Pinzon-Guzman, C., Asare, A., Ong, T., Pontano, L., Cotsarelis, G., Zediak, V. P., Velez, M., Bhandoola, A. & Brown, E. J. (2007). Deletion of the developmentally essential gene ATR in adult mice leads to age-related phenotypes and stem cell loss. *Cell Stem Cell,* 1**,** 113-26.
Saldivar, J. C., Cortez, D. & Cimprich, K. A. (2017). The essential kinase ATR: ensuring faithful duplication of a challenging genome. *Nat Rev Mol Cell Biol*.
Sancar, A., Lindsey-Boltz, L. A., Unsal-Kacmaz, K. & Linn, S. (2004). Molecular mechanisms of mammalian DNA repair and the DNA damage checkpoints. *Annu Rev Biochem,* 73**,** 39-85.
Shah, P., Wolf, K. & Lammerding, J. (2017). Bursting the Bubble - Nuclear Envelope Rupture as a Path to Genomic Instability? *Trends Cell Biol,* 27**,** 546-555.
Shanske, A., Caride, D. G., Menasse-Palmer, L., Bogdanow, A. & Marion, R. W. (1997). Central nervous system anomalies in Seckel syndrome: report of a new family and review of the literature. *Am J Med Genet,* 70**,** 155-8.

Shimada, M., Sagae, R., Kobayashi, J., Habu, T. & Komatsu, K. (2009). Inactivation of the Nijmegen breakage syndrome gene leads to excess centrosome duplication via the ATR/BRCA1 pathway. *Cancer Res,* 69**,** 1768-75.

Shull, E. R., Lee, Y., Nakane, H., Stracker, T. H., Zhao, J., Russell, H. R., Petrini, J. H. & Mckinnon, P. J. (2009). Differential DNA damage signaling accounts for distinct neural apoptotic responses in ATLD and NBS. *Genes Dev,* 23**,** 171-80.

Skau, C. T., Fischer, R. S., Gurel, P., Thiam, H. R., Tubbs, A., Baird, M. A., Davidson, M. W., Piel, M., Alushin, G. M., Nussenzweig, A., Steeg, P. S. & Waterman, C. M. (2016). FMN2 Makes Perinuclear Actin to Protect Nuclei during Confined Migration and Promote Metastasis. *Cell,* 167**,** 1571-1585 e18.

Smith, L., Liu, S. J., Goodrich, L., Jacobson, D., Degnin, C., Bentley, N., Carr, A., Flaggs, G., Keegan, K., Hoekstra, M. & Thayer, M. J. (1998). Duplication of ATR inhibits MyoD, induces aneuploidy and eliminates radiation-induced G1 arrest. *Nat Genet,* 19**,** 39-46.

Sokka, M., Rilla, K., Miinalainen, I., Pospiech, H. & Syvaoja, J. E. (2015). High levels of TopBP1 induce ATR-dependent shut-down of rRNA transcription and nucleolar segregation. *Nucleic Acids Res,* 43**,** 4975-89.

Sommer, L. A., Schaad, M. & Dames, S. A. (2013). NMR- and circular dichroism-monitored lipid binding studies suggest a general role for the FATC domain as membrane anchor of phosphatidylinositol 3-kinase-related kinases (PIKK). *J Biol Chem,* 288**,** 20046-63.

Stiff, T., Casar Tena, T., O'driscoll, M., Jeggo, P. A. & Philipp, M. (2016). ATR promotes cilia signalling: links to developmental impacts. *Hum Mol Genet,* 25**,** 1574-87.

Stokes, M. P., Rush, J., Macneill, J., Ren, J. M., Sprott, K., Nardone, J., Yang, V., Beausoleil, S. A., Gygi, S. P., Livingstone, M., Zhang, H., Polakiewicz, R. D. & Comb, M. J. (2007). Profiling of UV-induced ATM/ATR signaling pathways. *Proc Natl Acad Sci U S A,* 104**,** 19855-60.

Suetomi, K., Mereiter, S., Mori, C., Takanami, T. & Higashitani, A. (2013). Caenorhabditis elegans ATR checkpoint kinase ATL-1 influences life span through mitochondrial maintenance. *Mitochondrion,* 13**,** 729-35.

Sullivan, T., Escalante-Alcalde, D., Bhatt, H., Anver, M., Bhat, N., Nagashima, K., Stewart, C. L. & Burke, B. (1999). Loss of A-type lamin expression compromises nuclear envelope integrity leading to muscular dystrophy. *J Cell Biol,* 147**,** 913-20.

Supek, F., Bosnjak, M., Skunca, N. & Smuc, T. (2011). REVIGO summarizes and visualizes long lists of gene ontology terms. *PLoS One,* 6**,** e21800.

Syljuasen, R. G., Sorensen, C. S., Hansen, L. T., Fugger, K., Lundin, C., Johansson, F., Helleday, T., Sehested, M., Lukas, J. & Bartek, J. (2005). Inhibition of human Chk1 causes increased initiation of DNA replication, phosphorylation of ATR targets, and DNA breakage. *Mol Cell Biol,* 25**,** 3553-62.

Szklarczyk, D., Morris, J. H., Cook, H., Kuhn, M., Wyder, S., Simonovic, M., Santos, A., Doncheva, N. T., Roth, A., Bork, P., Jensen, L. J. & Von Mering, C. (2017). The STRING database in 2017: quality-controlled protein-protein association networks, made broadly accessible. *Nucleic Acids Res,* 45**,** D362-D368.

Thomas, D. G., Yenepalli, A., Denais, C. M., Rape, A., Beach, J. R., Wang, Y. L., Schiemann, W. P., Baskaran, H., Lammerding, J. & Egelhoff, T. T. (2015). Non-muscle myosin IIB is critical for nuclear translocation during 3D invasion. *J Cell Biol,* 210**,** 583-94.

Tibbetts, R. S., Cortez, D., Brumbaugh, K. M., Scully, R., Livingston, D., Elledge, S. J. & Abraham, R. T. (2000). Functional interactions between BRCA1 and the checkpoint kinase ATR during genotoxic stress. *Genes Dev,* 14**,** 2989-3002.

Tibelius, A., Marhold, J., Zentgraf, H., Heilig, C. E., Neitzel, H., Ducommun, B., Rauch, A., Ho, A. D., Bartek, J. & Kramer, A. (2009). Microcephalin and pericentrin regulate mitotic entry via centrosome-associated Chk1. *J Cell Biol,* 185**,** 1149-57.

Tivey, H. S., Rokicki, M. J., Barnacle, J. R., Rogers, M. J., Bagley, M. C., Kipling, D. & Davis, T. (2013). Small molecule inhibition of p38 MAP kinase extends the replicative life span of human ATR-Seckel syndrome fibroblasts. *J Gerontol A Biol Sci Med Sci,* 68**,** 1001-9.

Turgay, Y., Champion, L., Balazs, C., Held, M., Toso, A., Gerlich, D. W., Meraldi, P. & Kutay, U. (2014). SUN proteins facilitate the removal of membranes from chromatin during nuclear envelope breakdown. *J Cell Biol,* 204**,** 1099-109.

Valdes-Sanchez, L., De La Cerda, B., Diaz-Corrales, F. J., Massalini, S., Chakarova, C. F., Wright, A. F. & Bhattacharya, S. S. (2013). ATR localizes to the photoreceptor connecting cilium and deficiency leads to severe photoreceptor degeneration in mice. *Hum Mol Genet,* 22**,** 1507-15.

Vargas, J. D., Hatch, E. M., Anderson, D. J. & Hetzer, M. W. (2012). Transient nuclear envelope rupturing during interphase in human cancer cells. *Nucleus,* 3**,** 88-100.

Vergnolle, M. A. & Taylor, S. S. (2007). Cenp-F links kinetochores to Ndel1/Nde1/Lis1/dynein microtubule motor complexes. *Curr Biol,* 17**,** 1173-9.

Verstraeten, V. L., Ji, J. Y., Cummings, K. S., Lee, R. T. & Lammerding, J. (2008). Increased mechanosensitivity and nuclear stiffness in Hutchinson-Gilford progeria cells: effects of farnesyltransferase inhibitors. *Aging Cell,* 7**,** 383-93.

Vietri, M., Schink, K. O., Campsteijn, C., Wegner, C. S., Schultz, S. W., Christ, L., Thoresen, S. B., Brech, A., Raiborg, C. & Stenmark, H. (2015). Spastin and ESCRT-III coordinate mitotic spindle disassembly and nuclear envelope sealing. *Nature,* 522**,** 231-5.

Wang, N., Tytell, J. D. & Ingber, D. E. (2009). Mechanotransduction at a distance: mechanically coupling the extracellular matrix with the nucleus. *Nat Rev Mol Cell Biol,* 10**,** 75-82.

Webster, M., Witkin, K. L. & Cohen-Fix, O. (2009). Sizing up the nucleus: nuclear shape, size and nuclear-envelope assembly. *J Cell Sci,* 122**,** 1477-86.

Wei, F., Xie, Y., He, L., Tao, L. & Tang, D. (2011). ERK1 and ERK2 kinases activate hydroxyurea-induced S-phase checkpoint in MCF7 cells by mediating ATR activation. *Cell Signal,* 23**,** 259-68.

Weintraub, H. & Groudine, M. (1976). Chromosomal subunits in active genes have an altered conformation. *Science,* 193**,** 848-56.

Wu, C. S. & Zou, L. (2016). The SUMO (Small Ubiquitin-like Modifier) Ligase PIAS3 Primes ATR for Checkpoint Activation. *J Biol Chem,* 291**,** 279-90.

Yallapu, M. M., Katti, K. S., Katti, D. R., Mishra, S. R., Khan, S., Jaggi, M. & Chauhan, S. C. (2015). The roles of cellular nanomechanics in cancer. *Med Res Rev,* 35**,** 198-223.

Yu, J., Lei, K., Zhou, M., Craft, C. M., Xu, G., Xu, T., Zhuang, Y., Xu, R. & Han, M. (2011). KASH protein Syne-2/Nesprin-2 and SUN proteins SUN1/2 mediate nuclear migration during mammalian retinal development. *Hum Mol Genet,* 20**,** 1061-73.

Zeidman, I., Mc, C. M. & Coman, D. R. (1950). Factors affecting the number of tumor metastases; experiments with a transplantable mouse tumor. *Cancer Res,* 10**,** 357-9.

Zhang, C. Z., Spektor, A., Cornils, H., Francis, J. M., Jackson, E. K., Liu, S., Meyerson, M. & Pellman, D. (2015). Chromothripsis from DNA damage in micronuclei. *Nature,* 522**,** 179-84.
Zhang, S., Hemmerich, P. & Grosse, F. (2007a). Centrosomal localization of DNA damage checkpoint proteins. *J Cell Biochem,* 101**,** 451-65.
Zhang, X., Lei, K., Yuan, X., Wu, X., Zhuang, Y., Xu, T., Xu, R. & Han, M. (2009). SUN1/2 and Syne/Nesprin-1/2 complexes connect centrosome to the nucleus during neurogenesis and neuronal migration in mice. *Neuron,* 64**,** 173-87.
Zhang, X. H., Zhao, C. & Ma, Z. A. (2007b). The increase of cell-membranous phosphatidylcholines containing polyunsaturated fatty acid residues induces phosphorylation of p53 through activation of ATR. *J Cell Sci,* 120**,** 4134-43.
Zuleger, N., Robson, M. I. & Schirmer, E. C. (2011). The nuclear envelope as a chromatin organizer. *Nucleus,* 2**,** 339-49.
Zwerger, M., Ho, C. Y. & Lammerding, J. (2011). Nuclear mechanics in disease. *Annu Rev Biomed Eng,* 13**,** 397-428.

Acknowledgements

First and foremost, I would like to express my sincere gratitude to my supervisor Prof. Marco Foiani for this incredible opportunity, for his guidance and for his support through all these years. Besides Prof. Foiani, I also praise the guidance, teaching and help from my senior and predecessor Dr. Amit Kumar, who initiated this project with Prof. Foiani. I acknowledge the help from Irene Giovannetti, junior graduate student who will continue this mechano-biology project. A special thanks to funding agencies: Marie-Curie initial training network (European commission) and Associazione Italiana Per La Ricerca Sul Cancro (AIRC) for their generous support.

This project is the result of work by several researchers, who I wish to thank: Giulia Bastianello, Irene Giovannetti, Christopher Bruhn, Qingsen Li from our group; Andrea Disanza, Andrea Palamidessi, Emanuela Frittoli, Giorgio Scita, Vittoria Matafora, Umberto Restuccia, Angela Bachi, Paulina Nastaly, Paolo Maiuri, Kristina Havas, Marco Cosentino-Lagomarsino, Galina Beznusenko and Alexandre Mironov from the EM facility and other collaborators from IFOM; Marco Monticelli, Dario Valter Conca and Prof. Riccardo Bertacco from Politecnico di Milano; Matthieu Piel and Matthew Raab from Institute Curie, Paris; and Yannick Schwab from EMBL Heidelberg, I thank them all for their contributions. A special thank to the IFOM Imaging facility and Sorting facility, particularly Dario Parazzoli, Amanda Oldani, Sara Barozzi and Emanuele Martini for their sincere dedication towards our work. I am also grateful to the IFOM kitchen staff and to the cell culture staff for their assistance on a daily basis.

I would like to thank my internal and external supervisors, Prof. Vincenzo Costanzo and Prof. Jiri Bartek for their guidance and feedback. I also thank my examiners Nils Gauthier and Prof. Vincent Geli for their feedbacks and constructive criticism.

I extend my sincere gratitude towards my mentors, Ghadeer Shubassi, Chiara Lucca and Amit Kumar for their guidance through these years. I thank Yathish Achar,

Marek Adamowicz, Pawan singh, Martin Kosar, Hiroshi Arakawa, Michele Giannattasio and Paolo Maiuri for sharing their thoughts and expertise. My sincere thanks goes to Ghadeer Shubassi for critical reading of manuscripts and reports. I thank Giulia, Irene and Christopher for reading and correcting this thesis. I would like to thank members of Scita group, Fiore group, Bachi group, Costanzo group, Branzei group and Fagagna group for helping with reagents, protocols and discussions. Last but not least, I thank every past and present member of MF group for all the fun we have had in the last four and a half years, it was a memorable experience thank you for making it special.

A special acknowledgement goes to Anna Galgano, Laura Maggi, Aurelia Ramunni and "IFOM welcome office" members Mio Sumie and Marina Propenzi for taking care of foreign delegates, for handling all bureaucratic issues and making our stay easier and hassle free. I wish to acknowledge my friends Giulia Bastianello, Irene Giovannetti, Christopher Bruhn for all the "legendary" memories and my bench mate Arianna Colosio for all the gossips. I also like to thank all my friends from Milan especially my Bros Yathish, Pawan, Amit and Ram, my "Amore" Elisa Ferrari and Arta Ajazi for sharing her fantasies and the heated arguments. A special thanks goes to our TT group, for making every evening exciting and entertaining. I thank Eugenia Tabakaki and friends from ITN-ADDress network. I am grateful to Daniela Zechini for her friendship and kind help during early days of my Milan stay. I wish to thank the IFOM Indian community for all the food and for making me feel at home and our poker club for awesome games.

Finally, I want to thank my parents, my family and my friends back home for believing in me and for supporting me to reach my goal. I wish to dedicate this work to my mother Thulasi Amma, the reason behind my success. I am extremely grateful for her unconditional support and for the sacrifices that she made to see us achieve greater heights. Thanks you..